NONLINEAR ANALYSIS OF A TWO DOF PIECEWISE LINEAR AEROELASTIC SYSTEM

A Thesis

by

TAREK ADEL ABDELSALAM ELGOHARY

Submitted to the Office of Graduate Studies of
Texas A&M University
in partial fulfillment of the requirements for the degree of

MASTER OF SCIENCE

August 2010

Major Subject: Aerospace Engineering

NONLINEAR ANALYSIS OF A TWO DOF PIECEWISE LINEAR AEROELASTIC SYSTEM

A Thesis

by

TAREK ADEL ABDELSALAM ELGOHARY

Submitted to the Office of Graduate Studies of
Texas A&M University
in partial fulfillment of the requirements for the degree of

MASTER OF SCIENCE

Approved by:

Chair of Committee,	Tamás Kalmár-Nagy
Committee Members,	Thomas Strganac
	Jeffrey Falzarano
	Alan Palazzolo
Head of Department,	Dimitris Lagoudas

August 2010

Major Subject: Aerospace Engineering

ABSTRACT

Nonlinear Analysis of a Two DOF Piecewise Linear

Aeroelastic System. (August 2010)

Tarek Adel Abdelsalam Elgohary, B.S., American University in Cairo

Chair of Advisory Committee: Dr. Tamás Kalmár-Nagy

The nonlinear dynamic analysis of aeroelastic systems is a topic that has been covered extensively in the literature. The two main sources of nonlinearities in such systems, structural and aerodynamic nonlinearities, have analyzed numerically, analytically and experimentally. In this research project, the aerodynamic nonlinearity arising from the stall behavior of an airfoil is analyzed. Experimental data was used to fit a piecewise linear curve to describe the lift versus angle of attack behavior for a NACA 0012 2 DOF airfoil. The piecewise linear system equilibrium points are found and their stability analyzed. Bifurcations of the equilibrium points are analyzed and applying continuation software the bifurcation diagrams of the system are shown. Border collision and rapid/Hopf bifurcations are the two main bifurcations of the system equilibrium points. Chaotic behavior represented in the intermittent route to chaos was also observed and shown as part of the system dynamic analysis. Finally, sets of initial conditions associated with the system behavior are defined. Numerical simulations are used to show those sets, their subsets and their behavior with respect to the system dynamics. Poincaré sections are produced for both the periodic and the chaotic solutions of the system. The proposed piecewise linear model introduced some interesting dynamics for

such systems. The introduction of the border collision bifurcation and the existence of periodic and chaotic solutions for the system are some examples. The model also enables the understanding of the mapping of initial conditions as it defines clear boundaries with different dynamics that can be used as Poincaré sections to understand further the global system dynamics. One of the constraints of the system is its validity as it is dependent on the range of the experimental data used to generate the model. This can be addressed by adding more linear pieces to the system to cover a wider range of the dynamics.

DEDICATION

To my parents and my wife

ACKNOWLEDGMENTS

I would like to thank my committee chair, Dr. Kalmár-Nagy, and my committee members, Dr. Strganac, Dr. Falzarano and Dr. Palazzolo for their support and guidance throughout this research project. It has been a real pleasure working with all of my committee members and I benefited a lot from their experience whether in my research or in general.

I would also like to thank my advisor, Dr. Kalmár-Nagy, for all the effort and time he spent teaching and guiding me. It has been a pleasure working with him and I learned a lot from him. I must admit that I would not be here if he had not offered his support. Also with his guidance and help I became a much better student and researcher. Dr. T. I thank you for that, and I hope I that I have met your expectations as you were a great teacher, advisor and mentor to me.

I would also like to thank my family for all the support, financial and emotional, they unconditionally provided during the course of my study. I owe them everything I am now, and I owe them everything I will be.

Finally, to my fiancé and wife to be, I must say you gave me a reason to push forward and inspired me to continue and keep going. I thank you with all my heart and I cannot wait for the day of our wedding.

NOMENCLATURE

b	Semichord of the wing
s	Wing span
m	Mass of the system
k_y	Structural spring constant for vertical motion
k_α	Structural spring constant for rotational motion
c_y	Viscous damping coefficient for plunge DOF
c_α	Viscous damping coefficient for pitch DOF
C_{1_α}	Slope of the lift coefficient at zero angle of attack
I_{cg}	Mass moment of inertia about center of mass
ρ	Air density
M	Moment
L	Lift
α_{eff}	The effective angle of attack
α	Displacement coordinate for pitch DOF
y	Displacement coordinate for plunge DOF
U	Freestream velocity
μ	Non dimensional freestream velocity

TABLE OF CONTENTS

Page

LIST OF FIGURES

Page

Page

Page

Page

LIST OF TABLES

Page

1. INTRODUCTION

Nonlinear analysis of airfoils is a topic that is extensively covered in the literature. Many publications approached this problem analytically, numerically and experimentally. In general nonlinearities of airfoils can arise from two main sources; structural and aerodynamic nonlinearities. A comprehensive review of the literature covering both types of nonlinearities and the associated methods of solution can be found in Lee et al. (1999). In this review the equations of motion of a 2D airfoil oscillating in pitch and plunge with structural nonlinearity were derived. Three types of nonlinearities were investigated in details; cubic, free play and hysteresis. Also methods for solving the aerodynamic stall model were introduced with special emphasis on numerical simulations. Dowell et al. (2003) also introduced a good review for the problem discussing nonlinear aeroelasticity and its effects on flight and its association with limit cycle oscillations (LCO's). The paper also discussed both structural and aerodynamic nonlinearities and introduced results related to both. Gilliatt et al. (1997) investigated nonlinear aeroelastic behavior. In this paper both structural and aerodynamic nonlinearities were analyzed via measurements derived from wind-tunnel experiments and predictions derived from an analytical model. An emphasis was given to the aerodynamic nonlinearities arising from stall conditions.

This thesis follows the style of *Journal of Vibration and Control.*

Structural nonlinearities were tackled separately by many authors. O'Neil et al. (1996), O'Neil and Strganac (1998a) and O'Neil and Strganac (1998b) investigated the structural nonlinearity problem both analytically and experimentally. The emphasis in those papers was given to continuous nonlinearities that arise from spring hardening or softening effects. An experiment was set up and data was compared to analytical methods and was found to be consistent. Structural nonlinearities were also investigated by Price et al. (1995). In this paper the authors investigated the aeroelastic response of a 2D airfoil with bilinear and cubic structural nonlinearities. The results were introduced using numerical simulations by using the finite difference method. An analytical approach was also utilized using the describing function method and results were compared. LCO's were found to exist at a velocity below the divergent flutter limit. Chaotic behavior was investigated with the application of preload and bifurcation diagrams showing period doubling were plotted as a result. Woolston et al. (1957) approached the same problem and analyzed the three main models of structural nonlinearities namely freeplay, hysteresis and cubic nonlinearities. The flutter behavior of the airfoil was analyzed and it was found that with the structural nonlinearities flutter is highly dependent on initial conditions. The authors also introduced the LCO's behavior as a result of those nonlinearities.

Aerodynamics nonlinearities were tackled separately by Ueda and Dowell (1984). A typical airfoil section with transonic aerodynamic nonlinearities was analyzed. The describing function method was used for the analysis and results were compared to numerical methods. Results were very close especially for small amplitudes

of motion where the describing function method is very effective. Gilliatt (1997) and Gilliatt et al. (2003) examined internal resonances in an airfoil 2D model with aerodynamic nonlinearities, specifically nonlinearities arising from dynamic stall. The authors investigated the possible existence of internal resonances and showed evidence that for specific classes of aeroelastic systems internal resonance is present which gives rise to instabilities that are not predicted by traditional methods.

Analyzing an airfoil while combining both structural and aerodynamic nonlinearities was done by Tang and Dowell (1992) and Tang and Dowell (1993) where the authors investigated the nonlinear aeroelastic response of a non rotating helicopter blade. The airfoil model used is NACA 0012 and the paper investigated three cases of nonlinearities numerically. The three cases were nonlinear structure with linear aerodynamics where the stiffness of free play nonlinearity was used, linear structure with nonlinear aerodynamics where experimental data and curve fitting techniques were used to model the nonlinear lift coefficient and finally, nonlinear structure with nonlinear aerodynamics where the authors combined both cases. The flutter behavior in all cases was investigated and the amplitudes of LCO's were plotted and were found to be dependent on freestream velocity and initial conditions. Chaotic behavior was also investigated for forced and unforced cases and Poincaré maps sections were introduced for certain velocities. The authors also carried out an experiment to compare the previous analytical results with experimental results from the wind tunnel. The same airfoil section was used and results were found to be in good agreement between experimental and analytical methods confirming the results obtained previously. The

three main types of structural nonlinearities namely freeplay, cubic and hysteresis were investigated on 2 DOF and 3 DOF models. The existence of preload was investigated and it was shown that preload has a significant effect on flutter speed. The analysis confirmed that the flutter amplitudes largely depend on the initial conditions.

Analyzing nonlinear systems using the piecewise linear approximation is an approach that has been widely used and utilized in many problems. The main idea of the method is to divide a nonlinear dynamical system into linear regions where certain conditions are satisfied at which the local behavior of the system in each one of those regions is assumed to be linear. When combined together the overall nonlinear behavior of the system can be generated. This method has been introduced and discussed in several text books like Andronov et al. (1960) as several problems involving forced and free oscillations were introduced and analyzed using the piecewise linear approach. The same approach was used to investigate many different hysteretic systems. It was used by Kalmár-Nagy (2007) to study the hysteretic relay oscillator where the explicit solution of the problem was found and the Poincaré map of the system was constructed. Pratap et al. (1994a) and Pratap et al. (1994b) used the same approach to describe the behavior of an elasto-plastic beam model and showed the hysteretic behavior of the system after finding the closed form solution of the problem and constructing a map for the determination of the plastic cycles of the system. The two references describe the same problem with free oscillations and oscillations under periodic impulse forcing respectively. A piecewise linear oscillation model was analyzed by Shaw and Holmes (1983) where a single degree of freedom nonlinear oscillator was analyzed with the nonlinearity in the restoring force.

The force was modeled as a piecewise linear function with a single change of slope. The Poincaré map of the system was analyzed and harmonic, sub harmonic and chaotic motions were found and bifurcations leading to them were analyzed. Mahfouz and Badrakhan (1990a) and Mahfouz and Badrakhan (1990b) also analyzed similar piecewise linear systems and investigated their chaotic behavior. Two types of systems were introduced and analyzed in those references namely systems with set up springs and systems with clearance. Sub harmonic and chaotic motions of those systems were investigated and analyzed. Leine (2006) discussed bifurcations of equilibrium points for non smooth continuous systems. The so called 'multiple crossing bifurcations' where the Eigenvalues jump more than once over the imaginary axis was discussed for those types of systems. Examples of systems with that type of bifurcation were introduced and analyzed.

In this research project a complete nonlinear analysis for a 2 DOF aeroelastic system applying a piecewise linear stall model is conducted. The model is based on experimental data extracted from Sheldahl and Klimas (1981) and Gilliatt et al. (1997). The data is used and a piecewise linear curve fit is utilized to describe the lift versus the angle of attack behavior of a NACA 0012 airfoil oscillating in pitch and plunge. The equations of motion for the system are defined and nondimensionalized. The equilibrium points of the system are found and their stability analyzed. Bifurcation diagrams for each DOF are presented to describe the equilibrium points behavior as the no dimensional freestream velocity is varied. Numerical simulations are then used to show the system behavior at different regions of the bifurcation diagrams. Chaotic behavior is observed

and examined as part of the system dynamical analysis. Finally, sets of initial conditions associated with different dynamical behavior of the system are defined and analyzed. Numerical simulations were used to show those sets and their associated behavior. Also Poincaré sections for the stable periodic and the chaotic solutions are presented.

2. THE AEROELASTIC SYSTEM

The airfoil section used in this study is a NACA 0012 airfoil section. This is a typical 2 DOF, pitch and plunge, aeroelastic system with the assumption that the aeroelastic axis and the center of mass are collocated at three quarters of the chord length. Figure 1 shows a diagram of the system.

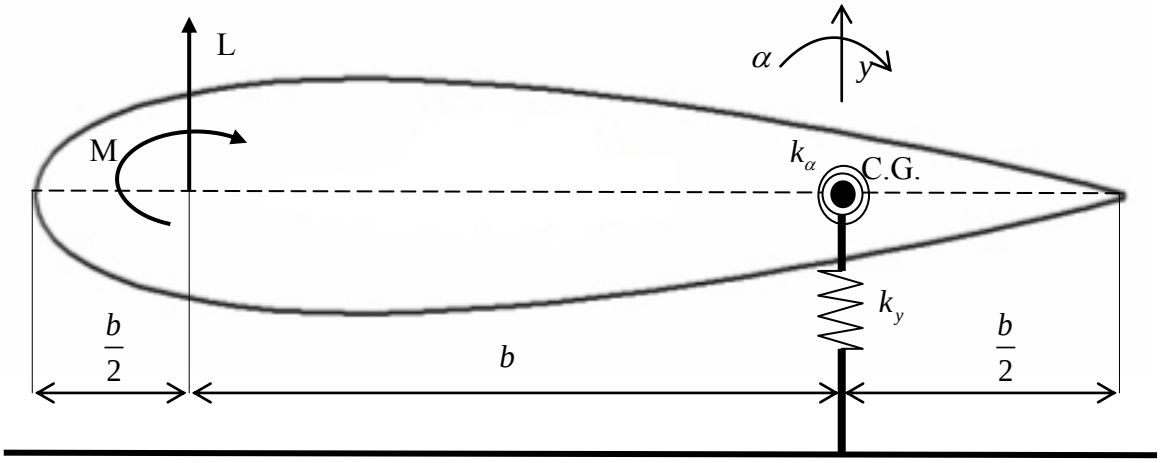

Figure 1: Airfoil section

The equations of motion of the shown system are

$$m\ddot{y} + c_y\dot{y} + k_y y = -L \tag{2.1}$$

$$I_{cg}\ddot{\alpha} + c_\alpha\dot{\alpha} + k_\alpha\alpha = M \tag{2.2}$$

where, the aerodynamic loads, lift and moment, are functions of the coefficient of lift and are expressed as

$$L = \rho U^2 bSC_l \tag{2.3}$$

$$M = \rho U^2 b^2 SC_l \tag{2.4}$$

2.1 The Aerodynamic Model

As the angle of attack of an airfoil increases, the lift coefficient also increases until a certain value of the angle of attack where the lift decreases as a result of flow separation. This behavior is what defines stall. Dynamic stall is the unsteady flow separation describing the stall of an airfoil oscillating into and out of stall. Two main approaches have been utilized to model dynamic stall. The first is a theoretical approach and the second is based on experimental data. In their NASA technical memo Reddy and Kaza (1987) conducted a comparative study of three dynamical stall models. The authors focused on three types of dynamic stall models that are based on experimental data (semi empirical models). The models were: (1) the corrected angle of attack approach where the effective angle of attack is utilized as a function of the rate of the angle of attack. The lift and moment coefficients are the then obtained from static airfoil data. (2) The synthesis procedure which involves three dynamic parameters defined to predict the stall event. The parameters are: (a) the instantaneous angle of attack, (b) the non-dimensional rate of the angle of attack and (c) a decay parameter which accounts for the change caused by the time history effects of the instantaneous angle of attack. (3) The ONERA model which uses ordinary differential equations to describe the change in lift and moment coefficients. The three models were used in simulations to describe dynamic stall in a typical airfoil section model and in a plate model. Results were compared and variations between the three models were highlighted especially the values of flutter speed and their offset from the calculated values using classical flutter analysis. McAlister et al. (1984) conducted a comprehensive study on the ONERA aerodynamic

model. The model was tested both numerically and experimentally and results were verified. The model was found to be consistent with experimental results for small amplitude responses. For higher angles the model was not able to accurately predict the physical behavior of the system. The authors also included some recommendations to include the hysteresis effects and the delay in stall due to the dynamic stall phenomena.

Table 3 in Appendix shows the experimental data used to construct the aerodynamic model for the presented aeroelastic system, Sheldahl and Klimas (1981). The experiments presented in that reference covered seven airfoils with angles of attack ranging from 0˚ to 360˚. The data for the NACA 0012 airfoil is used to construct two aerodynamic models for the system. The first is a continuous model and the second is a piecewise linear model. In the next sections each model will be presented with its equations of motion nondimensionalized and scaled.

2.1.1 The continuous aerodynamic model

As previously mentioned, experimental data extracted from Sheldahl and Klimas (1981) is used to construct the aerodynamic model. Figure 2 shows the model and the data points associated with the curve fit used.

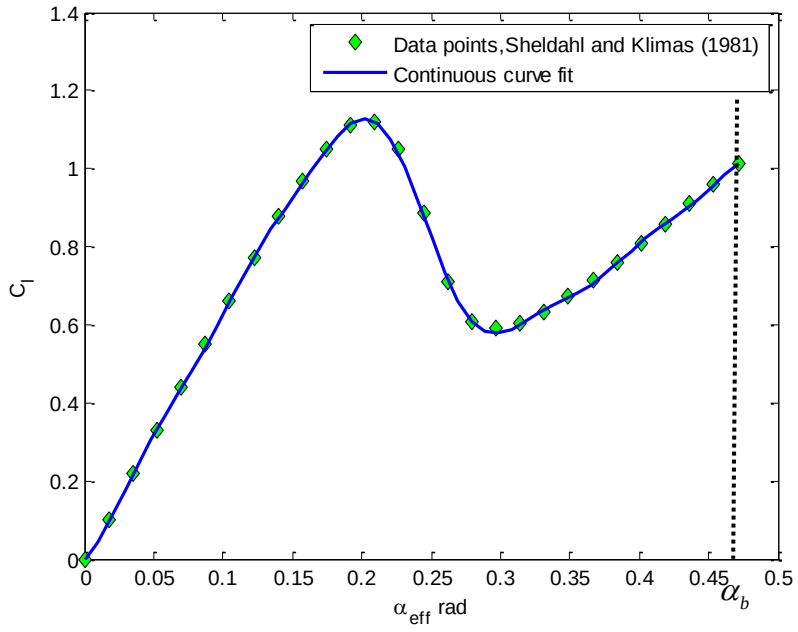

Figure 2: Continuous aerodynamic model

In this model the effective angle of attack resulting from instantaneous motion of the airfoil is used. The expression of the effective angle of attack for the presented aeroelastic system is

$$\alpha_{eff} = \alpha + \frac{\dot{y}}{U} \tag{2.5}$$

Based on various nonlinear fits the following function is found to be a very good approximation for the data points

$$C_l(\alpha_{eff}) = \operatorname{sgn}(\alpha_{eff})\left[\sum_{i=1}^{4} a_i \sin\left(b_i \left|\alpha_{eff}\right| + c_i\right) + C\right] \tag{2.6}$$

where, the sgn function is for the asymmetry of the model for negative values of α_{eff} and C is a constant used to adjust the curve fit to pass through the origin. All the parameters of the model are presented in Table 4 in the Appendix.

This model as well as the piecewise linear model, presented in the next section, will have the same range of angles of attack as shown in Figure 2 and Figure 3. The range of α is from 0 to α_b, where $\alpha_b = 0.4712\,rad$.

Now the aerodynamic loads in the equations of motion can be expressed as a function of the effective angle of attack as shown

$$m\ddot{y} + c_y\dot{y} + k_y y = -L\left(\alpha_{eff}\right) \tag{2.7}$$

$$I_{cg}\ddot{\alpha} + c_\alpha\dot{\alpha} + k_\alpha\alpha = M\left(\alpha_{eff}\right) \tag{2.8}$$

where, the aerodynamic loads, lift and moment are expressed as

$$L\left(\alpha_{eff}\right) = \rho U^2 bSC_l\left(\alpha_{eff}\right) \tag{2.9}$$

$$M\left(\alpha_{eff}\right) = \rho U^2 b^2 SC_l\left(\alpha_{eff}\right) \tag{2.10}$$

From (2.6) through (2.10) the dimensional form of the equations of motion for the continuous model can be obtained,

For the plunge DOF

$$m\ddot{y} + c_y\dot{y} + k_y y = -\rho U^2 bS\left[\operatorname{sgn}\left(\alpha_{eff}\right)\left[\sum_{i=1}^{4} a_i \sin\left(b_i\left|\alpha_{eff}\right| + c_i\right) + C\right]\right] \tag{2.11}$$

For the pitch DOF

$$I_{cg}\ddot{\alpha} + c_\alpha\dot{\alpha} + k_\alpha\alpha = \rho U^2 b^2 S\left[\operatorname{sgn}\left(\alpha_{eff}\right)\left[\sum_{i=1}^{4} a_i \sin\left(b_i\left|\alpha_{eff}\right| + c_i\right) + C\right]\right] \tag{2.12}$$

2.1.2 The piecewise linear aerodynamic model

The data points in Sheldahl and Klimas (1981) also suggested another type of curve fit. Instead of fitting a continuous function to the data points as was done in the previous section a piecewise linear function is fitted to the data. Switching points are defined and the system is divided into three sections with different linear functions describing the aerodynamic loads. Figure 3 shows the piecewise linear model.

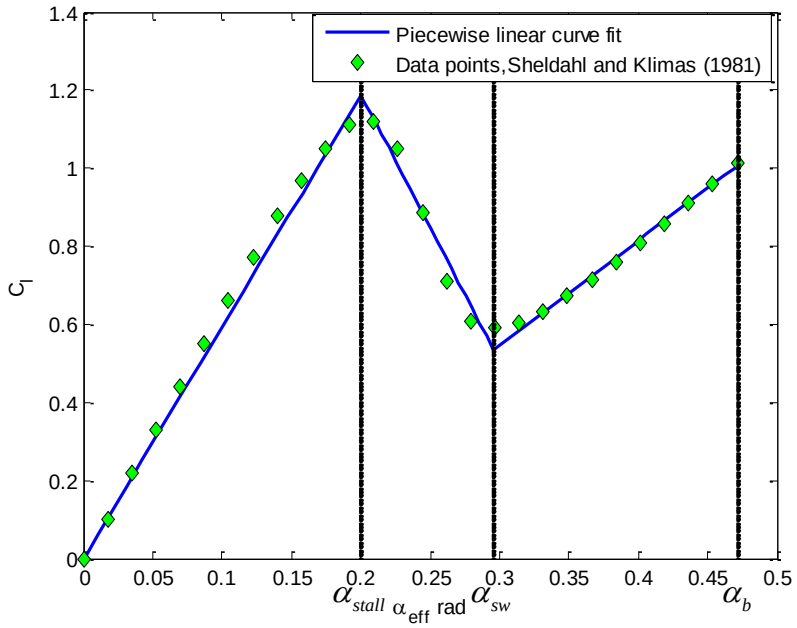

Figure 3: Piecewise linear aerodynamic model

The model represents the lift coefficient versus the angle of attack in three linear portions. The first region describes the linear increase in lift as we increase the angle of attack. This region bounds are between $\alpha = 0$ to $\alpha = \alpha_{stall}$ which corresponds to the stall angle of attack. The second region takes place after the value of the angle of attack exceeds the stall value and the airfoil starts to lose lift as the angle of attack increases.

This region ends at $\alpha = \alpha_{sw}$, which defines a third switching point and the beginning of the third region of the lift model. In this region the airfoil starts to regain lift as the angle of attack is increased until it reaches α_b that defines the bound of the aerodynamic model chosen from the experimental data in Sheldahl and Klimas (1981).

This piecewise linear model is only valid for angles of attack ranging from 0 to 0.4712 rad. Although experimental results are available for lift values at higher angles of attack, this range was chosen as it will sufficiently describe the physics of the problem for flight applications for the NACA 0012 airfoil.

The governing equations of motion of the system are

$$m\ddot{y} + c_y\dot{y} + k_y y = -L(\alpha_{eff}) \tag{2.13}$$

$$I_{cg}\ddot{\alpha} + c_\alpha\dot{\alpha} + k_\alpha\alpha = M(\alpha_{eff}) \tag{2.14}$$

where,

$$L(\alpha_{eff}) = \rho U^2 bSC_l(\alpha_{eff}) \tag{2.15}$$

$$M(\alpha_{eff}) = \rho U^2 b^2 SC_l(\alpha_{eff}) \tag{2.16}$$

and,

$$C_l(\alpha_{eff}) = \begin{cases} C_I = c_o\alpha_{eff} & -\alpha_{stall} \le \alpha_{eff} \le \alpha_{stall} \\ C_{II} = c_1\alpha_{eff} + \mathrm{sgn}(\alpha_{eff})c_2 & \alpha_{stall} \le \left|\alpha_{eff}\right| \le \alpha_{sw} \\ C_{III} = c_3\alpha_{eff} + \mathrm{sgn}(\alpha_{eff})c_4 & \alpha_{sw} \le \left|\alpha_{eff}\right| \le \alpha_b \end{cases} \tag{2.17}$$

where, α_{eff} is the effective angle of attack resulting from the instantaneous motion of the structure as presented in (2.5). Similar to the continuous model, the sgn function here is to represent the asymmetry of the model for negative values of α_{eff}. Table 5 in the

Appendix has a list of the different parameters values in the proposed piecewise linear lift function as well the values of the switching angles. A clear property of the proposed lift function in (2.17) is as follows

$$\begin{aligned} &At\left|\alpha_{eff}\right| = \alpha_{stall} && C_I = C_{II} \\ &At\left|\alpha_{eff}\right| = \alpha_{sw} && C_{II} = C_{III} \end{aligned} \tag{2.18}$$

Equation (2.18) will be very useful in the analysis of the system equilibrium points and the conditions of their existence presented in the next section.

Combining equations (2.13) through (2.17) will yield the final dimensional form of the equations of motion for the piecewise linear system.

For the plunge DOF

$$m\ddot{y} + c_y\dot{y} + k_y y = -\rho U^2 bS\left[c_o\left(\alpha + \frac{\dot{y}}{U}\right)\right] \qquad for -\alpha_{stall} \le \alpha_{eff} \le \alpha_{stall} \tag{2.19}$$

$$m\ddot{y} + c_y\dot{y} + k_y y = -\rho U^2 bS\left[c_1\left(\alpha + \frac{\dot{y}}{U}\right) + \mathrm{sgn}\left(\alpha_{eff}\right)c_2\right] \qquad for\ \alpha_{stall} \le |\alpha_{eff}| \le \alpha_{sw} \tag{2.20}$$

$$m\ddot{y} + c_y\dot{y} + k_y y = -\rho U^2 bS\left[c_3\left(\alpha + \frac{\dot{y}}{U}\right) + \mathrm{sgn}\left(\alpha_{eff}\right)c_4\right] \qquad for\ \alpha_{sw} \le |\alpha_{eff}| \le \alpha_b \tag{2.21}$$

For the pitch DOF

$$I_{cg}\ddot{\alpha} + c_\alpha\dot{\alpha} + k_\alpha\alpha = \rho U^2 b^2 S\left[c_o\left(\alpha + \frac{\dot{y}}{U}\right)\right] \qquad for\ -\alpha_{stall} \le \alpha_{eff} \le \alpha_{stall} \tag{2.22}$$

$$I_{cg}\ddot{\alpha} + c_\alpha\dot{\alpha} + k_\alpha\alpha = \rho U^2 b^2 S\left[c_1\left(\alpha + \frac{\dot{y}}{U}\right) + \mathrm{sgn}\left(\alpha_{eff}\right)c_2\right] \qquad for\ \alpha_{stall} \le |\alpha_{eff}| \le \alpha_{sw} \tag{2.23}$$

$$I_{cg}\ddot{\alpha} + c_\alpha\dot{\alpha} + k_\alpha\alpha = \rho U^2 b^2 S\left[c_3\left(\alpha + \frac{\dot{y}}{U}\right) + \mathrm{sgn}\left(\alpha_{eff}\right)c_4\right] \qquad for\ \alpha_{sw} \le |\alpha_{eff}| \le \alpha_b \tag{2.24}$$

2.2 Nondimensionalizing and Scaling

To continue with our analysis the equations of motion are nondimensionalized and scaled as follows.

Time and length scales are defined as

$$\tilde{y} = \frac{y}{L} \qquad \tilde{t} = \frac{t}{T} \tag{2.25}$$

Also a nondimensional freestream velocity is introduced as

$$\mu = \frac{U}{\Omega}, \text{ Where } \Omega = \frac{L}{T} \tag{2.26}$$

after substituting (2.25) and (2.26) into (2.5), The effective angle of attack is expressed as

$$\alpha_{eff} = \alpha + \frac{1}{\mu}\tilde{y}' \tag{2.27}$$

2.2.1 The continuous aerodynamic model

Substituting the scales presented in (2.25) and (2.26) into the continuous model equations of motion will produce the following equations,

For the plunge DOF,

$$\tilde{y}'' + T\frac{c_y}{m}\tilde{y}' + T^2\frac{k_y}{m}\tilde{y} + L\frac{\rho bs}{m}\mu^2 C_l\left(\alpha_{eff}\right) = 0 \tag{2.28}$$

For the pitch DOF,

$$\alpha'' + T\frac{c_\alpha}{I_{cg}}\alpha' + T^2\frac{k_\alpha}{I_{cg}}\alpha - L^2\frac{\rho b^2 s}{I_{cg}}\mu^2 C_l\left(\alpha_{eff}\right) = 0 \tag{2.29}$$

where, $C_l(\alpha_{eff})$ is expressed as

$$C_l(\alpha_{eff}) = \operatorname{sgn}\left(\alpha_{eff}\right)\left[\sum_{i=1}^{4} a_i \sin\left(b_i\left|\alpha_{eff}\right| + c_i\right) + C\right] \tag{2.30}$$

The following non dimensional quantities can be defined.

$$\gamma_1 = T\frac{c_y}{m} \qquad \gamma_4 = T\frac{c_\alpha}{I_{cg}}$$
$$\gamma_2 = L\frac{\rho bs}{m} \qquad \gamma_5 = T^2\frac{k_\alpha}{I_{cg}} \tag{2.31}$$
$$\gamma_3 = T^2\frac{k_y}{m} \qquad \gamma_6 = L^2\frac{\rho b^2 s}{I_{cg}}$$

A list of the system parameters and their values is presented in Table 2 in the Appendix. Table 6 in the Appendix includes the values and dimensional checks done on the quantities introduced in (2.31).

The following length and time scales are introduced to the problem.

$$L^2 = \frac{I_{cg}}{\rho b^2 s} \qquad \text{and} \qquad T^2 = \frac{m}{k_y} \tag{2.32}$$

Substituting (2.32) into our system, equations (2.28) and (2.29), the system equations will have the nondimensional form as follows

$$\tilde{y}'' + \frac{c_y}{\sqrt{k_y m}}\tilde{y}' + \tilde{y} + \mu^2\frac{\sqrt{\rho I_{cg} s}}{m}C_l(\alpha_{eff}) = 0 \tag{2.33}$$

$$\alpha'' + \frac{c_\alpha}{I_{cg}}\sqrt{\frac{m}{k_y}}\alpha' + \frac{k_\alpha m}{I_{cg}k_y}\alpha - \mu^2 C_l(\alpha_{eff}) = 0 \tag{2.34}$$

From (2.33) and (2.34) the following nondimensional parameters can be defined

$$p_1 = \frac{c_y}{\sqrt{mk_y}} \qquad p_3 = \frac{c_\alpha}{I_{cg}}\sqrt{\frac{m}{k_y}}$$
$$p_2 = \frac{\sqrt{\rho I_{cg} s}}{m} \qquad p_4 = \frac{k_\alpha m}{I_{cg} k_y} \tag{2.35}$$

Table 7 in the Appendix has the numerical values of these parameters and their dimensional check.

Substituting (2.35) in (2.33) and (2.34) will yield the following form of the nondimensional system equations

$$\tilde{y}'' + p_1\tilde{y}' + \tilde{y} + p_2\mu^2 C_l(\alpha_{eff}) = 0 \tag{2.36}$$

$$\alpha'' + p_3\alpha' + p_4\alpha - \mu^2 C_l(\alpha_{eff}) = 0 \tag{2.37}$$

For the purpose of numerical simulations the system is presented in the following first order from

$$x_1 = \tilde{y},\ x_2 = \tilde{y}',\ x_3 = \alpha, x_4 = \alpha' \tag{2.38}$$

$$\alpha_{eff} = x_3 + \frac{x_2}{\mu} \tag{2.39}$$

$$\begin{aligned} \dot{x}_1 &= x_2 \\ \dot{x}_2 &= -p_1 x_2 - x_1 - p_2\mu^2 C_l(\alpha_{eff}) \\ \dot{x}_3 &= x_4 \\ \dot{x}_4 &= -p_3 x_4 - p_4 x_3 + \mu^2 C_l(\alpha_{eff}) \end{aligned} \tag{2.40}$$

2.2.2 The piecewise linear aerodynamic model

Applying the same scales to the piecewise linear model and substituting into the equations of motion, the following set of equations are obtained,

The plunge DOF set of equations

$$\tilde{y}'' + T\frac{c_y}{m}\tilde{y}' + L\frac{\rho bs}{m}\mu c_o\tilde{y}' + T^2\frac{k_y}{m}\tilde{y} + L\frac{\rho bs}{m}\mu^2 c_o\alpha = 0 \qquad for\ -\alpha_{stall} \le \alpha_{eff} \le \alpha_{stall} \tag{2.41}$$

$$\tilde{y}'' + T\frac{c_y}{m}\tilde{y}' + L\frac{\rho bs}{m}c_1\tilde{y}' + T^2\frac{k_y}{m}\tilde{y} + L\frac{\rho bs}{m}\mu^2 c_1\alpha + \mathrm{sgn}\left(\alpha_{eff}\right)L\frac{\rho bs}{m}\mu^2 c_2 = 0 \qquad for\ \alpha_{stall} \le |\alpha_{eff}| \le \alpha_{sw} \tag{2.42}$$

$$\tilde{y}'' + T\frac{c_y}{m}\tilde{y}' + L\frac{\rho bs}{m}\mu c_3\tilde{y}' + T^2\frac{k_y}{m}\tilde{y} + L\frac{\rho bs}{m}\mu^2 c_3\alpha + \mathrm{sgn}\left(\alpha_{eff}\right)L\frac{\rho bs}{m}\mu^2 c_4 = 0 \qquad for\ \alpha_{sw} \le |\alpha_{eff}| \le \alpha_b \tag{2.43}$$

The pitch DOF set of equations

$$\alpha'' + T\frac{c_\alpha}{I_{cg}}\alpha' + T^2\frac{k_\alpha}{I_{cg}}\alpha - L^2\frac{\rho b^2 s}{I_{cg}}\mu^2 c_o\alpha - L^2\frac{\rho b^2 s}{I_{cg}}\mu c_o\tilde{y}' = 0 \qquad for\ -\alpha_{stall} \le \alpha_{eff} \le \alpha_{stall} \tag{2.44}$$

$$\alpha'' + T\frac{c_\alpha}{I_{cg}}\alpha' + T^2\frac{k_\alpha}{I_{cg}}\alpha - L^2\frac{\rho b^2 s}{I_{cg}}\mu^2 c_1\alpha - L^2\frac{\rho b^2 s}{I_{cg}}\mu c_1\tilde{y}' + \mathrm{sgn}\left(\alpha_{eff}\right)L^2\frac{\rho b^2 s}{I_{cg}}\mu^2 c_2 = 0 \qquad for\ \alpha_{stall} \le |\alpha_{eff}| \le \alpha_{sw} \tag{2.45}$$

$$\alpha'' + T\frac{c_\alpha}{I_{cg}}\alpha' + T^2\frac{k_\alpha}{I_{cg}}\alpha - L^2\frac{\rho b^2 s}{I_{cg}}\mu^2 c_3\alpha - L^2\frac{\rho b^2 s}{I_{cg}}\mu c_3\tilde{y}' + \mathrm{sgn}(\alpha_{eff})L^2\frac{\rho b^2 s}{I_{cg}}\mu^2 c_4 = 0 \qquad for\ \alpha_{sw} \le |\alpha_{eff}| \le \alpha_b \tag{2.46}$$

The same nondimensional quantities shown in (2.31) are defined here and their values and dimensional checks are presented in Table 6 in the Appendix.

$$\gamma_1 = T\frac{c_y}{m} \qquad \gamma_4 = T\frac{c_\alpha}{I_{cg}}$$
$$\gamma_2 = L\frac{\rho bs}{m} \qquad \gamma_5 = T^2\frac{k_\alpha}{I_{cg}} \tag{2.47}$$
$$\gamma_3 = T^2\frac{k_y}{m} \qquad \gamma_6 = L^2\frac{\rho b^2 s}{I_{cg}}$$

Introducing the same length and time scales as in (2.32)

$$L^2 = \frac{I_{cg}}{\rho b^2 s} \qquad \text{and} \qquad T^2 = \frac{m}{k_y} \tag{2.48}$$

Substituting into the equations of motion the following equations are obtained,

For the plunge DOF set of equations

$$\tilde{y}'' + \left(\frac{c_y}{\sqrt{mk_y}} + \frac{\sqrt{\rho I_{cg} s}}{m}\mu c_o\right)\tilde{y}' + \tilde{y} + \frac{\sqrt{\rho I_{cg} s}}{m}\mu^2 c_o \alpha = 0 \tag{2.49}$$
$$for\ -\alpha_{stall} \le \alpha_{eff} \le \alpha_{stall}$$

$$\tilde{y}'' + \left(\frac{c_y}{\sqrt{mk_y}} + \frac{\sqrt{\rho I_{cg} s}}{m}\mu c_1\right)\tilde{y}' + \tilde{y} + \frac{\sqrt{\rho I_{cg} s}}{m}\mu^2 c_1 \alpha + \mathrm{sgn}\left(\alpha_{eff}\right)\frac{\sqrt{\rho I_{cg} s}}{m}\mu^2 c_2 = 0$$
$$for\ \alpha_{stall} \le |\alpha_{eff}| \le \alpha_{sw} \tag{2.50}$$

$$\tilde{y}'' + \left(\frac{c_y}{\sqrt{mk_y}} + \frac{\sqrt{\rho I_{cg} s}}{m}\mu c_3\right)\tilde{y}' + \tilde{y} + \frac{\sqrt{\rho I_{cg} s}}{m}\mu^2 c_3 \alpha + \mathrm{sgn}\left(\alpha_{eff}\right)\frac{\sqrt{\rho I_{cg} s}}{m}\mu^2 c_4 = 0$$
$$for\ \alpha_{sw} \le |\alpha_{eff}| \le \alpha_b \tag{2.51}$$

For the pitch DOF set of equations

$$\alpha'' + \sqrt{\frac{m}{k_y}}\frac{c_\alpha}{I_{cg}}\alpha' + \left(\frac{k_\alpha m}{I_{cg}k_y} - \mu^2 c_o\right)\alpha - \mu c_0 \tilde{y}' = 0 \qquad for\ -\alpha_{stall} \le \alpha_{eff} \le \alpha_{stall} \tag{2.52}$$

$$\alpha'' + \sqrt{\frac{m}{k_y}}\frac{c_\alpha}{I_{cg}}\alpha' + \left(\frac{k_\alpha m}{I_{cg}k_y} - \mu^2 c_1\right)\alpha - \mu c_1 \tilde{y}' + \mathrm{sgn}\left(\alpha_{eff}\right)\mu^2 c_2 = 0 \qquad for\ \alpha_{stall} \le |\alpha_{eff}| \le \alpha_{sw} \tag{2.53}$$

$$\alpha'' + \sqrt{\frac{m}{k_y}}\frac{c_\alpha}{I_{cg}}\alpha' + \left(\frac{k_\alpha m}{I_{cg}k_y} - \mu^2 c_3\right)\alpha - \mu c_3 \tilde{y}' + \mathrm{sgn}\left(\alpha_{eff}\right)\mu^2 c_4 = 0 \qquad for\ \alpha_{sw} \le |\alpha_{eff}| \le \alpha_b \tag{2.54}$$

From equations (2.49) to (2.54) the same nondimensional parameters introduced in (2.35) are defined

$$p_1 = \frac{c_y}{\sqrt{mk_y}} \qquad p_3 = \frac{c_\alpha}{I_{cg}}\sqrt{\frac{m}{k_y}}$$
$$p_2 = \frac{\sqrt{\rho I_{cg} s}}{m} \qquad p_4 = \frac{k_\alpha m}{I_{cg}k_y} \tag{2.55}$$

Substituting (2.55) into the equations of motion will produce the following nondimensional form for the system equations.

The plunge DOF set of equations

$$\tilde{y}'' + \left(p_1 + p_2\mu c_o\right)\tilde{y}' + \tilde{y} + p_2\mu^2 c_o\alpha = 0 \qquad for -\alpha_{stall} \le \alpha_{eff} \le \alpha_{stall} \tag{2.56}$$

$$\tilde{y}'' + \left(p_1 + p_2\mu c_1\right)\tilde{y}' + \tilde{y} + p_2\mu^2 c_1\alpha + \mathrm{sgn}\left(\alpha_{eff}\right)p_2\mu^2 c_2 = 0 \qquad for\ \alpha_{stall} \le |\alpha_{eff}| \le \alpha_{sw} \tag{2.57}$$

$$\tilde{y}'' + \left(p_1 + p_2\mu c_3\right)\tilde{y}' + \tilde{y} + p_2\mu^2 c_3\alpha + \operatorname{sgn}\left(\alpha_{eff}\right)p_2\mu^2 c_4 = 0 \qquad for\ \alpha_{sw} \le |\alpha_{eff}| \le \alpha_b \tag{2.58}$$

The pitch DOF set of equations

$$\alpha'' + p_3\alpha' + \left(p_4 - \mu^2 c_o\right)\alpha - \mu c_o\tilde{y}' = 0 \qquad for -\alpha_{stall} \le \alpha_{eff} \le \alpha_{stall} \tag{2.59}$$

$$\alpha'' + p_3\alpha' + \left(p_4 - \mu^2 c_1\right)\alpha - \mu c_1\tilde{y}' + \operatorname{sgn}\left(\alpha_{eff}\right)\mu^2 c_2 = 0 \qquad for\ \alpha_{stall} \le |\alpha_{eff}| \le \alpha_{sw} \tag{2.60}$$

$$\alpha'' + p_3\alpha' + \left(p_4 - \mu^2 c_3\right)\alpha - \mu c_3\tilde{y}' + \operatorname{sgn}\left(\alpha_{eff}\right)\mu^2 c_4 = 0 \qquad for\ \alpha_{sw} \le |\alpha_{eff}| \le \alpha_b \tag{2.61}$$

Combining (2.56) with (2.59), (2.57) with (2.60) and (2.58) with (2.61), the system can be represented as three linear coupled second order differential equations as follows

$$\begin{aligned} &\tilde{y}'' + \left(p_1 + p_2\mu c_o\right)\tilde{y}' + \tilde{y} + p_2\mu^2 c_o\alpha = 0 \\ &\alpha'' + p_3\alpha' + \left(p_4 - \mu^2 c_o\right)\alpha - \mu c_o\tilde{y}' = 0 \end{aligned} \qquad for -\alpha_{stall} \le \alpha_{eff} \le \alpha_{stall} \tag{2.62}$$

$$\begin{aligned} &\tilde{y}'' + \left(p_1 + p_2\mu c_1\right)\tilde{y}' + \tilde{y} + p_2\mu^2 c_1\alpha + \operatorname{sgn}\left(\alpha_{eff}\right)p_2\mu^2 c_2 = 0 \\ &\alpha'' + p_3\alpha' + \left(p_4 - \mu^2 c_1\right)\alpha - \mu c_1\tilde{y}' + \operatorname{sgn}\left(\alpha_{eff}\right)\mu^2 c_2 = 0 \end{aligned} \qquad for\ \alpha_{stall} \le |\alpha_{eff}| \le \alpha_{sw} \tag{2.63}$$

$$\begin{aligned} &\tilde{y}'' + \left(p_1 + p_2\mu c_3\right)\tilde{y}' + \tilde{y} + p_2\mu^2 c_3\alpha + \operatorname{sgn}\left(\alpha_{eff}\right)p_2\mu^2 c_4 = 0 \\ &\alpha'' + p_3\alpha' + \left(p_4 - \mu^2 c_3\right)\alpha - \mu c_3\tilde{y}' + \operatorname{sgn}\left(\alpha_{eff}\right)\mu^2 c_4 = 0 \end{aligned} \qquad for\ \alpha_{sw} \le |\alpha_{eff}| \le \alpha_b \tag{2.64}$$

Equations (2.62) through (2.64) can be represented in state space form as shown in the following equations.

$$x_1 = \tilde{y}, x_2 = \tilde{y}', x_3 = \alpha, x_4 = \alpha' \tag{2.65}$$

The effective angle of attack equation

$$\alpha_{eff} = x_3 + \frac{1}{\mu} x_2 \tag{2.66}$$

For $-\alpha_{stall} \le \alpha_{eff} \le \alpha_{stall}$

$$\begin{bmatrix} \dot{x}_1 \\ \dot{x}_2 \\ \dot{x}_3 \\ \dot{x}_4 \end{bmatrix} = \begin{bmatrix} 0 & 1 & 0 & 0 \\ -1 & -(p_1 + p_2 \mu c_o) & -p_2 \mu^2 c_o & 0 \\ 0 & 0 & 0 & 1 \\ 0 & \mu c_o & -(p_4 - \mu^2 c_o) & -p_3 \end{bmatrix} \begin{bmatrix} x_1 \\ x_2 \\ x_3 \\ x_4 \end{bmatrix} \tag{2.67}$$

For $\alpha_{stall} \le |\alpha_{eff}| \le \alpha_{sw}$

$$\begin{bmatrix} \dot{x}_1 \\ \dot{x}_2 \\ \dot{x}_3 \\ \dot{x}_4 \end{bmatrix} = \begin{bmatrix} 0 & 1 & 0 & 0 \\ -1 & -(p_1 + p_2 \mu c_1) & -p_2 \mu c_1 & 0 \\ 0 & 0 & 0 & 1 \\ 0 & \mu c_1 & -(p_4 - \mu^2 c_1) & -p_3 \end{bmatrix} \begin{bmatrix} x_1 \\ x_2 \\ x_3 \\ x_4 \end{bmatrix} + \begin{bmatrix} 0 \\ -p_2 \mu^2 c_2 \\ 0 \\ \mu^2 \operatorname{sgn} c_2 \end{bmatrix} \operatorname{sgn}(\alpha_{eff}) \tag{2.68}$$

For $\alpha_{sw} \le |\alpha_{eff}| \le \alpha_b$

$$\begin{bmatrix} \dot{x}_1 \\ \dot{x}_2 \\ \dot{x}_3 \\ \dot{x}_4 \end{bmatrix} = \begin{bmatrix} 0 & 1 & 0 & 0 \\ -1 & -(p_1 + p_2 \mu c_3) & -p_2 \mu^2 c_3 & 0 \\ 0 & 0 & 0 & 1 \\ 0 & \mu c_3 & -(p_4 - \mu^2 c_3) & -p_3 \end{bmatrix} \begin{bmatrix} x_1 \\ x_2 \\ x_3 \\ x_4 \end{bmatrix} + \begin{bmatrix} 0 \\ -p_2 \mu^2 c_4 \\ 0 \\ \mu^2 c_4 \end{bmatrix} \operatorname{sgn}(\alpha_{eff}) \tag{2.69}$$

The state space representation of the system is convenient for running numerical simulations, checking stability and finding analytical solutions for the problem. In the next section a bilinear system is introduced based on equations (2.67) and (2.68). A dynamical analysis of the bilinear system is conducted which involves finding equilibrium points and analyzing their stability, studying the bifurcations associated with

those equilibriums and showing the bifurcation diagrams for each of the system DOF. Sets of initial conditions are defined and the dynamical behavior of the system associated with them is studied. Finally Poincaré sections are introduced to show periodic and the chaotic solutions of the system.

3. BILINEAR MODEL DYNAMIC ANALYSIS

3.1 The Bilinear Model

From the piecewise linear aerodynamic model introduced previously the bilinear model shown in Figure 4 will be analyzed. The analysis will focus on the bilinear model that describes the pre and post stall behavior of the airfoil based on the linear gain or loss of lift due to the occurrence of stall. Analyzing this simple bilinear model is a first step of defining a solution methodology to analyzing piecewise linear systems. It can be extended further for more complicated models with several linear sections as in the full piecewise linear model constructed before.

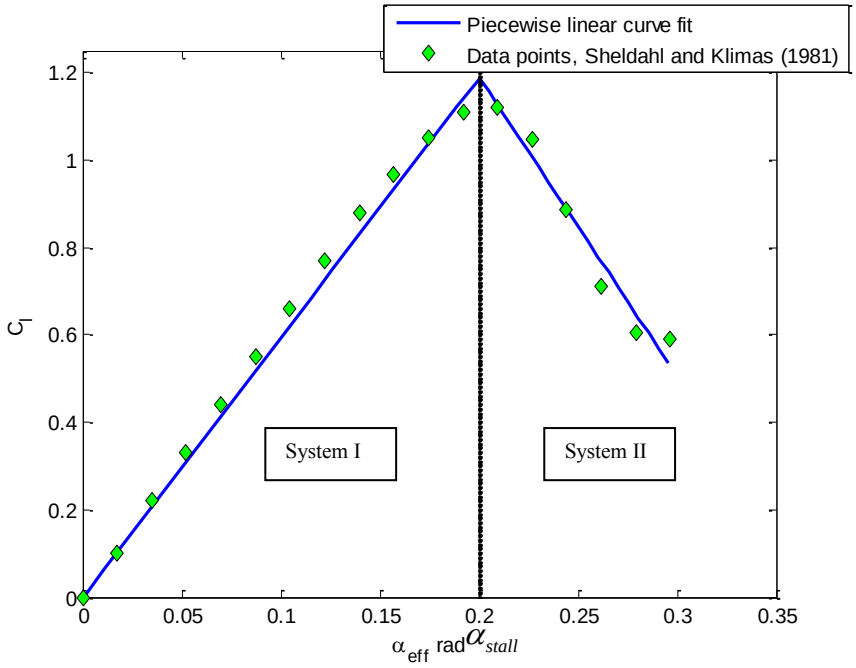

Figure 4: Bilinear aerodynamic model

The piecewise linear function of the lift coefficient can then be represented as

$$C_l(\alpha_{eff}) = \begin{cases} c_o\alpha_{eff} & -\alpha_{stall} \le \alpha_{eff} \le \alpha_{stall} \\ c_1\alpha_{eff} + \text{sgn}\left(\alpha_{eff}\right)c_2 & |\alpha_{eff}| \ge \alpha_{stall} \end{cases} \tag{3.1}$$

And the state space representation of the system will be only equations (2.67) and (2.68) as shown below

The effective angle of attack equation

$$\alpha_{eff} = x_3 + \frac{1}{\mu}x_2 \tag{3.2}$$

For $-\alpha_{stall} \le \alpha_{eff} \le \alpha_{stall}$

$$\begin{bmatrix} \dot{x}_1 \\ \dot{x}_2 \\ \dot{x}_3 \\ \dot{x}_4 \end{bmatrix} = \begin{bmatrix} 0 & 1 & 0 & 0 \\ -1 & -(p_1 + p_2\mu c_o) & -p_2\mu^2 c_o & 0 \\ 0 & 0 & 0 & 1 \\ 0 & \mu c_o & -(p_4 - \mu^2 c_o) & -p_3 \end{bmatrix} \begin{bmatrix} x_1 \\ x_2 \\ x_3 \\ x_4 \end{bmatrix} \tag{3.3}$$

For $|\alpha_{eff}| \ge \alpha_{stall}$

$$\begin{bmatrix} \dot{x}_1 \\ \dot{x}_2 \\ \dot{x}_3 \\ \dot{x}_4 \end{bmatrix} = \begin{bmatrix} 0 & 1 & 0 & 0 \\ -1 & -(p_1 + p_2\mu c_1) & -p_2\mu c_1 & 0 \\ 0 & 0 & 0 & 1 \\ 0 & \mu c_1 & -(p_4 - \mu^2 c_1) & -p_3 \end{bmatrix} \begin{bmatrix} x_1 \\ x_2 \\ x_3 \\ x_4 \end{bmatrix} + \begin{bmatrix} 0 \\ -p_2\mu^2 c_2 \\ 0 \\ \mu^2 c_2 \end{bmatrix} \text{sgn}\left(\alpha_{eff}\right) \tag{3.4}$$

In the following analysis equation (3.3) will be referred to as System I and equation (3.4) will be referred to as System II. Those are the two linear systems that construct the bilinear model that describes the system dynamics and will be used for the analysis to follow.

Equations (3.3) and (3.4) have the form

$$\dot{\mathbf{x}} = A\mathbf{x} + B\mathbf{u}(t) \tag{3.5}$$

Which has a general solution of the form

$$\mathbf{x}(t) = e^{At}\mathbf{x}(0) + \int_0^t e^{A(t-\tau)}B\mathbf{u}(\tau)d\tau \tag{3.6}$$

Equation (3.6) represents the general formula to obtain the closed form solution of a linear autonomous system. In Moler and Van Loan (2003), nineteen methods were introduced to solve for the matrix exponential e^{At} .The paper introduces 19 methods to calculate the matrix exponential and put them in 5 main categories; 1) the series methods, 2) the ordinary differential equation methods, 3) polynomial methods, 4) matrix decomposition methods and finally 5) splitting methods. Below an example from each category is presented.

1) Use Taylor series expansion to calculate the matrix exponential e^{A} as follows,

$$e^{A} = I + A + \frac{A^2}{2!} + \ldots,$$

Hence, using a computer and summing the terms in the series until a truncation point will give us a solution for the problem. The paper also highlights the importance of selecting the truncation value of the series to meet the convergence requirements for the problem.

2) Using an ODE solver to calculate the solution for the problem; $\dot{\mathbf{x}} = A\mathbf{x}$. In the paper several ODE solvers were tried and their accuracy analyzed. For the results presented here the ODE45 solver in MATLAB was used to obtain the numerical simulations results

3) From the Cayley-Hamilton theorem a solution for e^{At} can be obtained from the characteristic polynomial of A as follows,

Letting the characteristic polynomial of A to be represented as

$$f(\lambda) = \det(\lambda I - A) = \lambda^n - \sum_{k=0}^{n-1} a_k \lambda^k$$

And since according to the Cayley-Hamilton theorem that a square matrix satisfies its own characteristic polynomial then

$$f(A) = 0$$

Hence,

$$a_0 I + a_1 A + \cdots + a_{n-1} A^{n-1} = A^n$$

And for any power of A the following relation was expressed

$$A^k = \sum_{j=0}^{n-1} \beta_{kj} A^j$$

It follows that,

$$e^{At} = \sum_{k=0}^{\infty} \frac{t^k A^k}{k!} = \sum_{k=0}^{\infty} \frac{t^k}{k!} \left[\sum_{j=0}^{n-1} \beta_{kj} A^j \right]$$

where β_{kj} is presented as a recursive function that was presented in the referred paper.

4) Use similarity transformation utilizing the eigenvectors of A and obtain a diagonal matrix with the eigenvalues of A. Whereas,

$$D = V^{-1} A V = diag(\lambda_1 \cdots \lambda_n)$$

$$e^{Dt} = diag(e^{\lambda_1 t} \cdots e^{\lambda_n t})$$

Hence,

$$e^{At} = V e^{Dt} V^{-1}$$

5) The final method presented in the referred paper is the splitting method. It suggests the approximation of e^A by splitting A into $B+C$ and using the Trotter product property,

$$e^{B+C} = \lim_{m\to\infty}\left(e^{B/m}e^{C/m}\right)^m$$

Hence,

$$e^A \simeq \left(e^{B/m}e^{C/m}\right)^m$$

Based on the polynomial methods and by utilizing the characteristic polynomial of the coefficient matrix, Weaver et al. (1990) tackled the free vibrations problem for a 2 DOF system with viscous damping (two-mass system with dashpot dampers). The analysis assumes the eigenvalues of the system are neither real and positive nor complex with positive real parts. It also assumes small damping hence the solution can be represented in complex conjugate pairs with negative real parts. Based on these assumptions a closed form solution for the problem was presented. For our system of equations the coefficients of the characteristic polynomial vary as we vary the non dimensional freestream velocity μ which represents the bifurcation parameter of the bilinear system. Hence a closed form solution of the problem can't be obtained as we can't assume small damping or all positive coefficients for the characteristic polynomial.

Based on the above the equilibrium points of the system are found and analyzed. Also a linear stability analysis is conducted on each part of the bilinear system and the interaction between the two systems is examined based on the stability and the existence of equilibrium points of each system separately.

3.2 Equilibrium Points

Since our system is divided into two linear systems finding the equilibrium points of the whole system requires finding the equilibriums of each system separately and finding the conditions for those equilibrium points to exist. In this section the system equilibrium points will be expressed as well as the conditions for their existence.

System I has the general form of $\dot{\mathbf{x}} = A_I \mathbf{x}$. Hence, the equilibrium of System I is found to be

$$\mathbf{x}_{Ieq} = \begin{bmatrix} 0 & 0 & 0 & 0 \end{bmatrix}^T \tag{3.7}$$

System II has the general form of $\dot{\mathbf{x}} = A_{II} \mathbf{x} + \mathbf{b}$. Hence, the equilibrium of System II can be calculated as follows.

$$\mathbf{x}_{IIeq} = -A^{-1}\mathbf{b} \tag{3.8}$$

Finding the inverse of A and substituting in (3.8) will give us the following expression.

$$\mathbf{x}_{IIeq} = \pm \begin{bmatrix} \dfrac{p_1 p_4 - p_1 \mu^2 c_1 + p_2 \mu c_1 p_4}{-p_4 + \mu^2 c_1} & -1 & \dfrac{p_2 \mu^2 c_1 p_3}{-p_4 + \mu^2 c_1} & \dfrac{p_2 \mu^2 c_1}{-p_4 + \mu^2 c_1} \\ -1 & 0 & 0 & 0 \\ \dfrac{\mu c_1}{-p_4 + \mu^2 c_1} & 0 & \dfrac{-p_3}{-p_4 + \mu^2 c_1} & \dfrac{-1}{-p_4 + \mu^2 c_1} \\ 0 & 0 & -1 & 0 \end{bmatrix} \begin{bmatrix} 0 \\ -p_2 \mu^2 c_2 \\ 0 \\ \mu^2 c_2 \end{bmatrix} \tag{3.9}$$

The $\pm$ sign in those calculations is replacing the sgn function introduced earlier in the construction of the system dynamics. It signifies that depending on the sign of α_{eff} the equilibrium point of System II will either exist in the positive or the negative

domain of the system state space. After doing the above matrix multiplication the following expression is obtained for the equilibrium of System II.

$$\mathbf{x}_{IIeq} = \begin{bmatrix} x_{1IIeq} \\ x_{2IIeq} \\ x_{3IIeq} \\ x_{4IIeq} \end{bmatrix} = \pm \begin{bmatrix} -p_2\mu^2 c_2 + \dfrac{p_2\mu^4 c_1 c_2}{-p_4 + \mu c_1} \\ 0 \\ -\dfrac{\mu^2 c_2}{-p_4 + \mu^2 c_1} \\ 0 \end{bmatrix} \tag{3.10}$$

This equilibrium point will exit only if it lies in the domain of System II. From this we can find the value of μ at which System II equilibrium point exists in its domain.

This value can be found from substituting the expression in (3.10) into the expression of the effective angle of attack (3.2) to satisfy the condition for which System II exists in (3.4).

The condition in (3.4) can be expressed as

$$\begin{aligned} &\left|\alpha_{eff}\right| \geq \alpha_{stall} \\ &\left|x_3 + \frac{1}{\mu} x_2\right| \geq \alpha_{eff} \end{aligned} \tag{3.11}$$

Hence, for the equilibrium point of System II to exist in its domain it has to satisfy the condition in (3.11).

Substituting (3.10) into (3.11)

$$\begin{aligned} &\left|x_{3IIeq}\right| \geq \alpha_{stall} \\ &\frac{\mu^2 c_2}{-p_4 + \mu^2 c_1} \geq \alpha_{stall} \end{aligned} \tag{3.12}$$

Hence, an inequality that μ must satisfy for the equilibrium point of System II to exist can be expressed as.

$$\mu_{IIeq}^2 \geq \frac{\alpha_{stall} p_4}{(c_2 + \alpha_{stall} c_1)} \tag{3.13}$$

At $\mu_{IIeq}^2 = \frac{\alpha_{stall} p_4}{(c_2 + \alpha_{stall} c_1)}$ System II equilibrium exists exactly on the switching line that separates System I and II. This fact along with the stability analysis of the system will be used to analyze the bifurcations the system undergoes as we change the value of μ.

In the next section the stability of these equilibrium points will be examined and the values of μ at which each system loses stability will be obtained both analytically and numerically.

3.3 Linear Stability Analysis

From (3.3) and (3.4) the characteristic polynomial of each system is obtained as follows.

For System I

$$f_I(\lambda) = \lambda^4 + (p_3 + p_1 + p_2\mu c_o)\lambda^3 + (1 + p_4 - \mu^2 c_o + p_3 p_1 + p_3 p_2 \mu c_o)\lambda^2 + (p_4 p_1 + p_4 p_2 \mu c_o - \mu^2 c_o p_1 + p_3)\lambda + p_4 - \mu^2 c_o \tag{3.14}$$

For System II

$$f_{II}(\lambda) = \lambda^4 + (p_3 + p_1 + p_2\mu c_1)\lambda^3 + (1 + p_4 - \mu^2 c_1 + p_3 p_1 + p_3 p_2 \mu c_1)\lambda^2 + (p_4 p_1 + p_4 p_2 \mu c_1 - \mu^2 c_1 p_1 + p_3)\lambda + p_4 - \mu^2 c_1 \tag{3.15}$$

The above polynomials can be expressed as

$$a_0\lambda^4 + a_1\lambda^3 + a_2\lambda^2 + a_3\lambda + a_4 = 0 \tag{3.16}$$

where, for System I

$$\begin{aligned} a_0 &= 1 \\ a_1 &= p_3 + p_1 + p_2\mu c_o \\ a_2 &= 1 + p_4 - \mu^2 c_o + p_3 p_1 + p_3 p_2 \mu c_o \\ a_3 &= p_4 p_1 + p_4 p_2 \mu c_o - \mu^2 c_o p_1 + p_3 \\ a_4 &= p_4 - \mu^2 c_o \end{aligned} \tag{3.17}$$

and for System II

$$\begin{aligned} a_0 &= 1 \\ a_1 &= p_3 + p_1 + p_2\mu c_1 \\ a_2 &= 1 + p_4 - \mu^2 c_1 + p_3 p_1 + p_3 p_2 \mu c_1 \\ a_3 &= p_4 p_1 + p_4 p_2 \mu c_1 - \mu^2 c_1 p_1 + p_3 \\ a_4 &= p_4 - \mu^2 c_1 \end{aligned} \tag{3.18}$$

Applying Routh-Hurwitz stability theorem to the above equations we can determine when the system will lose stability (roots crossing to the right half plane). The necessary and sufficient condition for the polynomial in (3.16) to have all roots in the left half plane is

$$\Delta_1 > 0, \Delta_2 > 0, \Delta_3 > 0, \Delta_4 > 0 \tag{3.19}$$

where,

$$\begin{aligned}
\Delta_1 &= a_1 \\
\Delta_2 &= \begin{vmatrix} a_1 & a_3 \\ a_o & a_2 \end{vmatrix} \\
\Delta_3 &= \begin{vmatrix} a_1 & a_3 & 0 \\ a_0 & a_2 & a_4 \\ 0 & a_1 & a_3 \end{vmatrix} \\
\Delta_4 &= \begin{vmatrix} a_1 & a_3 & 0 & 0 \\ a_0 & a_2 & a_4 & 0 \\ 0 & a_1 & a_3 & 0 \\ 0 & a_0 & a_2 & a_4 \end{vmatrix}
\end{aligned} \tag{3.20}$$

The above determinants are called the Hurwitz determinants. Applying the Routh-Hurwitz theorem to find the closed form of the minimum value μ that will cause the system to be unstable is very difficult as the above Hurwitz determinants will produce highly nonlinear inequalities in μ. Those inequalities can be solved numerically and are presented in the Appendix.

To avoid solving the nonlinear inequalities generated from the Hurwitz determinants presented above another check was made by using the Liénard – Chipart criterion, see Gantmacher (1959). The Criterion is actually a supplement to the Routh-

Hurwitz theorem as it draws the connection between the sign of the coefficients of the polynomial and the Hurwitz determinants in (3.20).

According to this stability criterion for the fourth order polynomial in (3.16) a necessary and sufficient condition to have all the roots in the left half plane is

$$\begin{aligned} &a_1 > 0, a_2 > 0, a_3 > 0, a_4 > 0 \\ &and \\ &\Delta_3 > 0 \end{aligned} \tag{3.21}$$

For System I the inequality that will yield the minimum value of μ for which the system will lose stability is

$$p_4 - \mu_I^2 c_o \geq 0 \tag{3.22}$$

$$\mu_I^2 \leq \frac{p_4}{c_o} \tag{3.23}$$

This expression of μ came from substituting $\lambda = 0$ in System I characteristic polynomial and checking for the minimum value of μ at which System I will lose stability applying the Liénard – Chipart stability criterion.

For System II stability the value of μ at which the system loses stability can be obtained from (3.15) by substituting

$$\begin{aligned} \lambda_{1,2} &= i\omega_1 \\ \lambda_{3,4} &= -r \pm i\omega_2 \end{aligned} \tag{3.24}$$

where, $\lambda_{1,2}$ represents a pair of complex conjugate eigenvalues crossing the imaginary axis at the instability point of System II and $\lambda_{3,4}$ represents the other two pair with a negative real part.

Applying (3.24) as roots for a fourth order polynomial will yield the following form of System II characteristic polynomial

$$f(\lambda) = \lambda^4 + 2r\lambda^3 + \left(\omega_2^2 + \omega_1^2 + r^2\right)\lambda^2 + 2r\omega_1^2\lambda + \left(\omega_1^2 r^2 + \omega_1^2\omega_2^2\right) \tag{3.25}$$

Equating the coefficients of (3.25) and (3.15) will yield the following four equations,

$$\begin{aligned} 2r &= p_3 + p_1 + p_2 c_1 \mu \\ \omega_1^2 + \omega_2^2 + r^2 &= 1 + p_4 + p_3 p_1 - c_1\mu^2 + p_3 p_2 c_1 \mu \\ 2r\omega_1^2 &= p_4 p_1 + p_3 - p_1 c_1 \mu^2 + p_4 p_2 c_1 \mu \\ \omega_1^2 r^2 + \omega_1^2\omega_2^2 &= p_4 - \mu^2 c_1 \end{aligned} \tag{3.26}$$

from (3.26) an expression for μ can be extracted from

$$\frac{p_4 p_1 + p_3 - p_1 c_1 \mu^2 + p_4 p_2 c_1 \mu}{p_3 + p_1 + p_2 c_1 \mu}\left(\begin{array}{l} 1 + p_4 + p_3 p_1 - c_1\mu^2 + p_3 p_2 c_1 \mu \\ -\dfrac{p_4 p_1 + p_3 - p_1 c_1 \mu^2 + p_4 p_2 c_1 \mu}{p_3 + p_1 + p_2 c_1 \mu} \end{array}\right) = p_4 - \mu^2 c_1 \tag{3.27}$$

Solving (3.27) for μ gives the value of μ at which System II loses stability, $\mu = 0.3043$

Another method utilized to obtain the minimum value of μ at which System II loses stability was from solving the fifth order polynomial generated from the Hurwitz determinant Δ_3.

Hence, for System I the value of μ at which the system loses stability is $\mu_I = 0.2152$ and for System II $\mu_{II} = 0.3034$.

Figure 5 shows the eigenvalues behavior of System I as the value of μ is varied.

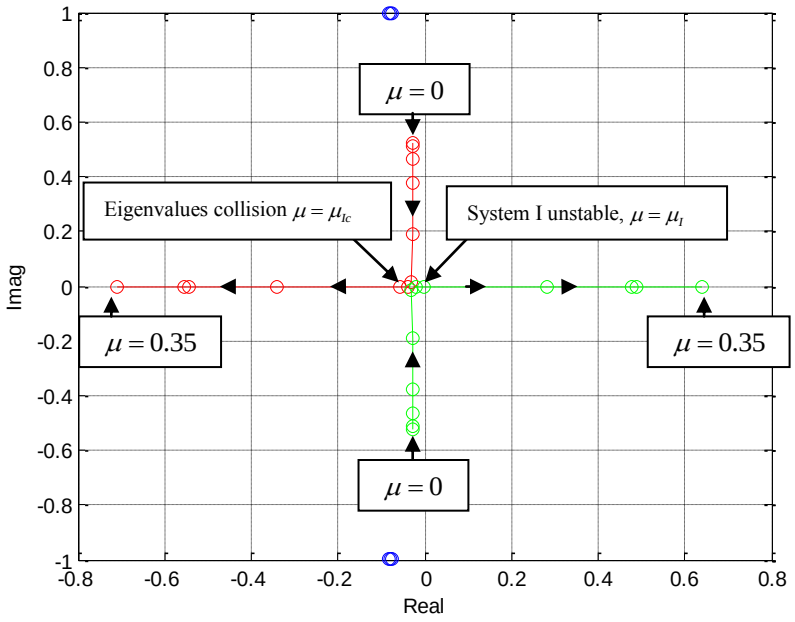

Figure 5: Eigenvalues behavior of System I

An interesting phenomenon observed in the eigenvalues behavior of System I is that a certain value of μ, $\mu = \mu_{Ic}$, a pair of complex conjugate eigenvalues collide with each other yielding two real eigenvalues. One of the real eigenvalues moves towards the imaginary axis and crosses to the right half plane which results in the instability of System I equilibrium point. In Seiranyan (1994) the collision of eigenvalues in linear oscillatory system was examined and analyzed. This phenomenon was found to explain some interesting behavior of linear systems such as the shift of the normal mode of vibrations and the loss of stability for systems with weak damping. In the case presented here and due to this collision between a pair of System I eigenvalues, the solution shifted from oscillatory to exponential as it converges towards System I equilibrium point. Figure 6 shows the time evolution of the pitch DOF as the system converges to its

equilibrium point. As it's clearly shown the system starts off with an oscillatory behavior and then exponential decay occurs till it converges to the equilibrium point. The phase portrait in Figure 7 also shows this jump between the oscillatory and exponential behavior for the pitch DOF. This jump between the two different responses is due to the collision of a pair of System I eigenvalues as it results in a change in the mode of vibration of the system.

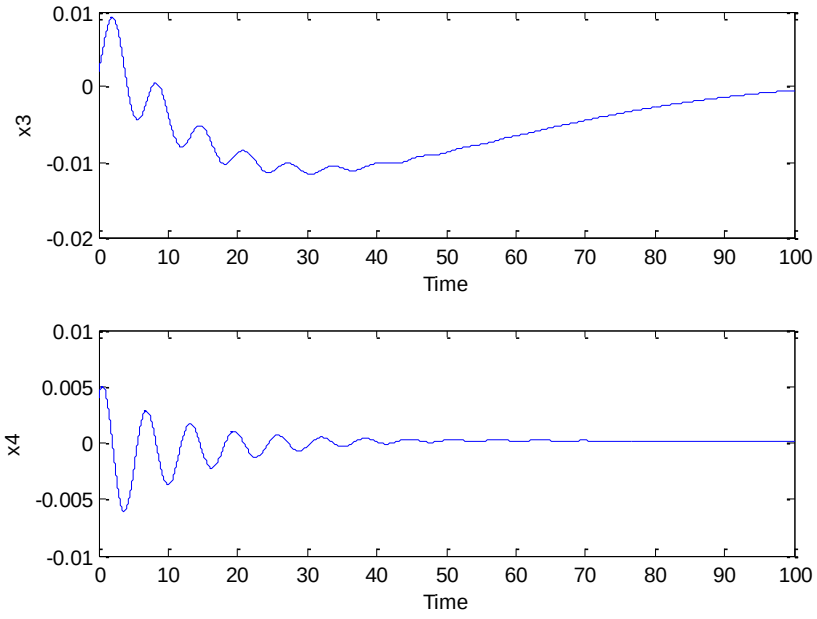

Figure 6: Time evolution, pitch DOF at $\mu = \mu_{Ic}$

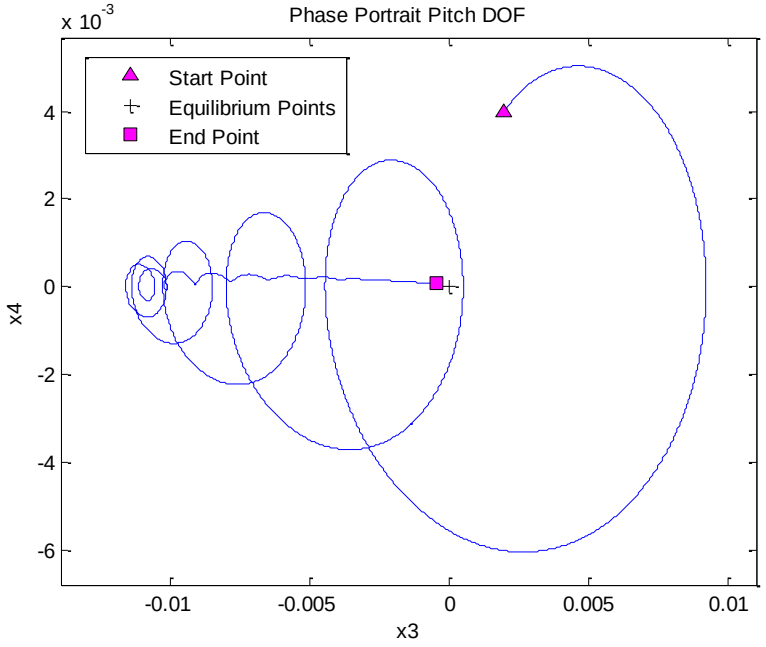

Figure 7: Phase portrait pitch DOF at $\mu = \mu_{Ic}$

To obtain the value of μ at which this phenomenon takes place the eigenvalues of System I will have the following form

$$\begin{aligned} \lambda_{1,2} &= -r_1, -r_1 \\ \lambda_{3,4} &= r_2 \pm i\omega \end{aligned} \tag{3.28}$$

Applying (3.28) as roots for a fourth order polynomial will yield the following form for System I characteristic polynomial

$$f(\lambda) = \lambda^4 + \left(2r_1 + 2r_2\right)\lambda^3 + \begin{pmatrix} 4r_1 r_2 + r_2^2 \\ +\omega^2 + r_1^2 \end{pmatrix}\lambda^2 + \begin{pmatrix} 2r_1^2 r_2^2 + \\ 2r_1\omega^2 + 2r_1^2 r_2 \end{pmatrix}\lambda + \left(r_1^2 r_2^2 + r_1^2\omega^2\right) \tag{3.29}$$

Equating the coefficients of (3.29) and (3.14) will yield the following set of nonlinear algebraic equations

$$
\begin{aligned}
&2r_1 + 2r_2 = p_3 + p_1 + p_2\mu c_o \\
&4r_1r_2 + r_2^2 + \omega^2 + r_1^2 = 1 + p_4 - \mu^2 c_o + p_3p_1 + p_3p_2\mu c_o \\
&2r_1^2r_2^2 + 2r_1\omega^2 + 2r_1^2 r = p_4p_1 + p_4p_2\mu c_o - \mu^2 c_o p_1 + p_3 \\
&r_1^2r_2^2 + r_1^2\omega^2 = p_4 - \mu^2 c_o
\end{aligned}
\tag{3.30}
$$

The equations presented in (3.30) are solved numerically to obtain the value of μ at which the eigenvalues collision occurs, $\mu_{Ic} = 0.2148$.

As the value of μ is increased one of the real eigenvalues of System I moves towards the imaginary axis till it crosses to the right half plane at $\mu = \mu_I$ causing System I to be unstable.

Similar to System I, Figure 8 shows the eigenvalues behavior of System II as the value of μ is changed. At $\mu = \mu_{II}$ a pair of complex conjugate eigenvalues of System II cross to the right half plane. As μ is increased beyond μ_{II} System I and II are unstable.

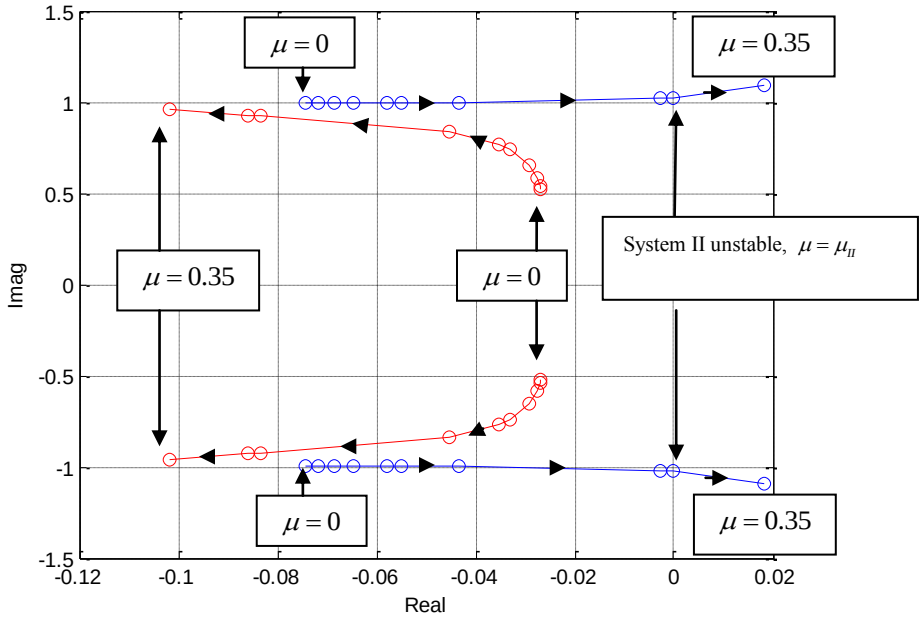

Figure 8: Eigenvalues behavior of System II

3.4 System Bifurcations

The stability analysis conducted in the previous section will lead to the development of the bifurcation diagram of the bilinear system.

Based on the eigenvalues analysis conducted in the previous section, System I starts with a stable equilibrium at $\mathbf{x}_{Ieq} = \begin{bmatrix} 0 & 0 & 0 & 0 \end{bmatrix}^T$. This stable equilibrium remains stable until μ reaches the critical value of System I μ_I at which System I loses stability.

The value at which System I loses its stability is obtained in (3.23) this expression when compared with the condition of the existence of System II equilibrium expressed in (3.13) will lead to a type of bifurcation associated with piecewise smooth Systems called border collision bifurcation.

Border collision bifurcation occurs when an equilibrium point hits the border or the switching surface of a piecewise smooth dynamical system. As a result this equilibrium loses stability and may give rise to another stable point, a stable periodic orbit or even chaos. This type of bifurcations is analyzed in di Bernardo et al. (2008) and Zhusubaliyev and Mosekilde (2003) as a characteristic of piecewise smooth dynamical systems and many examples were presented to show the different system behaviors that can arise from this type of bifurcations.

In the case of our system the following analysis is conducted to prove that System I loses stability exactly when System II equilibrium exists at the border or the switching surface that separates the two pieces of the bilinear model.

As mentioned earlier from the stability analysis of System I, the stability is lost at the following value of μ.

$$\mu_I^2 = \frac{p_4}{c_o} \tag{3.31}$$

Also System II equilibrium exists in its domain at

$$\mu_{IIeq}^2 = \frac{p_4 \alpha_{stall}}{\left(c_1 \alpha_{stall} + c_2\right)} \tag{3.32}$$

Multiplying both the numerator and denominator of (3.31) by α_{stall}, we will have

$$\mu_I^2 = \frac{p_4 \alpha_{stall}}{c_o \alpha_{stall}} \tag{3.33}$$

Since at $\left|\alpha_{eff}\right| = \alpha_{stall}$, we have $C_{lI} = C_{lII}$,from the construction of the piecewise linear function of the lift coefficient presented in Section 2, then

$$c_o \alpha_{stall} = c_1 \alpha_{stall} + c_2 \tag{3.34}$$

From (3.34) it is clear that System I loses stability exactly at the same value of μ at which System II stable equilibrium lies in its domains, in other words exists.

Hence,

$$\mu_I = \mu_{IIeq} \tag{3.35}$$

The relationship proved in (3.35) is a case of border collision bifurcation as System II equilibrium lies on the border or the switching surface of the bilinear system at the same instant System I equilibrium becomes unstable.

Based on these results bifurcation diagrams for both the plunge and pitch DOF are developed using MATCONT, a numerical continuation toolbox developed for MATLAB, see Dhooge et al. (2003).

The analysis of the bilinear model has a limitation defined by the range of the data points the model was based on. This limitation also has a physical meaning that is if the linear model was extended beyond a certain value of the angle of attack and due to the negative slope of the line representing System II aerodynamic forces the lift will acquire a negative value. The value of α at which the lift becomes zero will define the physical limitation of the model.

$$\alpha_p = 0.37\, rad \tag{3.36}$$

Hence the bifurcation analysis presented in this section will be limited to values of α below this value to be within the physically valid region of the model.

Figure 9 shows the bifurcation diagram for the plunge DOF.

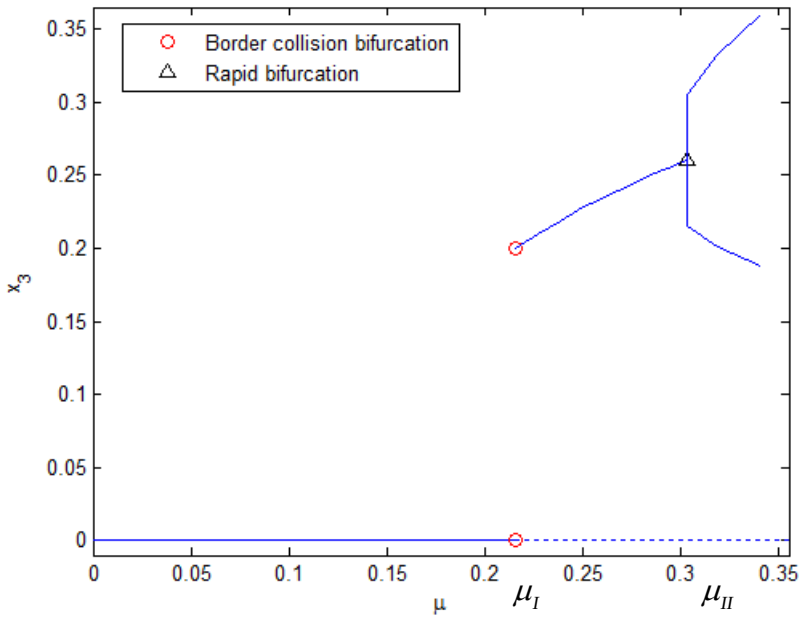

Figure 9: Bifurcation diagram, pitch DOF

As shown System I equilibrium, $\mathbf{x}_{Ieq} = \begin{bmatrix} 0 & 0 & 0 & 0 \end{bmatrix}^T$, is stable until μ reaches the critical value of System I, μ_I, at which System I equilibrium loses stability. At the same instant System II equilibrium exists on the border between the two systems and becomes stable in a border collision bifurcation. System II equilibrium is stable until the value of μ_{II} at which a pair of complex conjugate eigenvalues cross the imaginary axis causing the onset of a stable limit cycle in a rapid bifurcation. A rapid bifurcation in piecewise dynamical systems is analogous to a degenerate Hopf bifurcation in continuous systems. The degenerate Hopf bifurcation occurs when at the bifurcation value there exists no isolated limit cycle. Instead there exists a set of closed orbits surrounding the point at which the bifurcation occurs, Figure 10. In that case, at the bifurcation value the fixed point becomes a nonlinear center, Strogatz (2000). The rapid bifurcation is discussed in Kriegsmann (1987) and Freire et al. (1999). One of the differences between a rapid and a Hopf bifurcation is in the amplitude propagation of the limit cycle as it does not follow the square root scaling rule where the amplitude is not proportional to $O(\mu^{\frac{1}{2}})$. Figure 11shows a 3D plot for the limit cycle propagation for the plunge DOF starting at the instant of the rapid bifurcation.

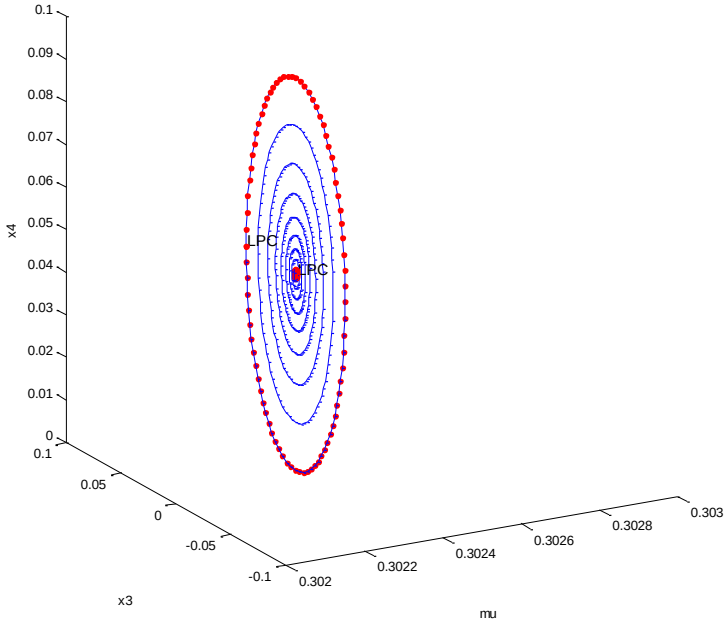

Figure 10: Degenerate Hopf bifurcation, pitch DOF

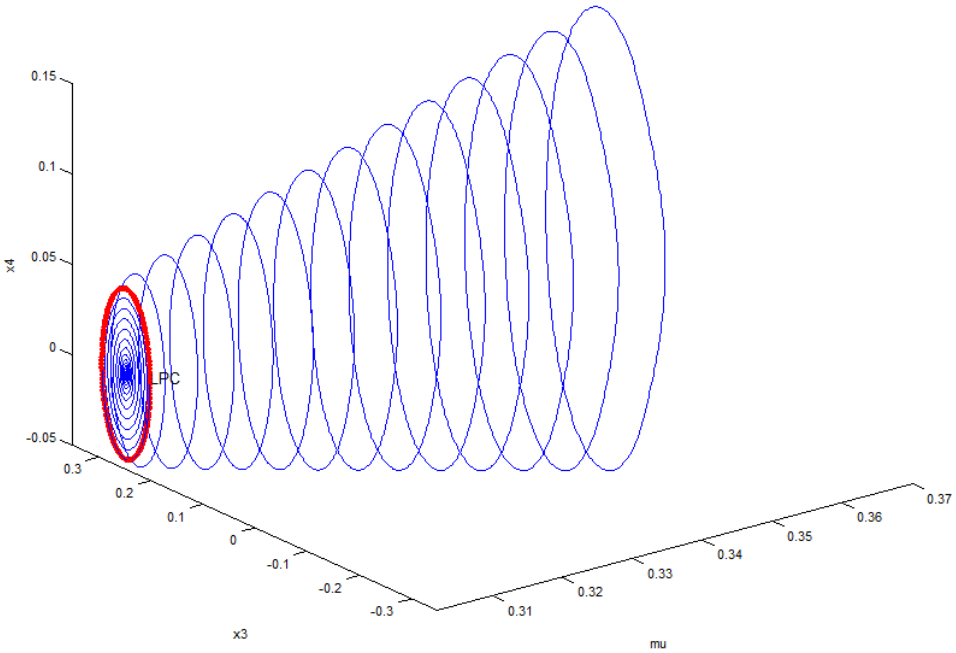

Figure 11: LCO propagation, pitch DOF

Similar to the pitch DOF, A similar bifurcation diagram is developed for the plunge DOF, Figure 12.

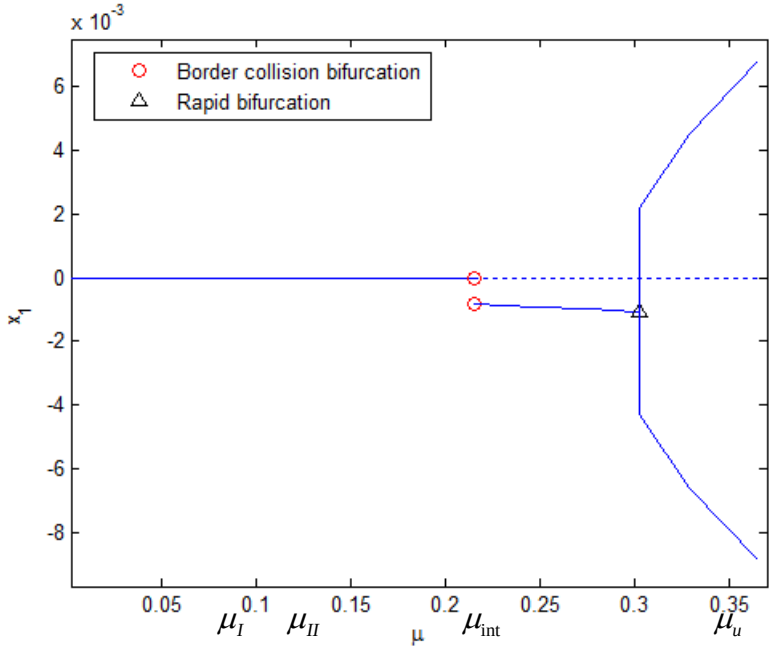

Figure 12: Bifurcation diagram, plunge DOF

The degenerate Hopf bifurcation and the limit cycle propagation for the plunge DOF are shown in Figure 13 and Figure 14 respectively.

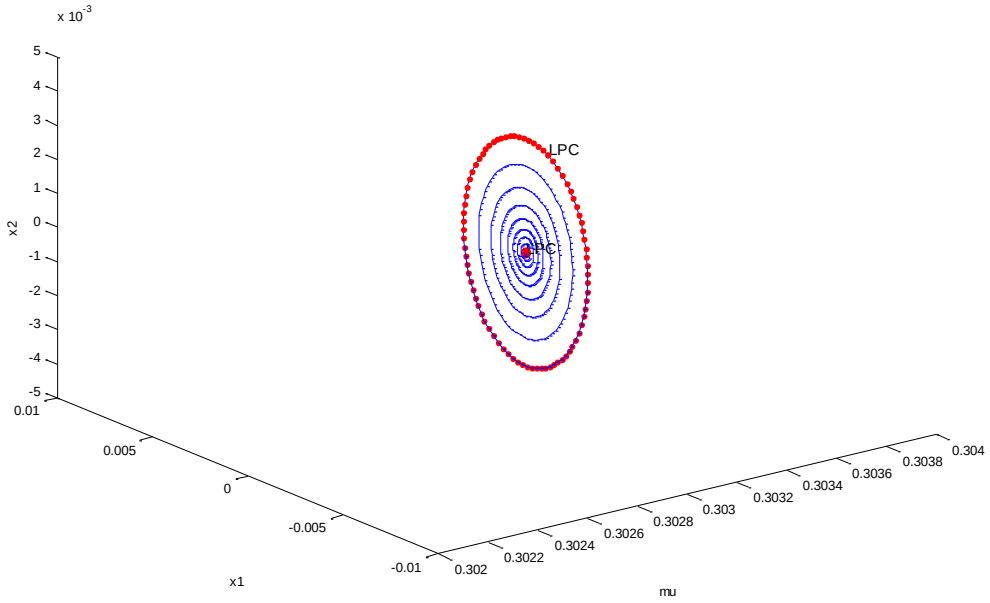

Figure 13: Degenerate Hopf bifurcation, plunge DOF

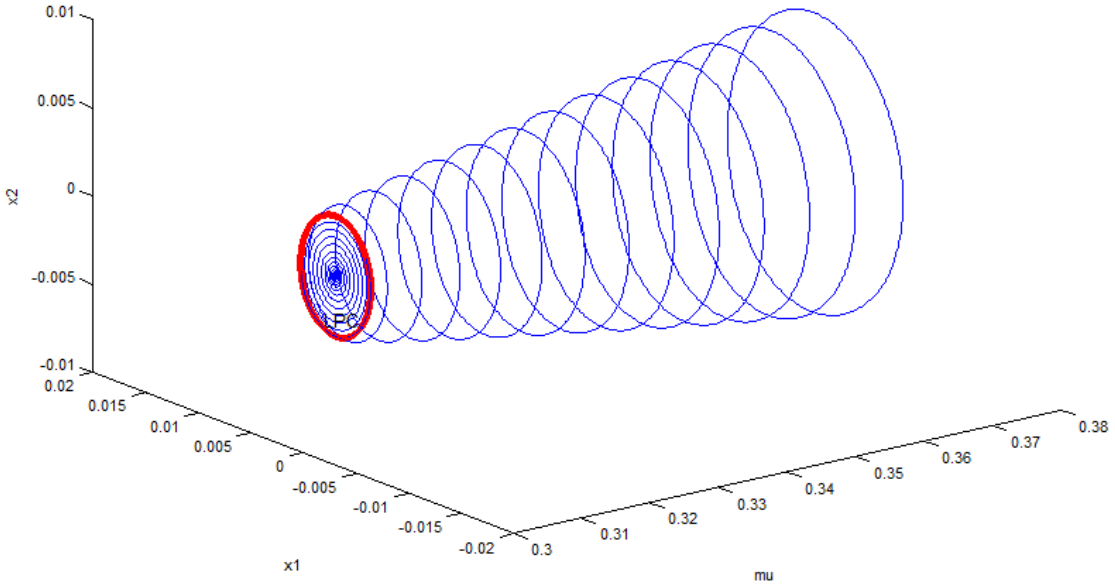

Figure 14: LCO propagation, plunge DOF

The bifurcation diagrams shown are the results of the analysis using the continuation software MATCONT. The results have also been verified by using numerical simulation for different values of μ to make sure that there exists no other dynamical behavior than the behavior presented. In the physical validity region of the model and in regions where linear stability holds the system will either converge to System I or System II equilibrium points depending on the value of μ. At the rapid bifurcation both System I and System II have eigenvalues with positive real parts. In this region and to make sure that the bifurcation diagrams are capturing all the dynamics of the system, combinations of the values of μ with various initial conditions were tried to make sure that the limit cycle is the only response of the system. It was found that the bifurcation diagrams of the bilinear system generated by MATCONT captured all the system dynamics within the physically valid region of the bilinear model.

To further understand the global behavior of our system and to establish a method of analyzing and finding other system responses than the ones detected by MATCONT or numerical simulations sets of initial conditions will be introduced and analyzed in later sections to verify and understand both the local and global behaviors of the bilinear system.

In the next section numerical simulations will be shown to verify the system behavior within the various regions of the bifurcation diagrams.

3.5 Numerical Simulation Results

In this section numerical simulations are done to verify the analysis presented in the previous section. The simulations were done using the ODE45 function in MATLAB and by utilizing the event locator option in the ODE solver to calculate the instances at which the switching between System I and System II takes place.

Based on the bifurcation diagrams of the system values of μ will be along with initial conditions to represent the behavior of the system at a certain region of the bifurcation diagrams.

This section will also include numerical simulation results of the continuous system presented before and a comparison will be made between the results from the bilinear model and the results from the continuous system.

3.5.1 Results for the bilinear model

The first set of plots will show the system behavior at a value of μ where System I equilibrium is stable. The time evolution and the phase portrait of the plunge DOF is shown in Figure 15 and Figure 16 respectively.

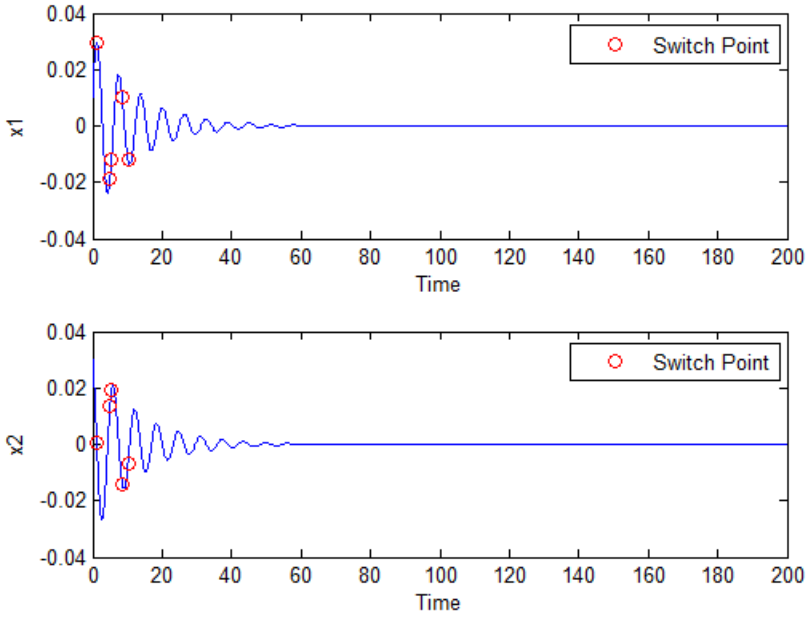

Figure 15: Time evolution plunge DOF $\mu < \mu_I, (\mu = 0.15)$

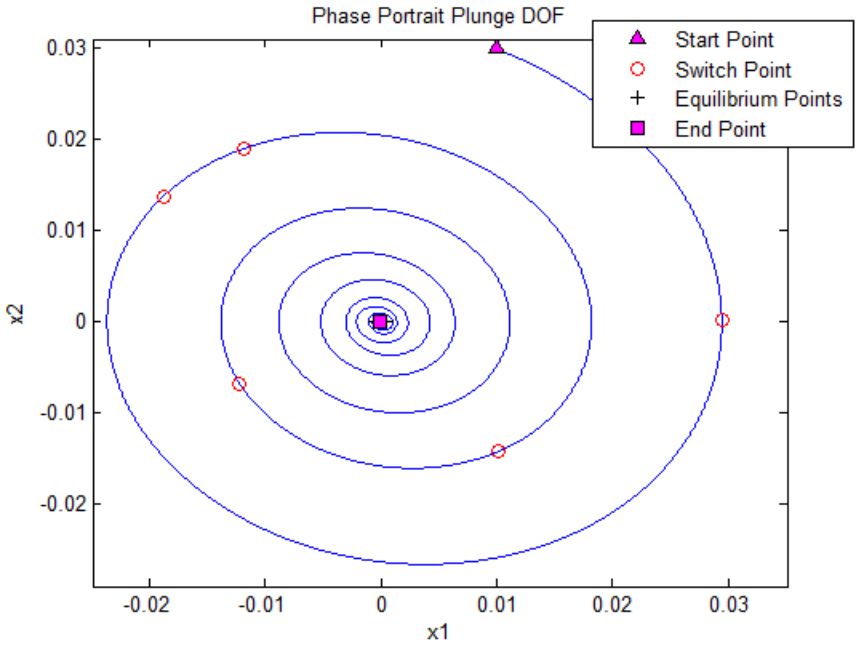

Figure 16: Phase portrait plunge DOF $\mu < \mu_I, (\mu = 0.15)$

The time evolution and the phase portrait of the pitch DOF are shown in Figure 17 and Figure 18 respectively.

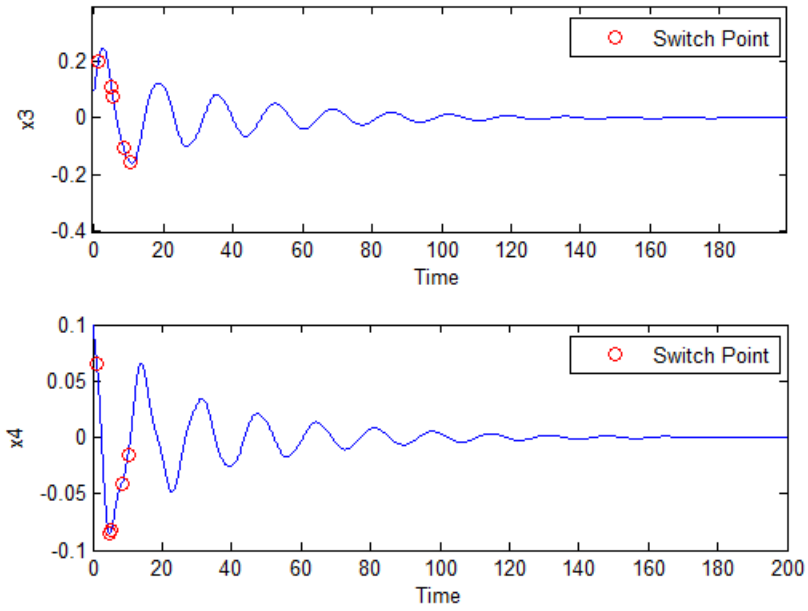

Figure 17: Time evolution pitch DOF $\mu < \mu_1, (\mu = 0.15)$

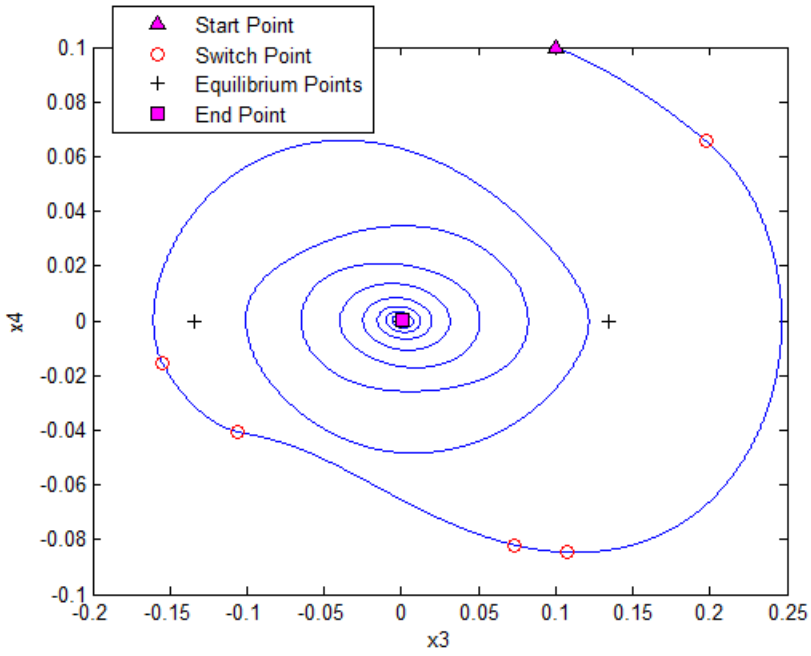

Figure 18: Phase portrait pitch DOF $\mu < \mu_I, (\mu = 0.15)$

Figure 19 shows a projection of the phase portrait in the x2-x3 plane. This projection is of interest as it is the plane where the switch condition, defined by the straight line equation, $x_2 = \mu(\alpha_{stall} - x_3)$, between System I and II exits.

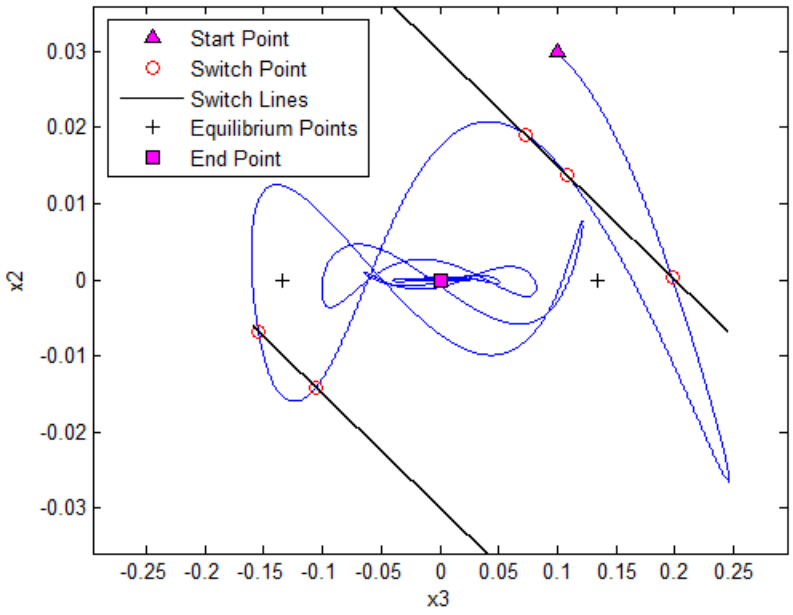

Figure 19: x3-x2 plane phase portrait projection $\mu < \mu_I, (\mu = 0.15)$

As it is shown in the plots the system converges to System I stable equilibrium. Also in Figure 19 the points at which the switch between System I and System II takes place are highlighted. Those points on the switch line are of interest as they will be used as the basis for the construction of the Poincaré sections of the bilinear system. Figure 20 shows the lift versus the angle of attack generated from the numerical simulations results. This plot is shown as a double check that the simulations did not exceed the physical limit of the bilinear aerodynamic model.

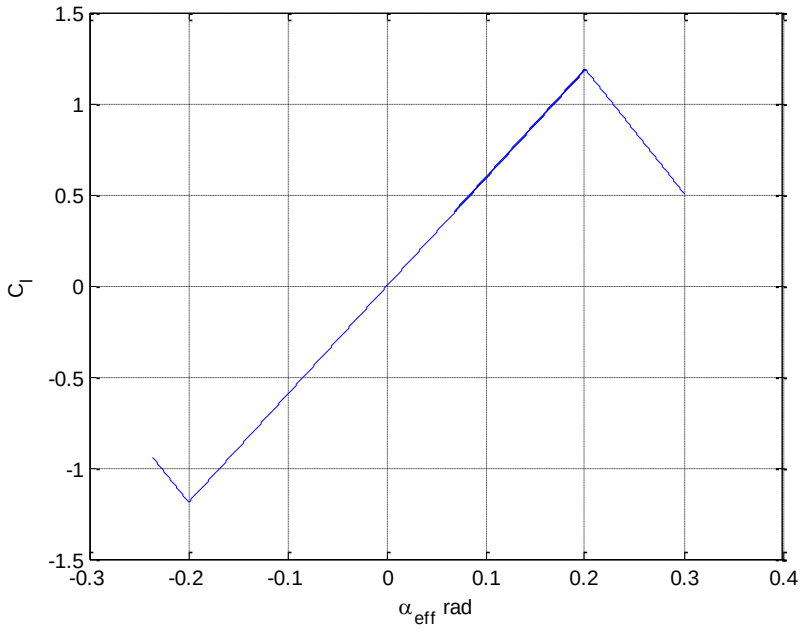

Figure 20: Lift vs. α_{eff} generated from simulations $\mu = 0.15$

The next group of plots will show the behavior of the system at a value of μ at which System II equilibrium exists and is stable while System I equilibrium loses stability.

The time evolution and the phase portrait of the plunge DOF are shown in Figure 21 and Figure 22 respectively.

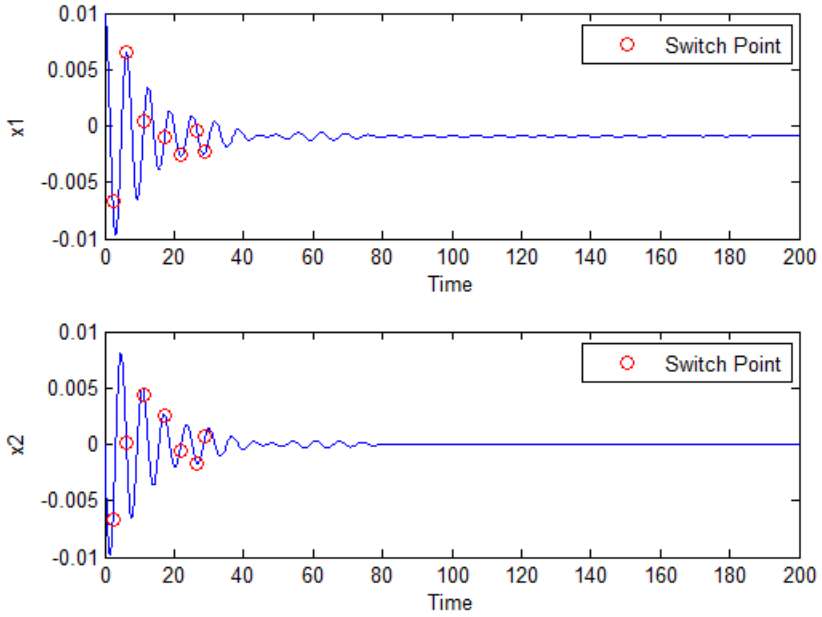

Figure 21: Time evolution plunge DOF $\mu_I < \mu < \mu_{II}, (\mu = 0.25)$

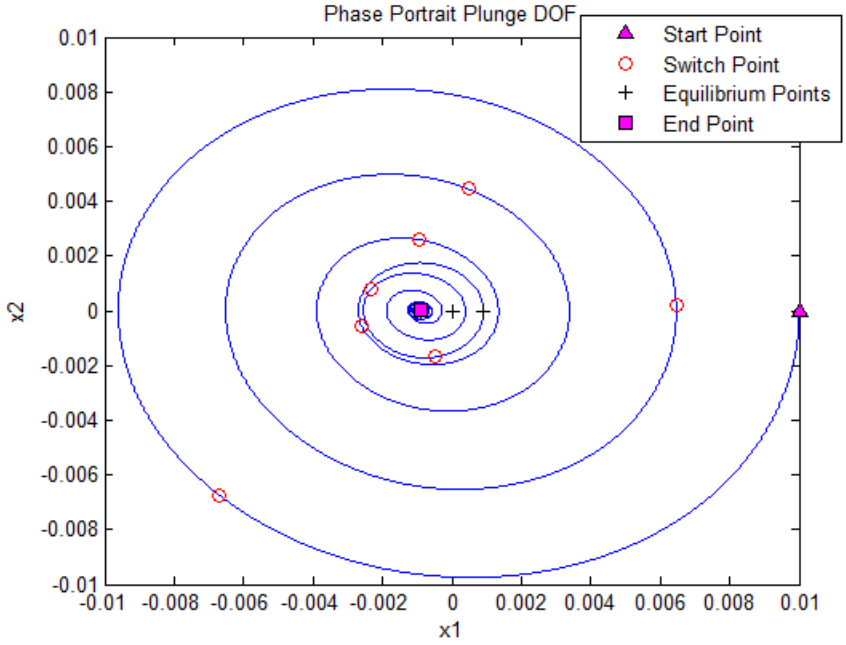

Figure 22: Phase portrait plunge DOF $\mu_I < \mu < \mu_{II}, (\mu = 0.25)$

The time evolution and the phase portrait of the pitch DOF are shown in Figure 23 and Figure 24 respectively.

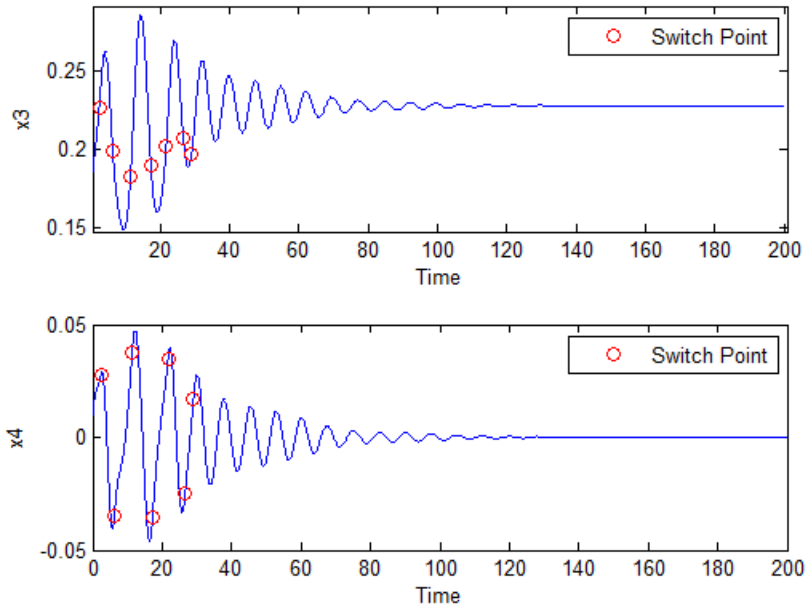

Figure 23: Time evolution pitch DOF $\mu_I < \mu < \mu_{II}, (\mu = 0.25)$

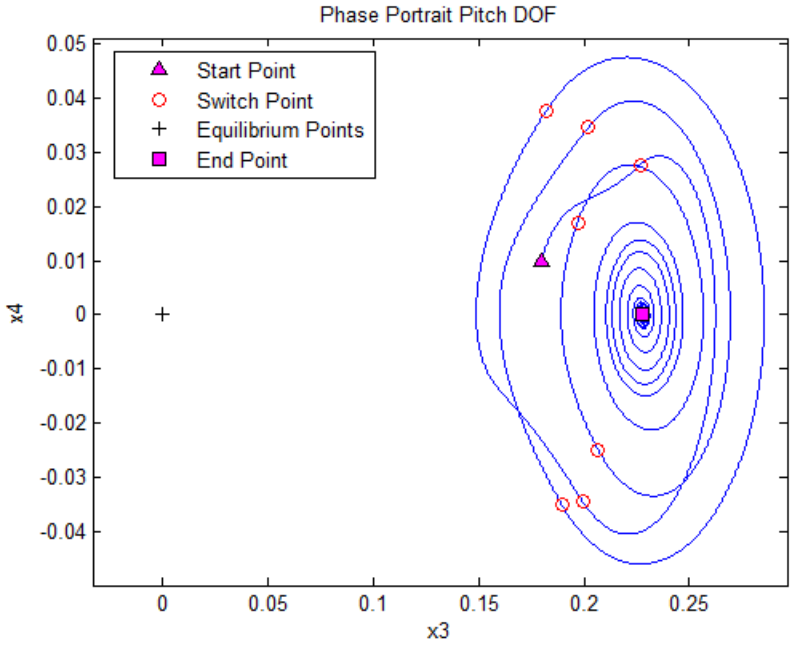

Figure 24: Phase portrait pitch DOF $\mu_I < \mu < \mu_{II}, (\mu = 0.25)$

At this value of μ System II equilibrium point is stable and hence the trajectories converge to that point. Figure 25 shows the x3-x2 phase projection which shows the convergence of the trajectories to System II stable equilibrium which at that value of μ lies in System II domain. Figure 26 the lift versus the angle of attack curve is extracted from the simulation results to prove that the results generated are within the physical limitation of the proposed aerodynamic bilinear model.

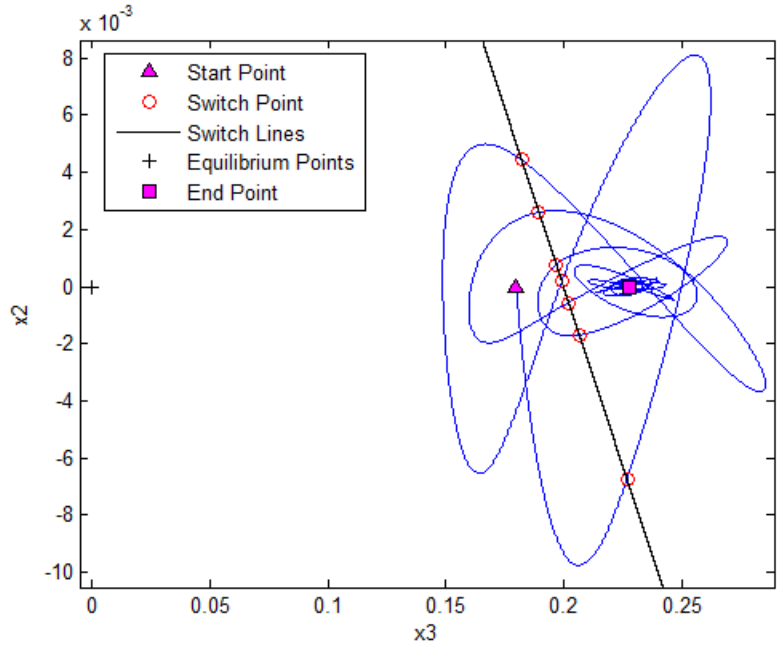

Figure 25: x3-x2 plane phase portrait projection $\mu_I < \mu < \mu_{II}$,, $(\mu = 0.25)$

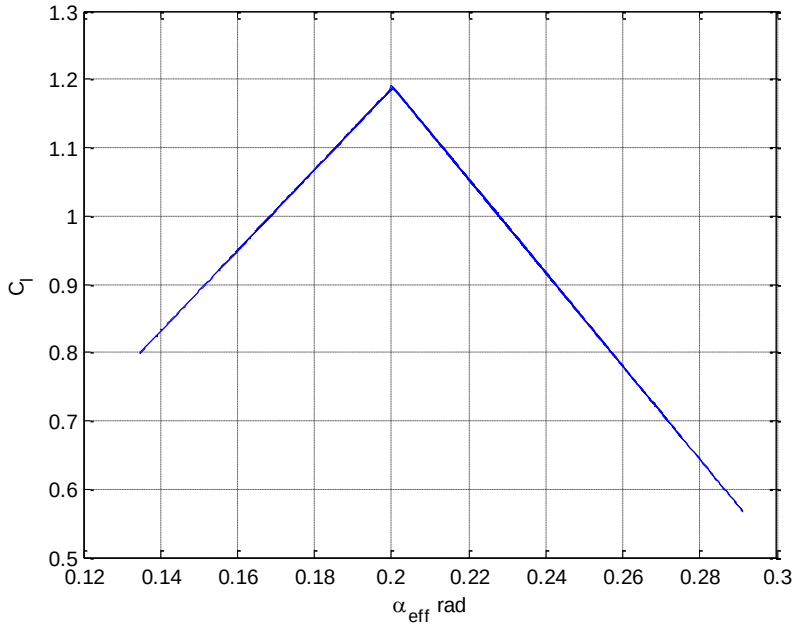

Figure 26: Lift vs. α_{eff} **generated from simulations** $\mu = 0.25$

As the value of μ is increased the system converges to the stable limit cycle that resulted from the rapid bifurcation occurring at the value of μ where a complex conjugate pair of System II eigenvalues cross to the right half of the complex plane simultaneously. The periodic behavior of the plunge DOF is illustrated in Figure 27 and Figure 28.

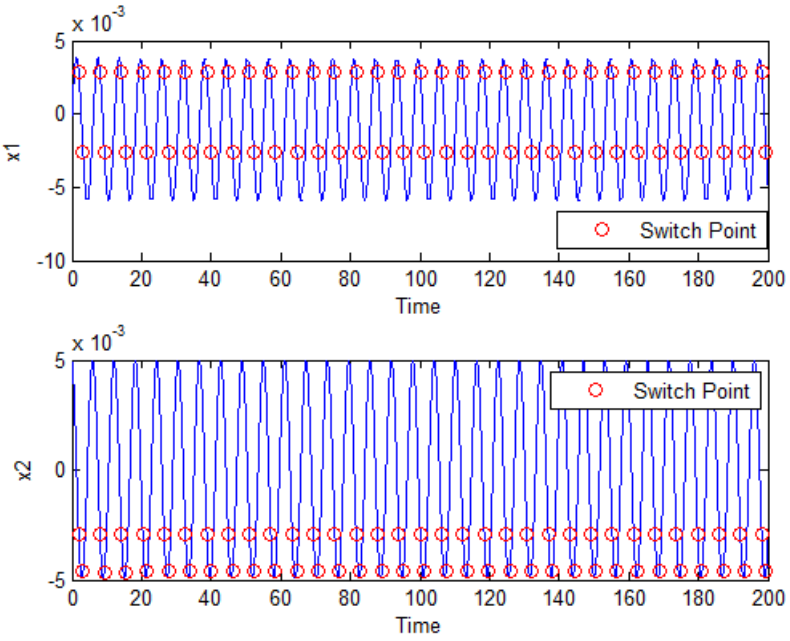

Figure 27: Time evolution plunge DOF $\mu > \mu_{II}, (\mu = 0.32)$

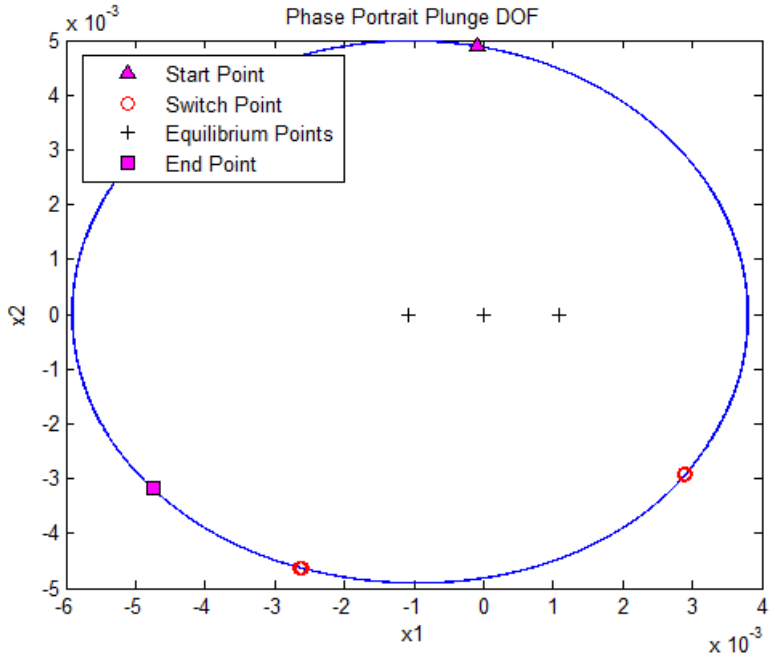

Figure 28: Phase portrait plunge DOF $\mu > \mu_{II}, (\mu = 0.32)$

Similarly, the same behavior is observed for the pitch DOF as shown in Figure 29 and Figure 30.

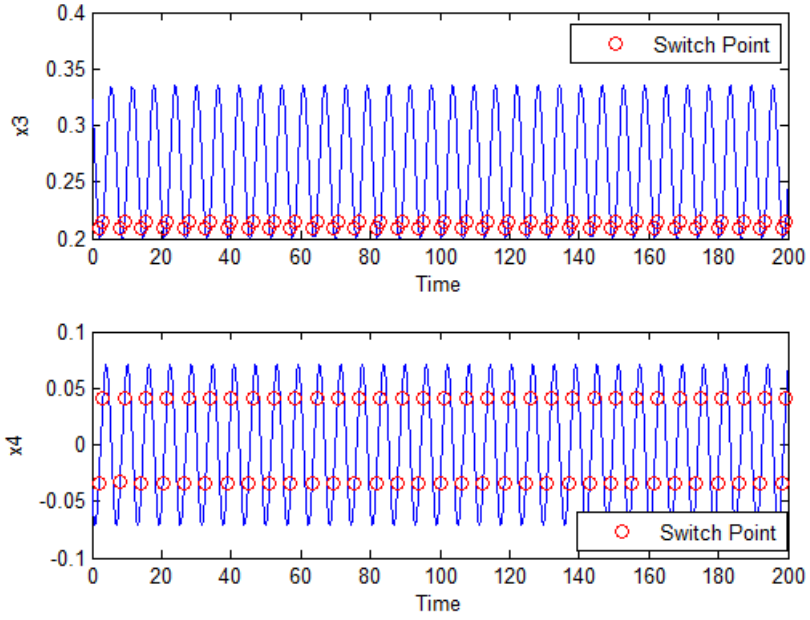

Figure 29: Time evolution pitch DOF $\mu > \mu_{II}, (\mu = 0.32)$

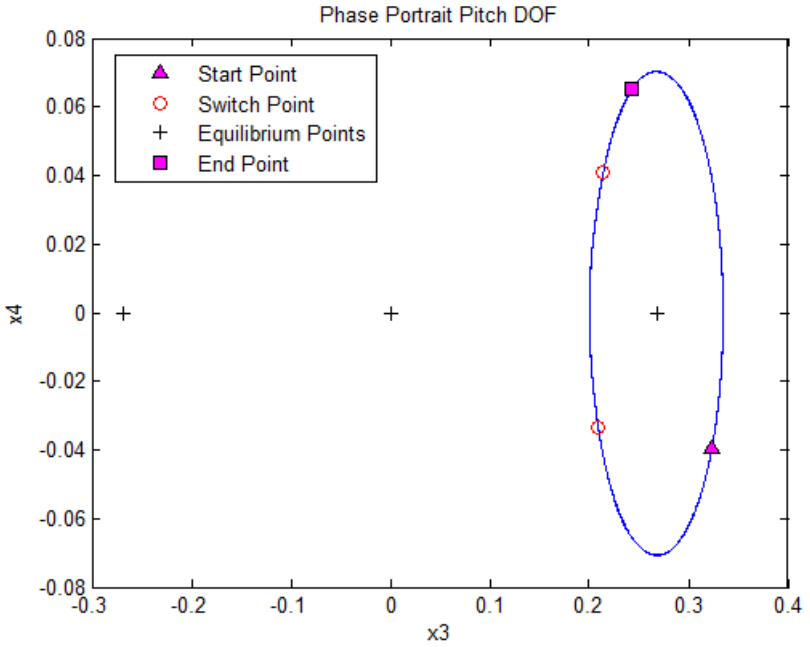

Figure 30: Phase portrait pitch DOF $\mu > \mu_{II}, (\mu = 0.32)$

In the x3-x2 plane the projection of the limit cycle is shown in Figure 31.

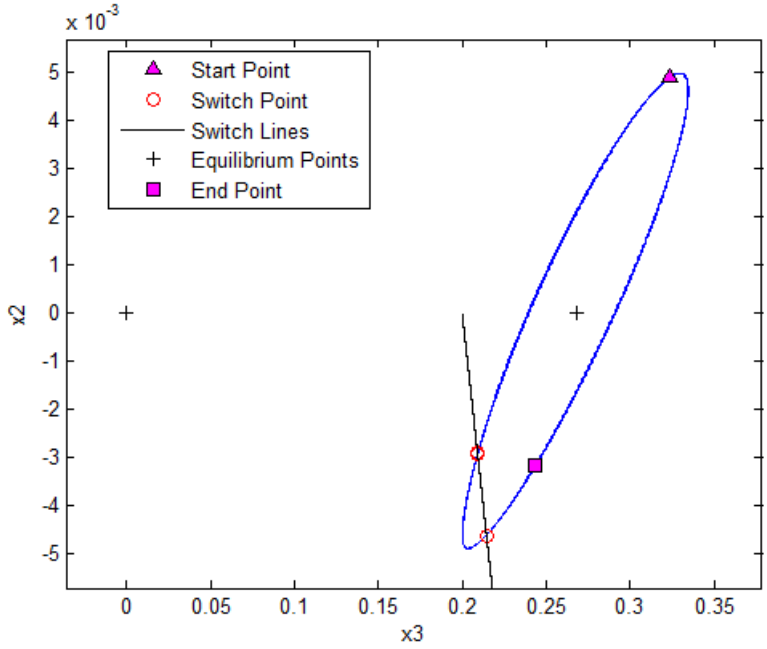

Figure 31: x2-x3 plane phase portrait projection $\mu > \mu_{II}, (\mu = 0.32)$

As shown in the figure the limit cycle behavior is a result from the continuous switching between System I and System II.

To further analyze the periodic behavior of the system power spectral analysis is used to examined the frequencies of the periodic behavior shown in the previous figures. The spectrum analysis of the plunge DOF and the pitch DOF is shown in Figure 32 and Figure 33 respectively.

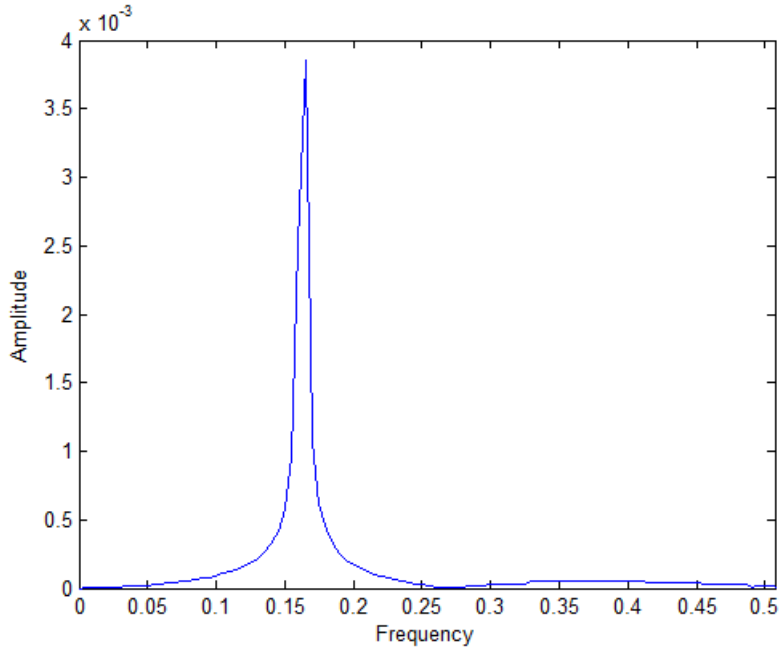

Figure 32: Power spectrum plunge DOF $\mu > \mu_{II}, (\mu = 0.32)$

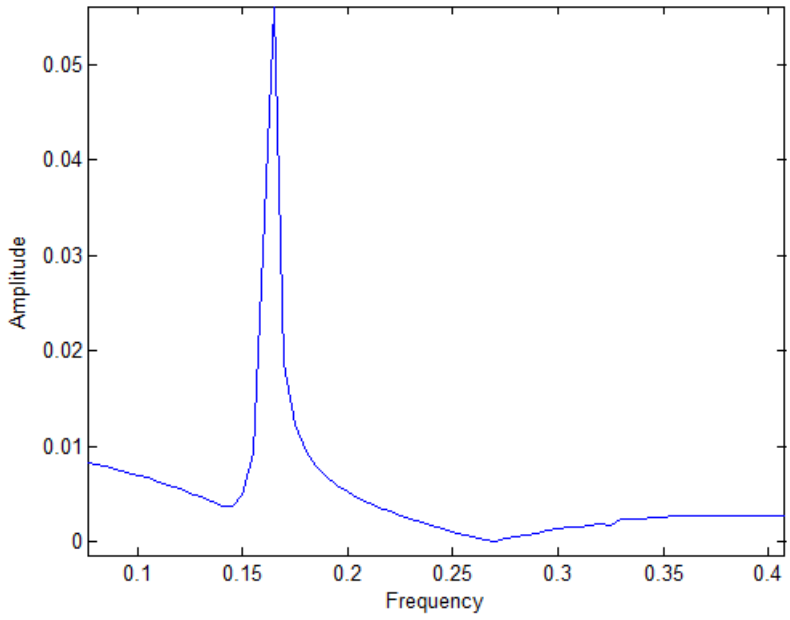

Figure 33: Power spectrum pitch DOF $\mu > \mu_{II}, (\mu = 0.32)$

The spectrum analysis supports the bifurcation diagram and the numerical simulation as it shows the existence of only one limit cycle (one peak) and hence proves the purely periodic behavior of the system at the indicated values of μ.

As a final on the physical validity of the results in this region the lift versus the angle of attack curve is generated from the numerical simulation results as shown in Figure 34.

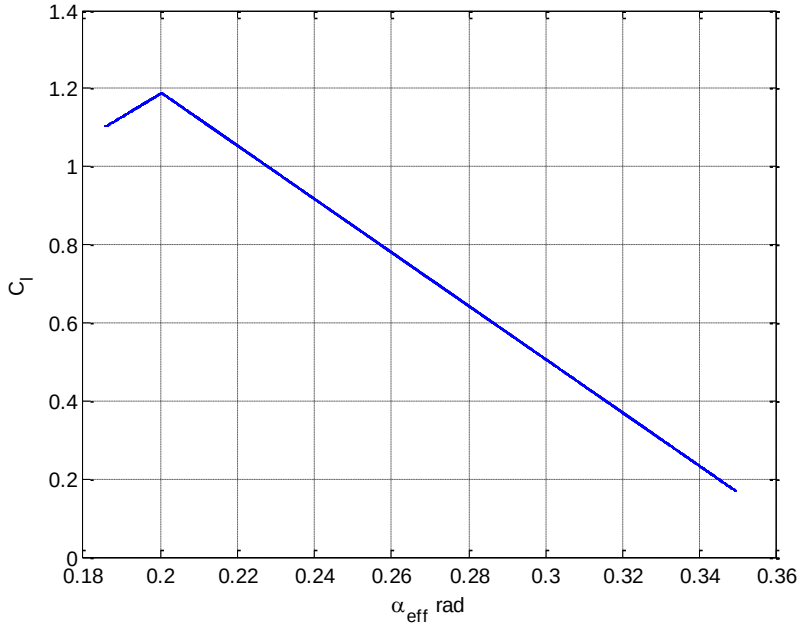

Figure 34: Lift vs. α_{eff} generated from simulations $\mu = 0.32$

As shown in the figure the results generated are within the physically valid region of the bilinear aerodynamic model.

3.5.2 Results for the bilinear model beyond the physically valid region

The motivation behind this section is to further explore the dynamics of the system to provide further understanding and methods of analyzing bilinear systems with

similar behavior. In this section the model will be pushed to values of α beyond the physical limit of the aeroelastic problem to further explore the dynamics of the system and apply a methodology of analysis that can be utilized for similar systems. In the literature one of the systems that can take the full advantage of that analysis is the Wien bridge oscillator presented in Kriegsmann (1987) and Freire et al. (1999).

First the bifurcation diagrams of the plunge DOF and the pitch DOF are reintroduced in Figure 35 and Figure 36 respectively.

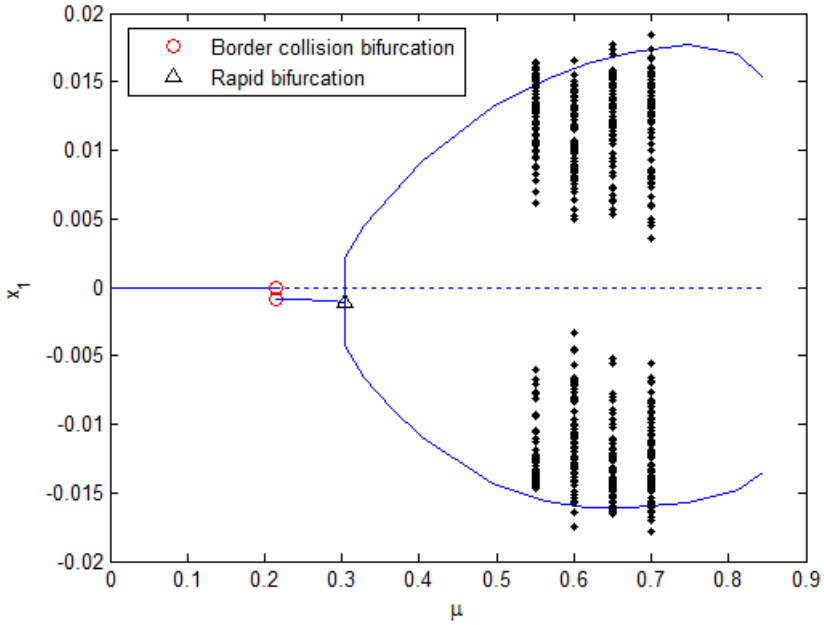

Figure 35: Full bifurcation diagram plunge DOF

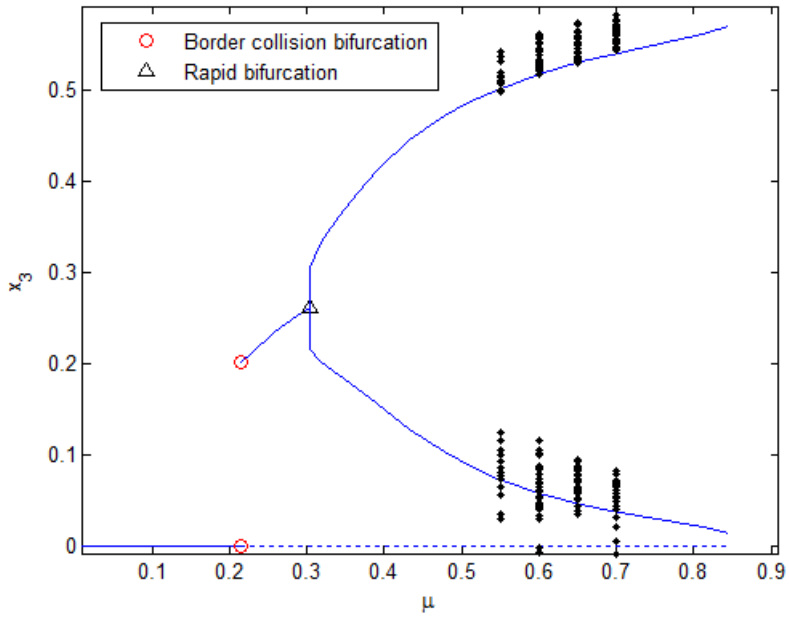

Figure 36: Full bifurcation diagram pitch DOF

As shown in the bifurcation diagrams the limit cycle continues to exist beyond the physical limit of the model. Another observation was also made that there exists a chaotic window at which the both the chaotic and the periodic behaviors coexist. The chaotic window shown in the bifurcation diagrams starts at $\mu = 0.55$ and ends at $\mu = 0.7$. In the presented bifurcation diagrams sampling of the chaotic behavior is added to the bifurcation in steps of 0.5 to show that there exists a chaotic response that coexist with the periodic response calculated using MATCONT.

There are three main routes to chaos in dynamical systems, Hilborn (2000). The first route to chaos is through a series of period doubling of limit cycles in a series of supercritical Hopf bifurcations that eventually lead to chaotic behavior. This kind of behavior can be found in many dynamical systems and iterated maps. The most widely used example in the literature for period doubling is the logistic map function. The

second route to chaos is via a quasi-periodic behavior. The difference between this case and the period doubling case is that the frequencies at which the system oscillates are not commensurate. This means that in the case of period doubling the frequencies of the system can be represented in the form $\frac{f_1}{f_2} = \frac{p}{q}$ where p and q are integers. An example for a quasi-periodic route to chaos can be found in the forced Rayleigh-Bénard convection. The third route to chaos is through intermittency. In the case of intermittency the system exhibits a periodic solution with bursts of chaotic behavior. As the bifurcation parameter is increased the periodic behavior becomes less dominant where as the chaotic behavior dominance increases. The intermittent route to chaos has four types. Type I is the tangent bifurcation intermittency or the stable intermittency. This type occurs as one of the Floquet multipliers crosses the unit circle along the real axis at +1. This type of intermittency leads to bursts of chaotic behavior with the existence of the stable periodic amplitudes hence the name stable intermittency. This type has been widely observed in many experiments such as in Jeffries and Perez (1982), Yeh and Kao (1982) and Hayashi and Ishizuka (1983). The second type is a less observed type of intermittency associated with the occurrence of a Hopf bifurcation along with bursts of chaotic behavior hence the name Hopf bifurcation intermittency. This type has been observed in Huang and Kim (1987). The third type is associated with a period doubling behavior accompanied with bursts of chaos. The third type of intermittency is called period-doubling intermittency. In this type the sub harmonic frequency of the system becomes more dominant as the main frequency loses dominance

as the bifurcation parameter is increased. This type has been observed experimentally in Dubois et al. (1983). The last type of intermittency is called the on-off intermittency where the system alternates between a very stable behavior and bursts of chaos. The on-off intermittency has been examined in Platt et al. (1993) and Hammer et al. (1994).

For our system a type I intermittency has been observed. As the value of μ is increased the chaotic behavior becomes more dominant and the system loses its periodicity. The following set of figures will show this behavior as we increase the value of μ. Figure 37 shows the time evolution and Figure 38 shows the phase portrait of the pitch DOF at the value of μ at which the intermittent chaotic behavior was observed. A power spectrum analysis is also used to further examine the system chaotic behavior as shown in Figure 39.

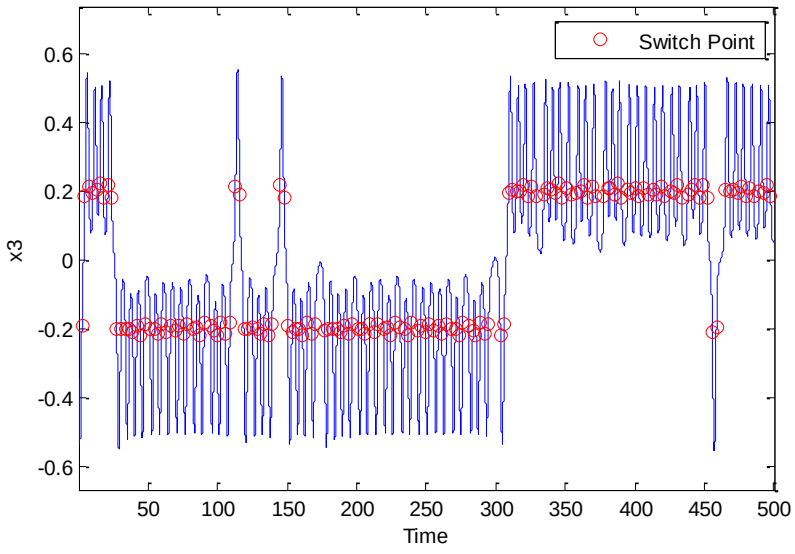

Figure 37: Time evolution, pitch DOF at $\mu = 0.55$

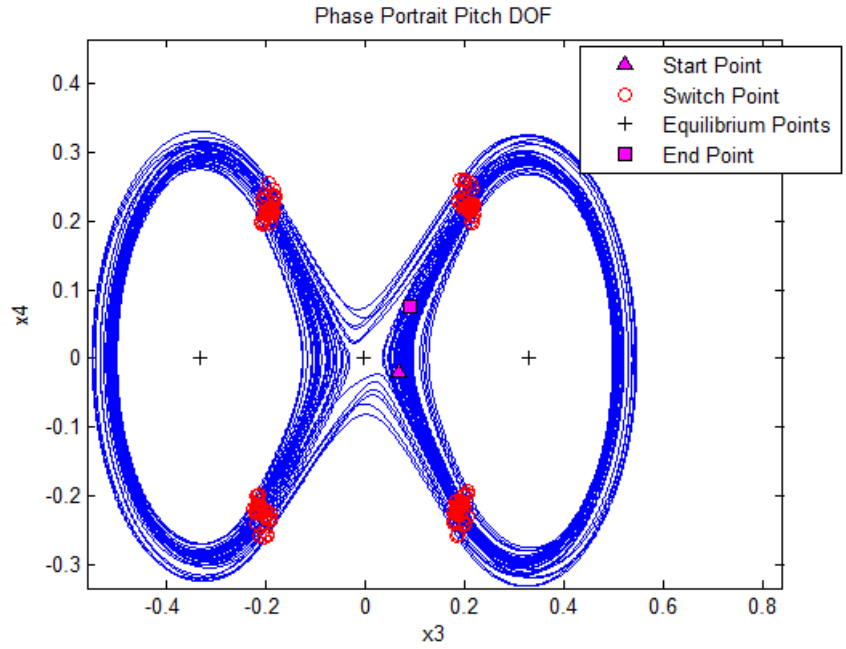

Figure 38: Phase portrait pitch DOF at $\mu = 0.55$

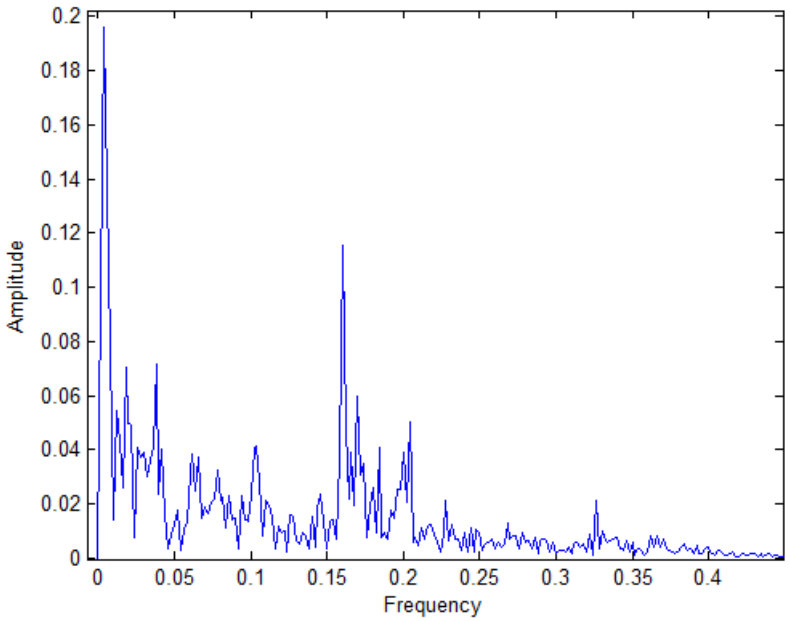

Figure 39: Power spectrum pitch DOF at $\mu = 0.55$

As shown in the figure the periodic response of the system is dominating the system behavior with small jumps of aperiodicity. In Figure 38 the periodic behavior is observed at the equilibrium points of System II while the aperiodicity is generated as a result of the jumps between those two equilibriums. As μ is increased the chaotic behavior becomes more dominant and with less periodicity in the system response. The time evolution, the phase portrait and the power spectrum for the pitch DOF at $\mu = 0.6$ is shown in Figure 40, Figure 41 and Figure 42 respectively.

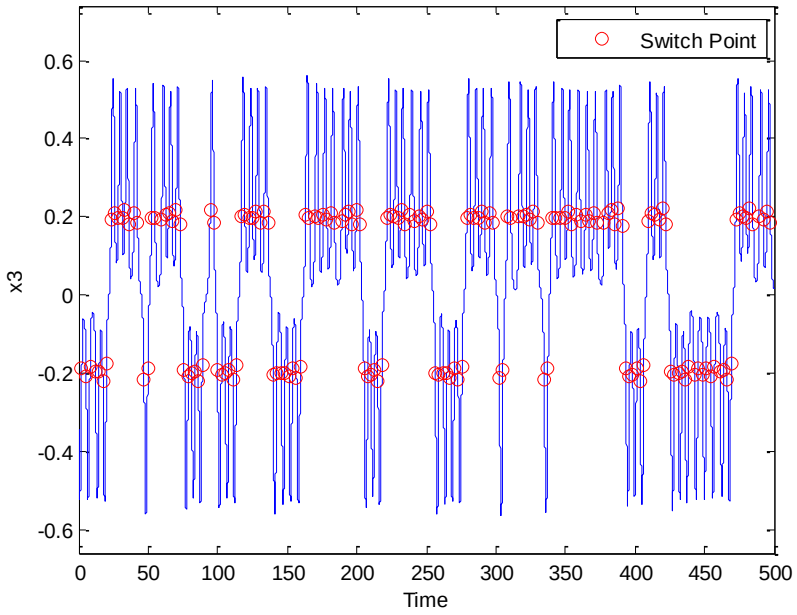

Figure 40: Time evolution, Pitch DOF at $\mu = 0.6$

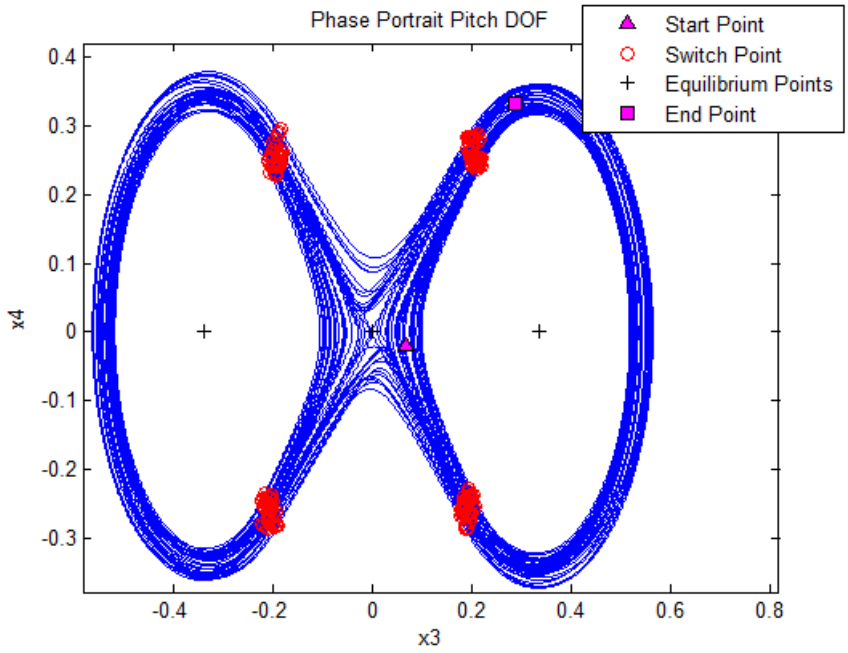

Figure 41: Phase portrait pitch DOF at $\mu = 0.6$

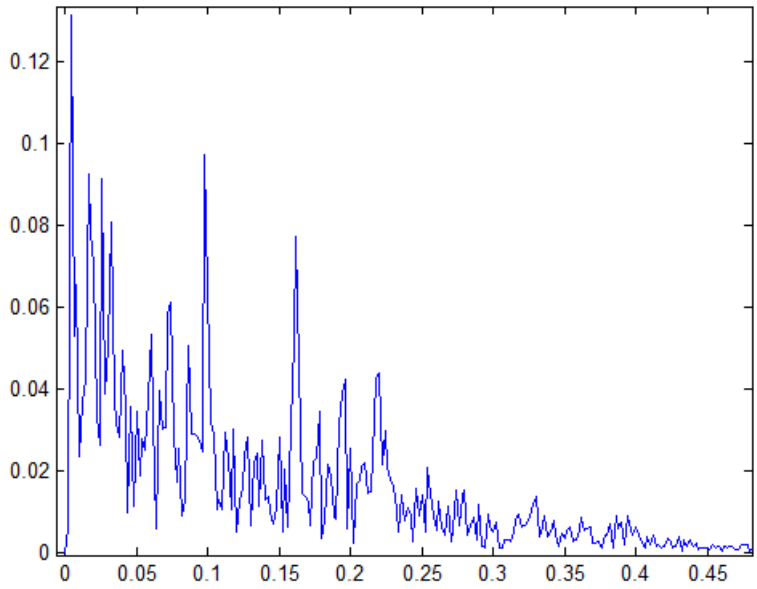

Figure 42: Power spectrum pitch DOF at $\mu = 0.6$

At $\mu = 0.65$ similar results are shown in Figure 43 thorugh Figure 45.

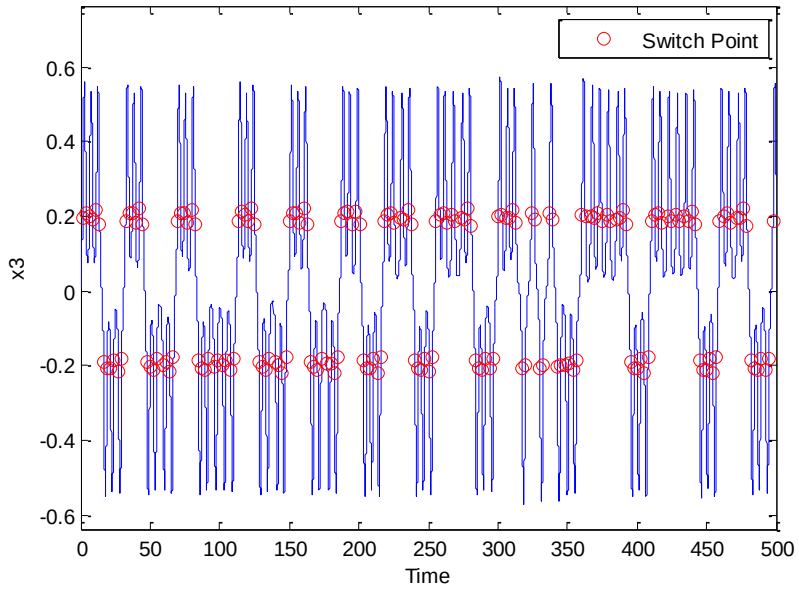

Figure 43: Time evolution, pitch DOF at $\mu = 0.65$

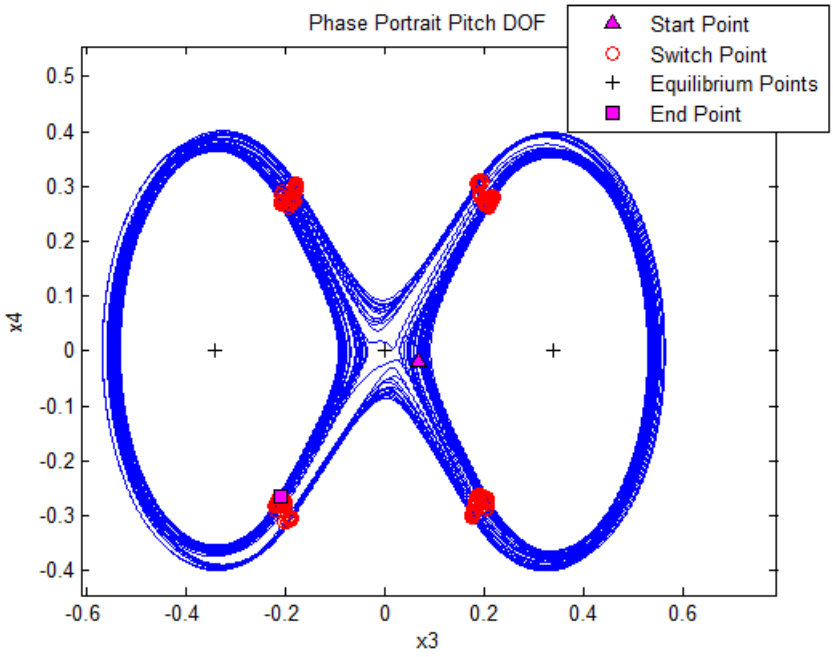

Figure 44: Phase portrait, pitch DOF at $\mu = 0.65$

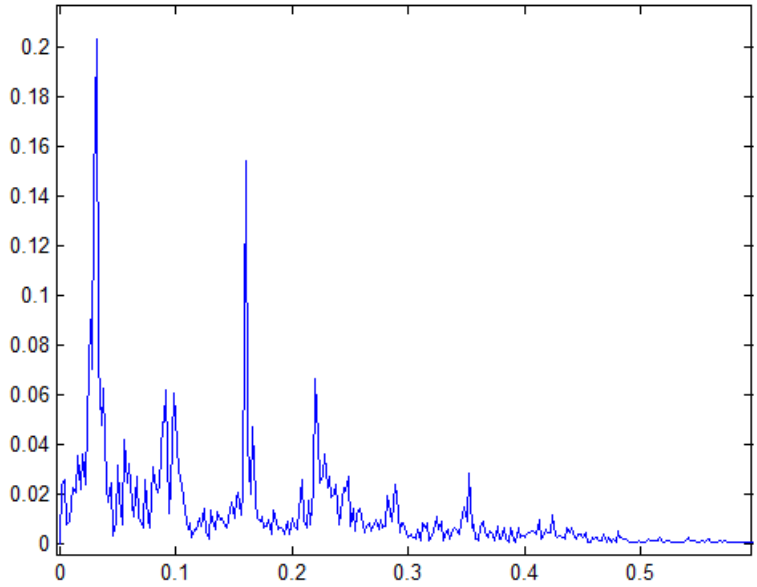

Figure 45: Power spectrum pitch DOF at $\mu = 0.65$

As shown as the value of μ increases the periodicity becomes less dominant and the chaotic jumps becomes the dominant behavior of the system. Figure 46 through Figure 48 show the time evolution, the phase portrait and the power spectrum for the pitch DOF at $\mu = 0.7$.

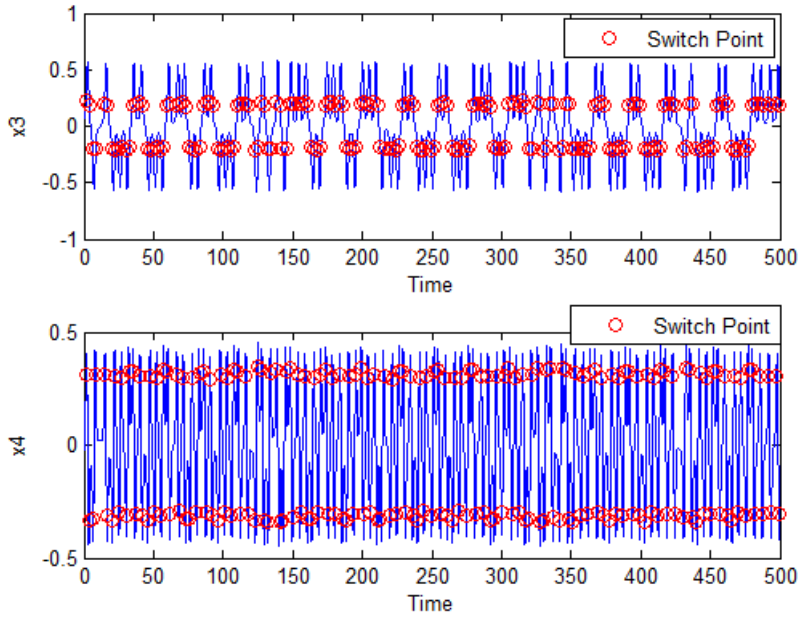

Figure 46: Time evolution pitch DOF at $\mu = 0.7$

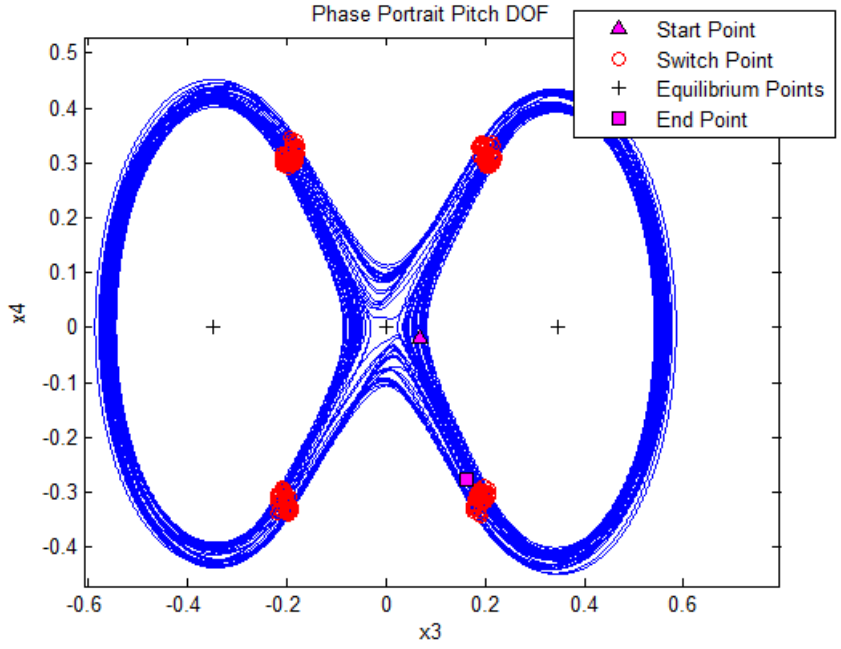

Figure 47: Phase portrait, pitch DOF at $\mu = 0.7$

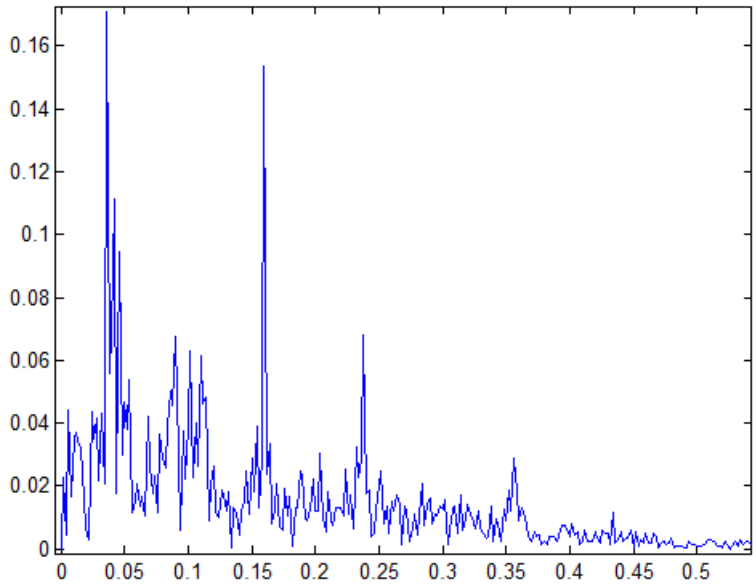

Figure 48: Power spectrum pitch DOF at $\mu = 0.7$

Another observation is that the periodic solution obtained with the continuation software also exists for the same values of μ that exhibits the intermittent chaotic behavior, Figure 49 and Figure 50. This suggests the existence of a global chaotic solution for the system and the jump between the two solutions is extremely sensitive to initial conditions.

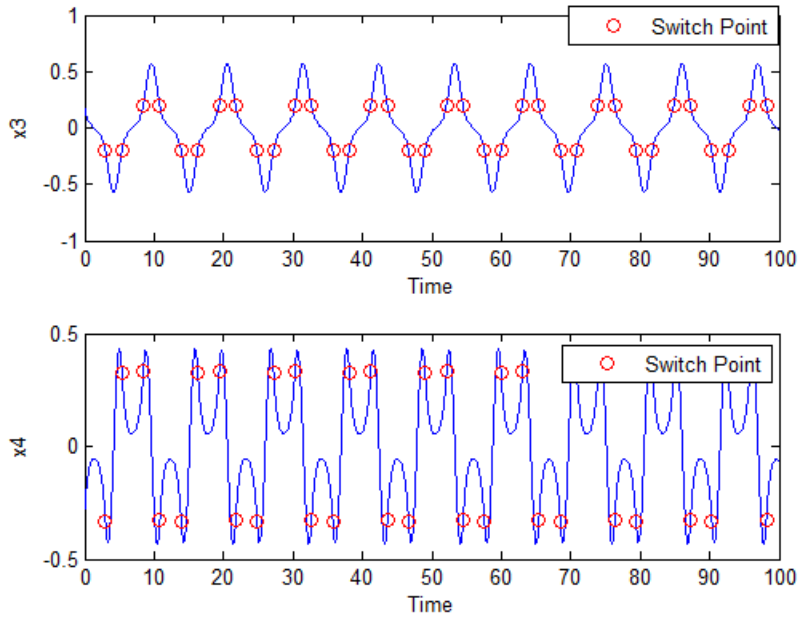

Figure 49: Time evolution pitch DOF at $\mu = 0.7$

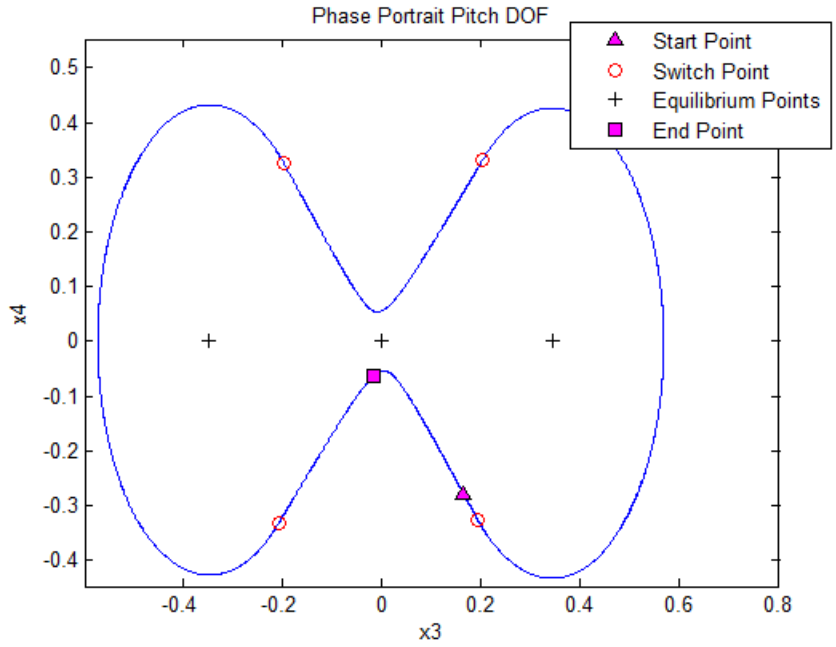

Figure 50: Phase portrait pitch DOF at $\mu = 0.7$

Figure 51 shows the power spectrum analysis for the pitch DOF at $\mu = 0.7$.

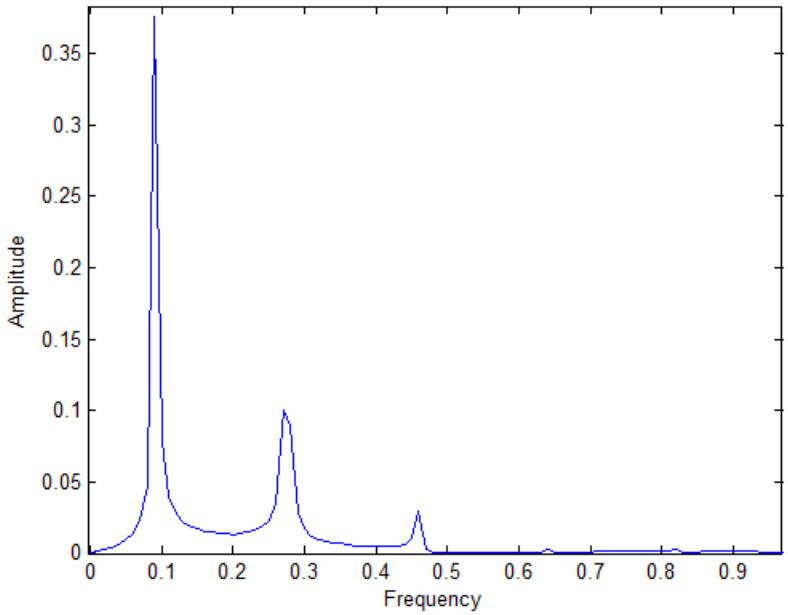

Figure 51: Power spectrum pitch DOF at $\mu = 0.7$

As shown in the figure there is no trace of the chaotic behavior and shown previously at the same value of μ. The analysis shows a major peak which describe the frequency of the limit cycle and two smaller peaks which can be attributed to the interaction of System I and System II and their frequencies.

It should be noted that the chaotic behavior of the system is observed via numerical simulations and to rigorously investigate it can be part of a future investigation of the system chaotic behavior.

3.4.3 Results for the continuous aerodynamic model

As a final step of the numerical analysis of the system the continuous aerodynamic model presented earlier will be analyzed numerically and results will be

compared to the bilinear linear model. The same values of μ and the same initial conditions will be used in this analysis to have a good comparison between the two models.

First we will start with the value of μ at which the origin is the stable equilibrium. The time evolution and the phase portrait for the plunge DOF are shown in Figure 52 and Figure 53 respectively.

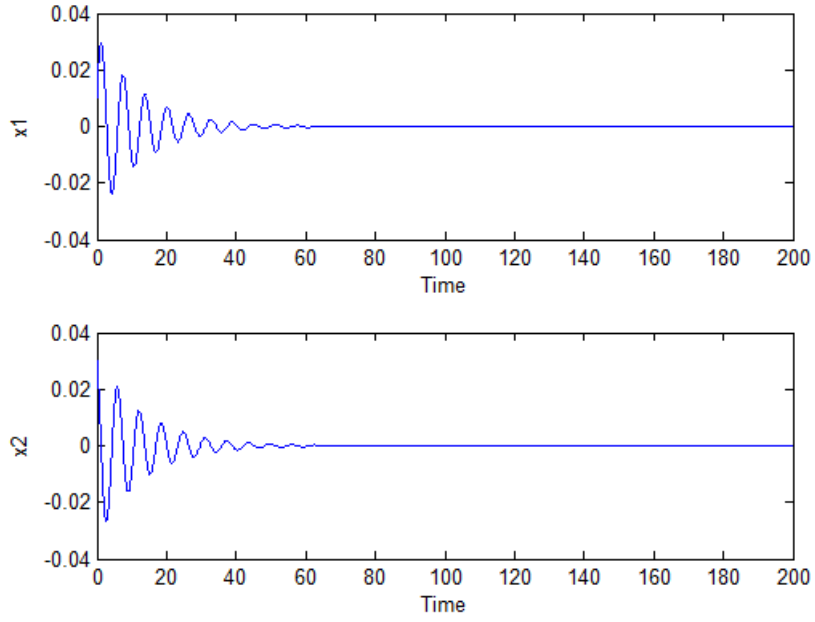

Figure 52: Time evolution plunge DOF at $\mu = 0.15$

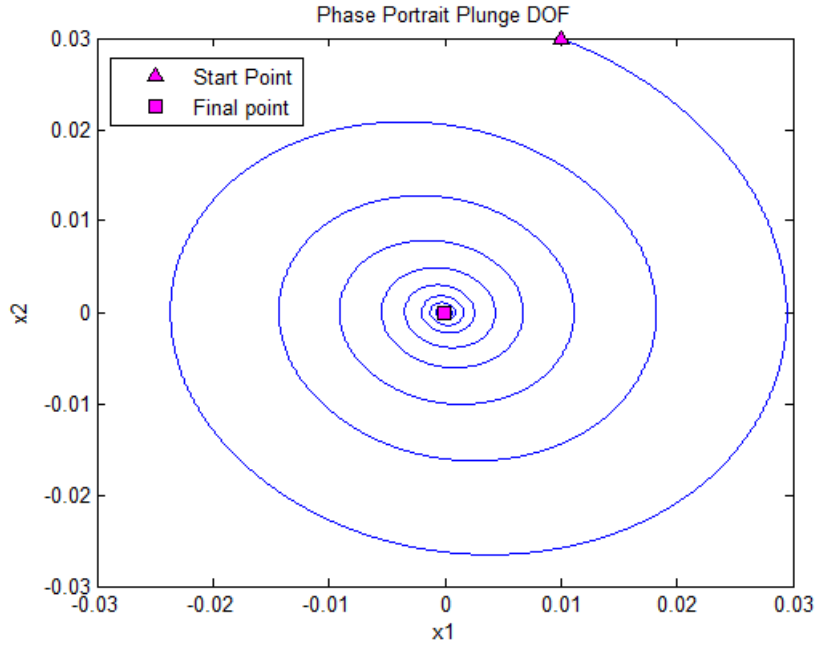

Figure 53: Phase portrait plunge DOF at $\mu = 0.15$

Similarly the pitch DOF response is shown in Figure 54 and Figure 55.

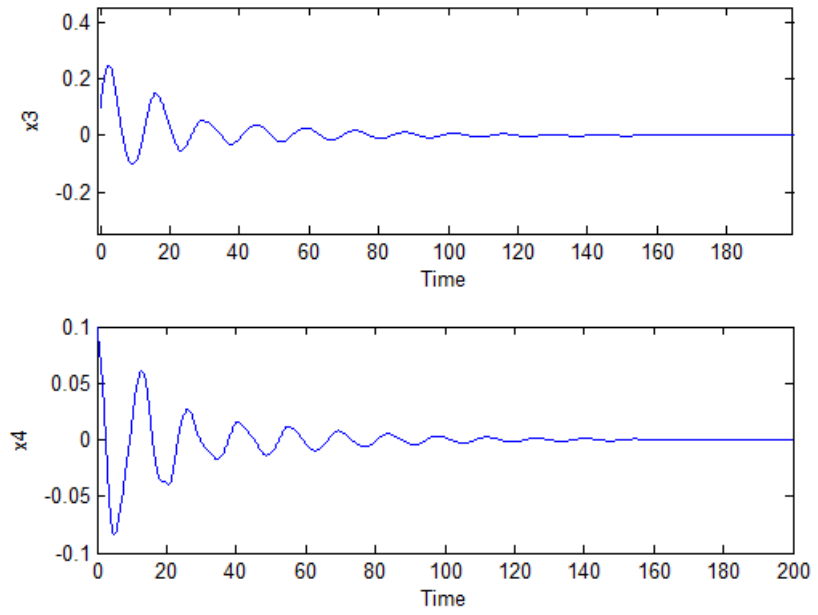

Figure 54: Time evolution pitch DOF at $\mu = 0.15$

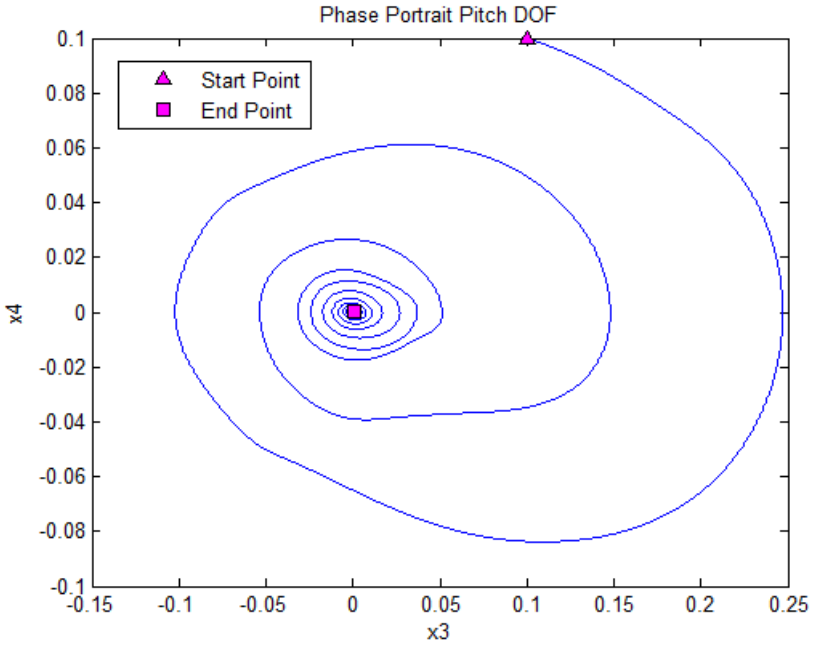

Figure 55: Phase portrait pitch DOF at $\mu = 0.15$

As it is clearly shown in the figures the system has the same response as the bilinear system. There are some minor differences in the trajectories between the two models. These differences arise from the difference in the function describing the aerodynamic loads as the range of the continuous model is wider than the bilinear model and covers the exact behavior of the system as extracted from the experimental data points. Figure 56 shows the lift versus α curve which is different from the one generated from the bilinear model as it goes with the data points for a wider range of α .

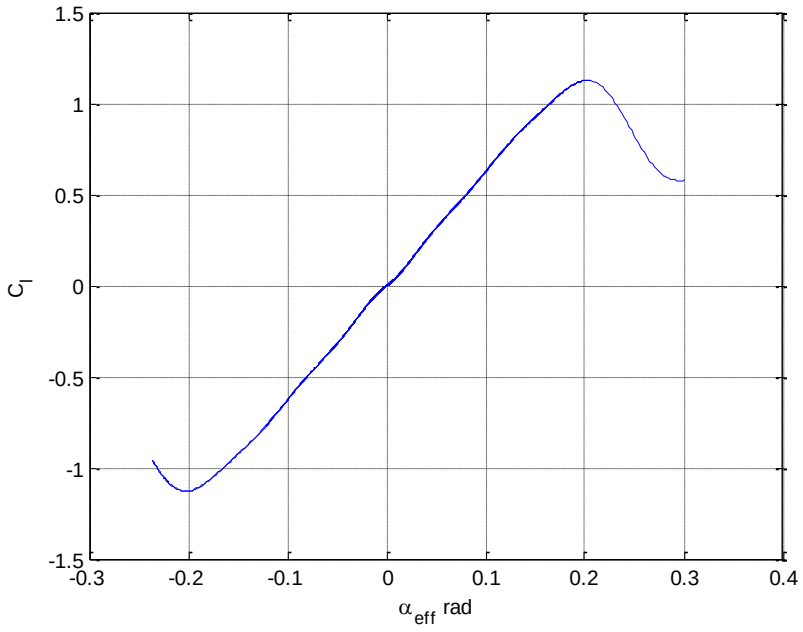

Figure 56: Lift vs. α_{eff} generated from simulations at $\mu = 0.15$

The next set of results is for a value of $\mu = 0.25$, which in case of the bilinear system lies within the stable domain of System II equilibrium. The same initial conditions are used for the simulation and the results are shown in the next set of figures. The response of the plunge DOF is shown in Figure 57 and Figure 58.

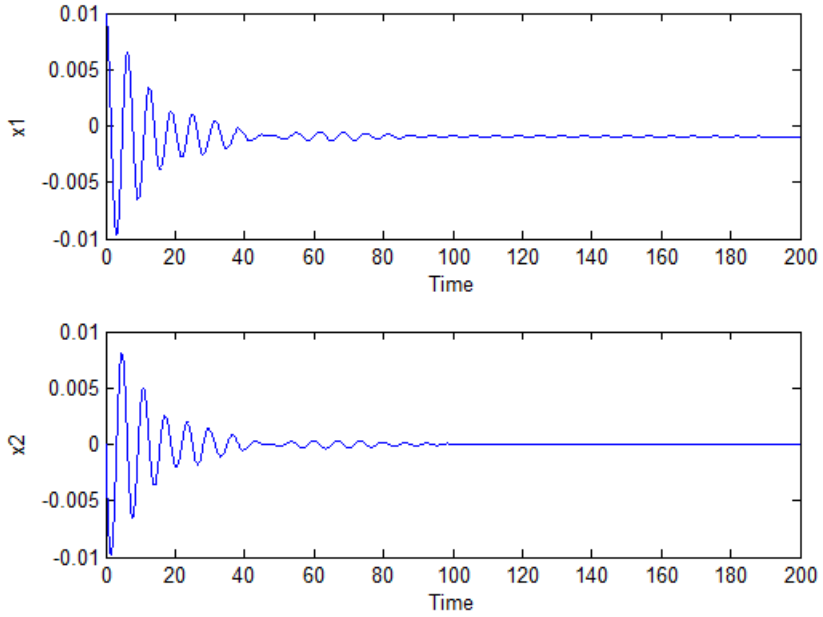

Figure 57: Time evolution plunge DOF at $\mu = 0.25$

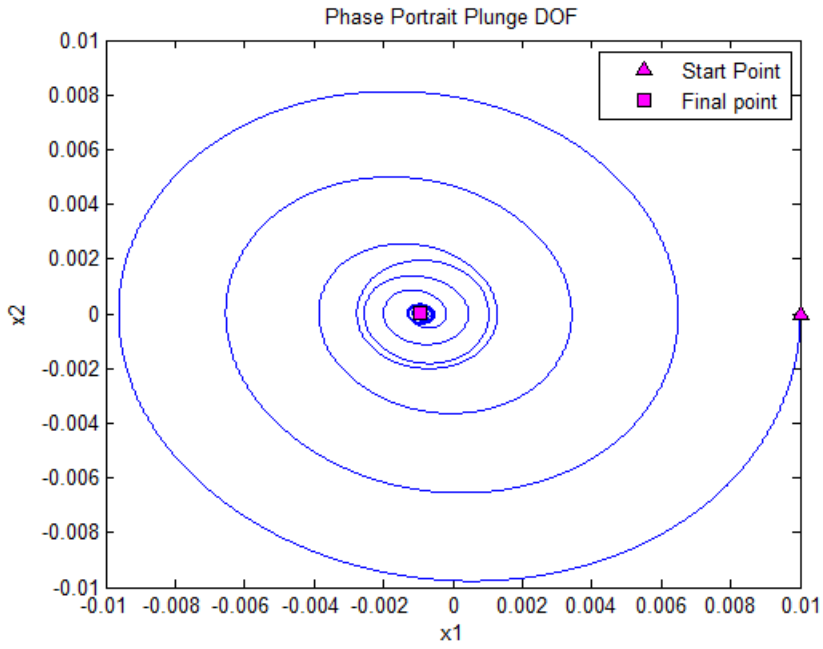

Figure 58: Phase portrait plunge DOF at $\mu = 0.25$

The response of the pitch DOF is shown in Figure 59 and Figure 60.

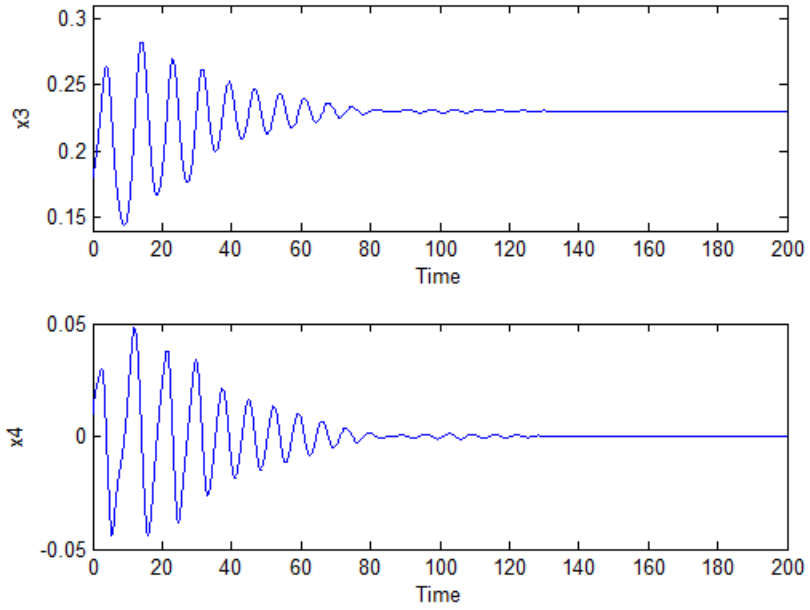

Figure 59: Time evolution pitch DOF at $\mu = 0.25$

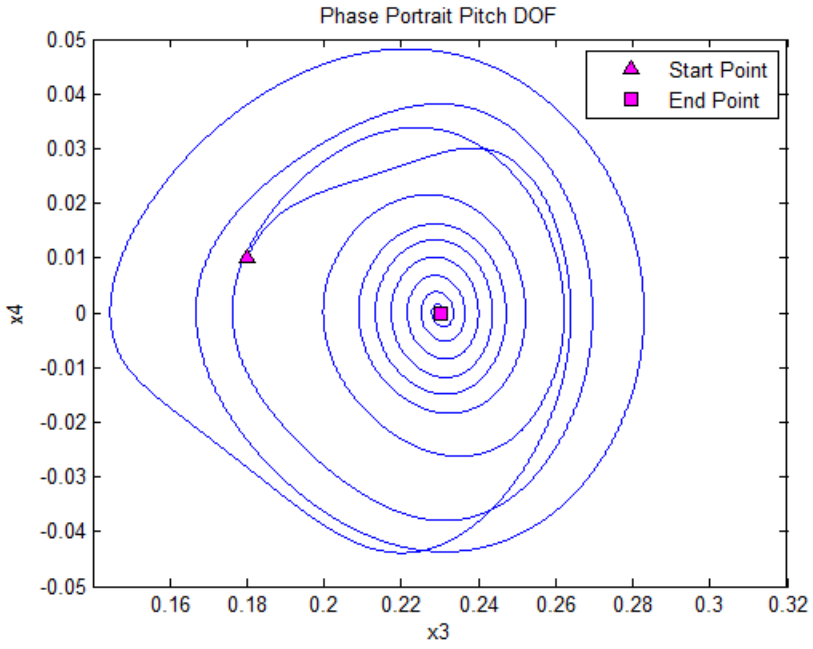

Figure 60: Phase portrait pitch DOF at $\mu = 0.25$

As in the bilinear system the continuous system also converged to the equilibrium point of System II. Figure 61 shows the lift versus α curve generated from the simulation results which lies within the same region of the previously presented bilinear system.

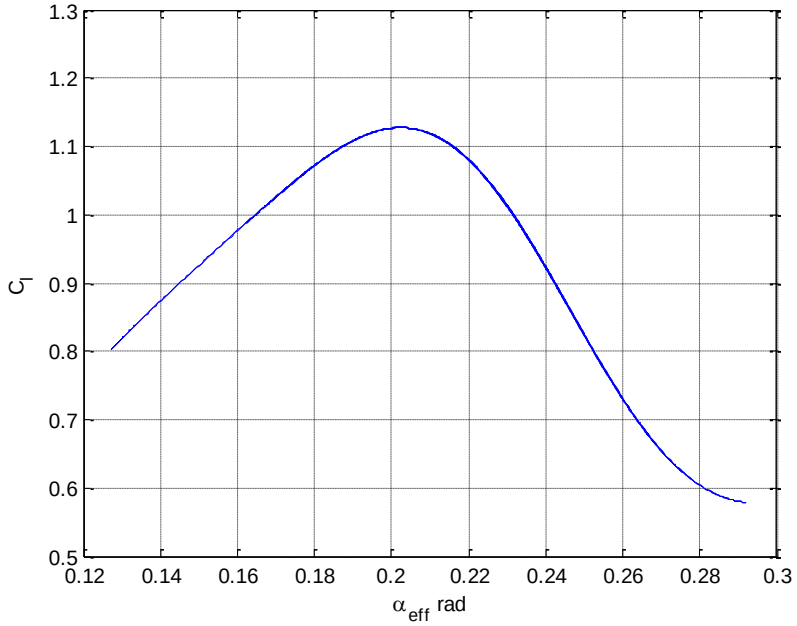

Figure 61: Lift vs. α_{eff} generated from simulations at $\mu = 0.25$

For the final values of μ for which the bilinear model simulations are shown the same initial conditions with the same value of $\mu = 0.32$ are used to simulate the continuous model. Figure 62 and Figure 63 show the plunge DOF response.

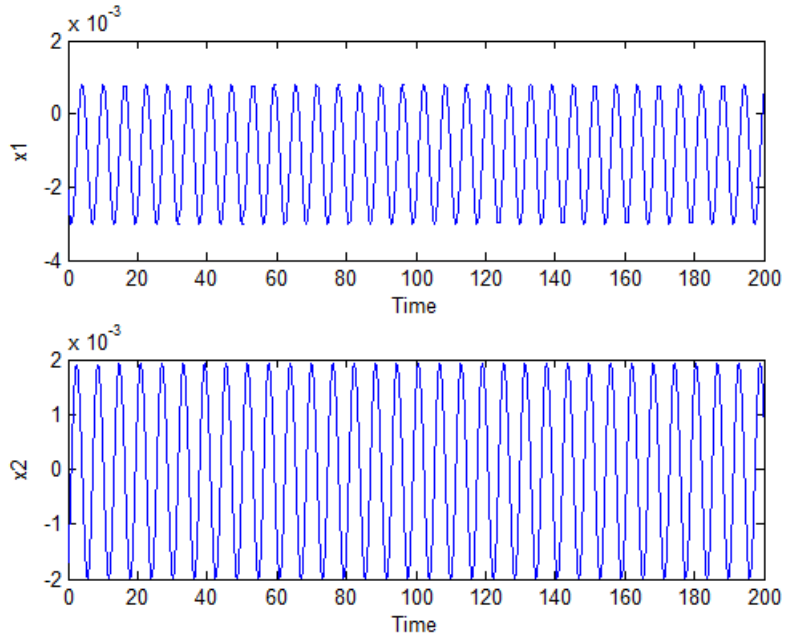

Figure 62: Time evolution plunge DOF at $\mu = 0.32$

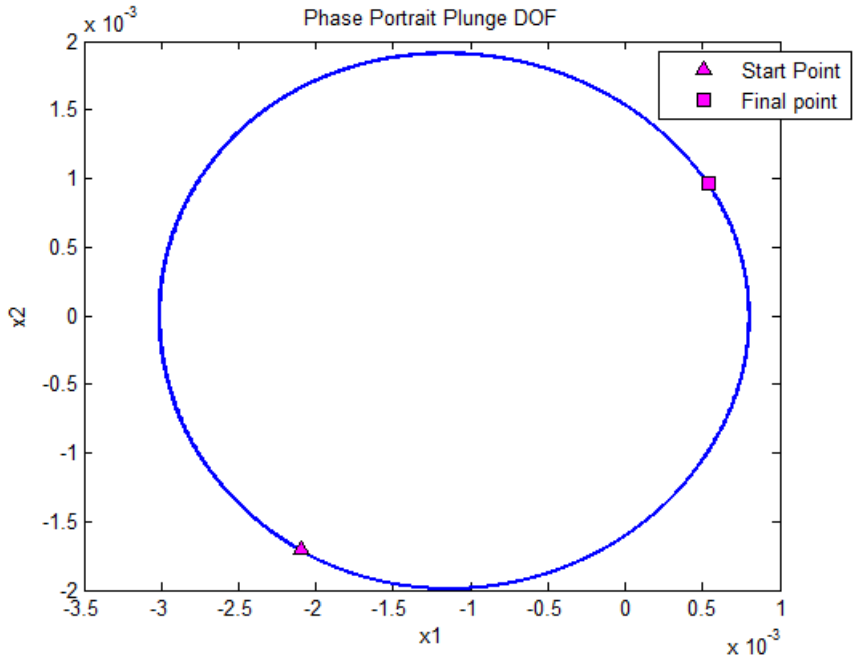

Figure 63: Phase portrait plunge DOF at $\mu = 0.32$

Figure 64 and Figure 65 show the pitch DOF response.

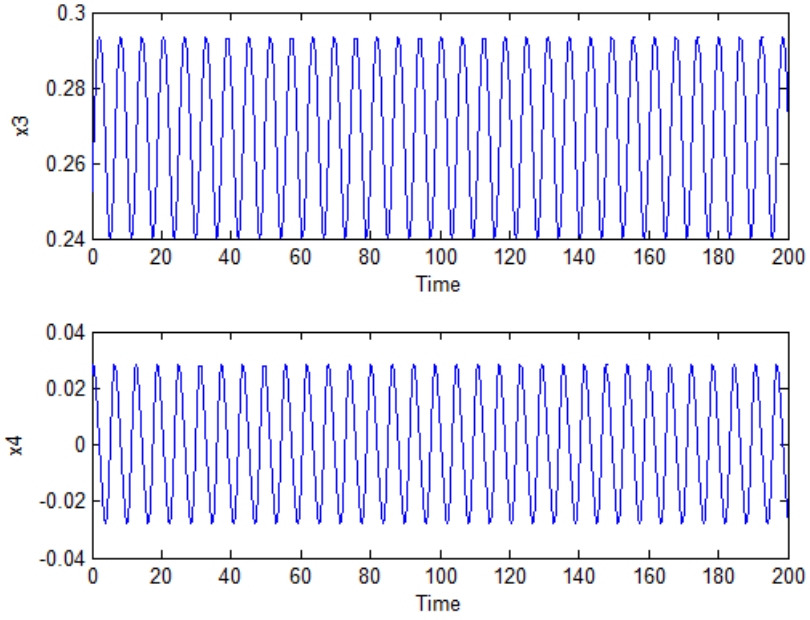

Figure 64: Time evolution pitch DOF at $\mu = 0.32$

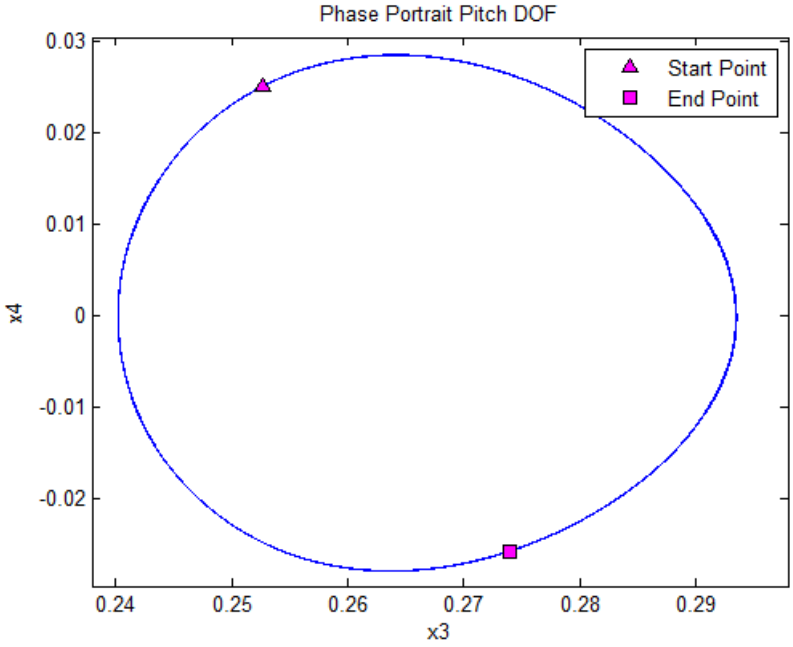

Figure 65: Phase portrait pitch DOF at $\mu = 0.32$

As shown there exist a limit cycle at the same value of μ as in the bilinear system. The power spectrum for the plunge and the pitch DOF are shown in Figure 66 and Figure 67 respectively.

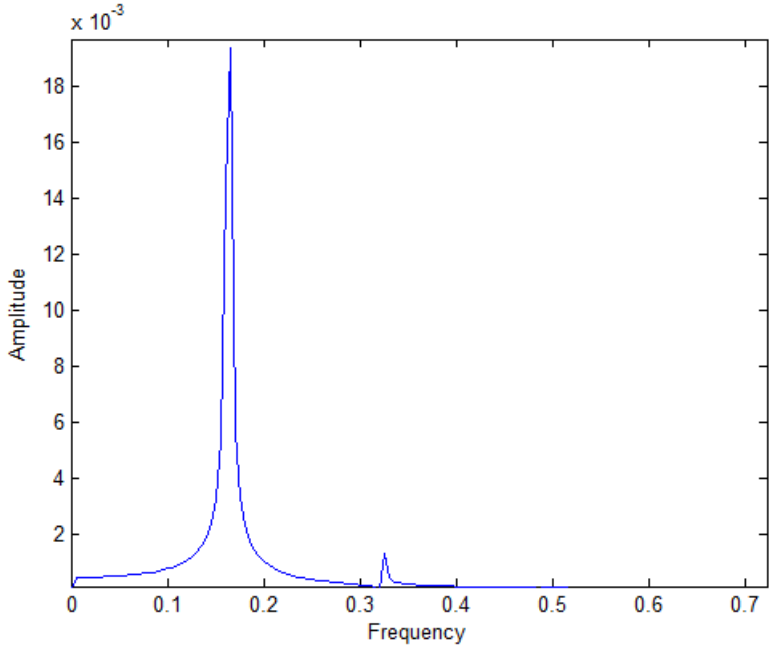

Figure 66: Power spectrum plunge DOF at $\mu = 0.32$

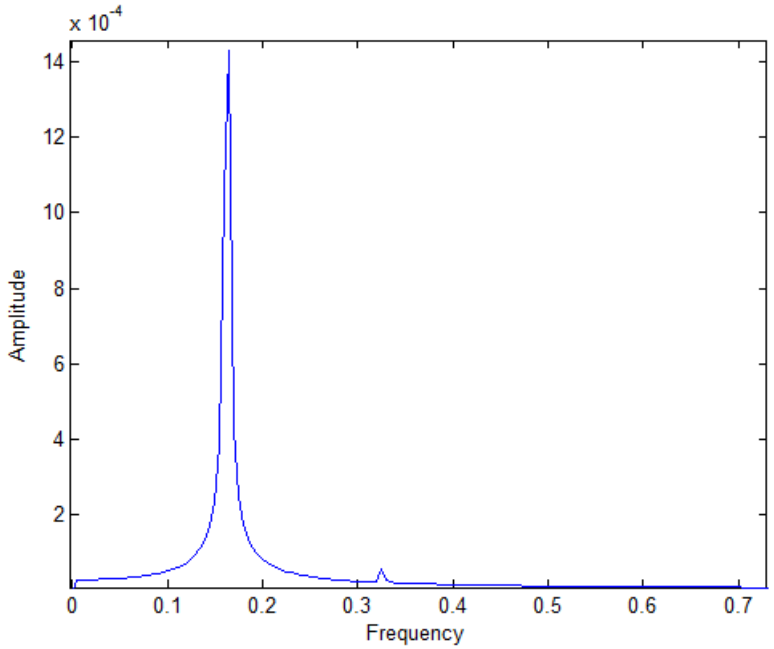

Figure 67: Power spectrum pitch DOF at $\mu = 0.32$

Finally the lift versus α curve is generated from the numerical results in Figure 68.

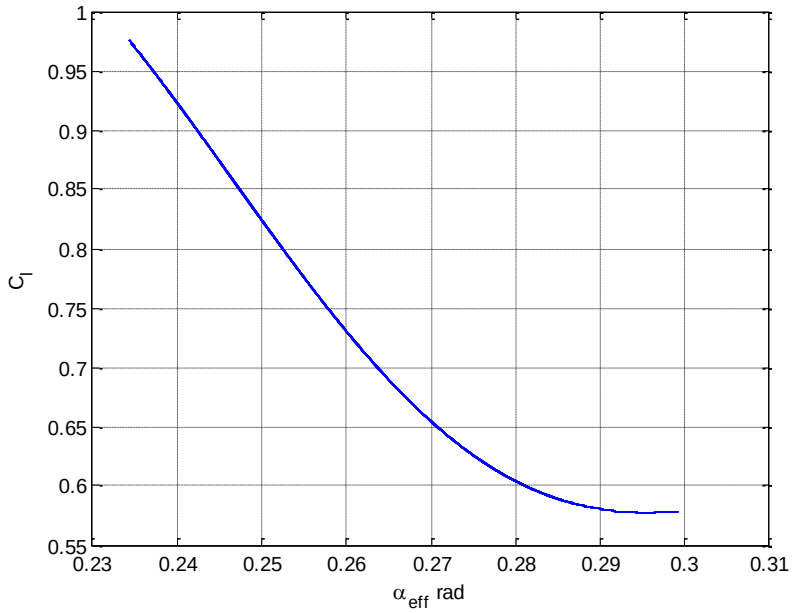

Figure 68: Lift vs. α generated from simulations at $\mu = 0.32$

As a final comparison between the bilinear model results and the continuous model the bifurcation diagrams of the continuous model are generated using MATCONT and overlaid on the bifurcation diagram of the bilinear model. The bifurcation diagrams for the plunge DOF and the pitch DOF are shown in Figure 69 and Figure 70 respectively.

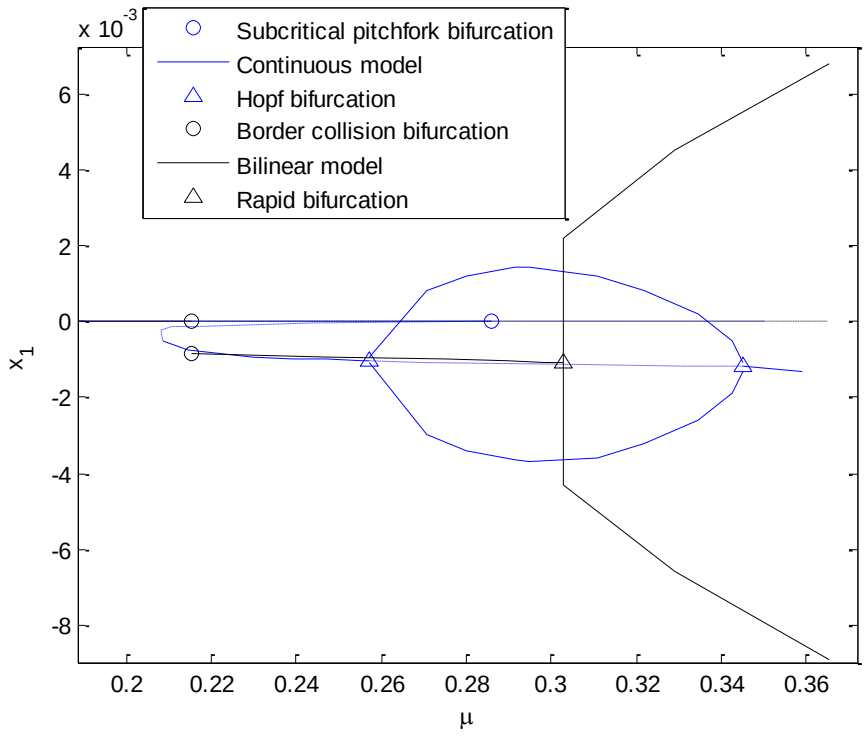

Figure 69: Bifurcation diagram plunge DOF, continuous vs. bilinear model

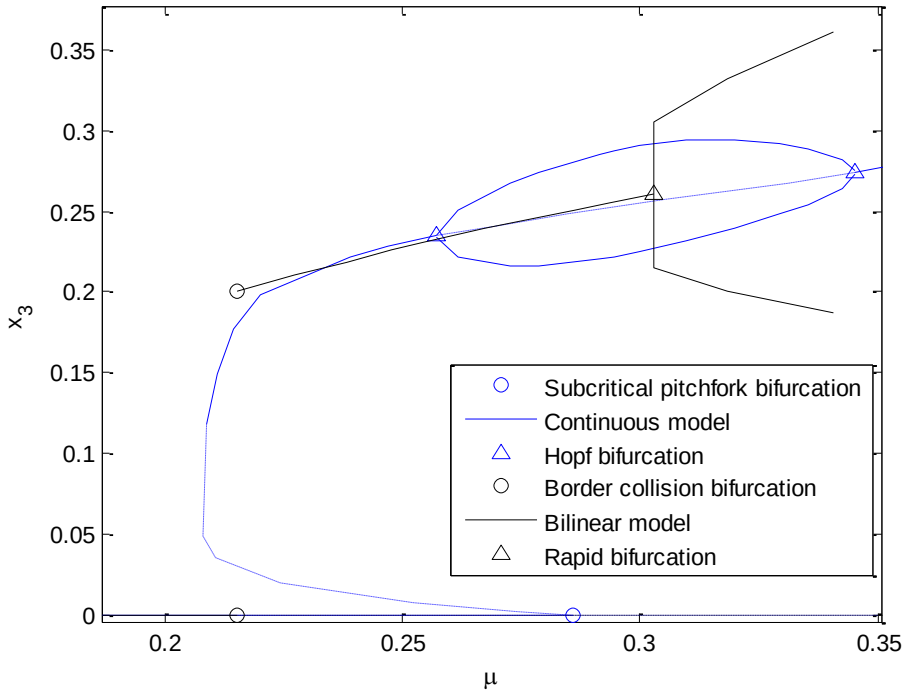

Figure 70: Bifurcation diagram pitch DOF, continuous vs. bilinear model

Qualitatively both models can be called similar. The general behavior of the continuous and the bilinear models follows the same pattern. The system starts with the origin as a stable equilibrium, this point loses stability as the value of μ is changed and another stable equilibrium attracts the system. As the value of μ is changed the second equilibrium loses stability to a stable limit cycle.

The differences between the two models can be noted in the values at which the bifurcations take place. There is also notable difference in the amplitude and the propagation of the limit cycles. Finally in the continuous system and as the origin loses stability it does not jump the other stable equilibrium does not exist suddenly as in the case of the bilinear model, instead a subcritical pitchfork bifurcation takes as shown in

the diagrams. Due to the hysteresis nature of this bifurcation a jump from one equilibrium to the other can take place within the region of which both equilibrium points exist and are stable, see Strogatz (2000). Those differences can be attributed to the nature of the piecewise linear model as it is a non smooth system with an abrupt jump from one dynamical system to the other whereas the continuous model is a smooth dynamical system. Another reason is due to the differences in the functions describing the aerodynamic loads. Due to the difference in the dynamics and instead of having a limit cycle that will increase in amplitude as μ is increased the bifurcation diagrams of the continuous model show a rise of a third equilibrium point in a reverse Hopf bifurcation.

In conclusion both the bilinear and the continuous system have similar behavior at the same values of μ applying the same initial conditions. The bifurcation diagrams showed some differences in the limit cycle behavior and the values at which the bifurcations occur but in general the behavior of both systems is very similar qualitatively. This can be considered as an indication that a bilinear approximation or in general a piecewise linear approximation is a good approximation to be used in such systems. It generates very similar results to the continuous system but has the advantage of applying linear systems techniques which are simpler, tractable and can produce analytical results as shown previously.

3.6 Sets of Initial Conditions and Poincaré Sections

As part of the dynamical analysis of the bilinear system, this section deals with defining sets of initial conditions that lie on the switching surface between System I and System II and the system behavior associated with those sets. Understanding the behavior of the system using those sets will give us better understanding of the dynamics of the system. It will also lead to showing Poincaré sections for the system at the switching surface that will shed more understanding on how the system behaves and will provide more understanding and explanation for the system behavior shown in the previous section simulations.

First we are interested in starting on the switch line between System I and II hence, the equation of the switch line (3.2) must be satisfied as follows.

$$x_2 = \mu(\pm\alpha_{stall} - x_3) \tag{3.37}$$

This condition guarantees that the system will start on the switch line between System I and II. Using the relation in (3.37) the first set of initial conditions L can be defined. L is the set of initial conditions that lie on the switch line between System I and System II. It can be formally defined as,

$$L = \{\mathbf{x} \mid x_2 = \mu(\pm\alpha_{stall} - x_3)\} \tag{3.38}$$

where, $\mathbf{x} = \begin{bmatrix} x_1 & x_2 & x_3 & x_4 \end{bmatrix}^T$.

For initial conditions that are elements of L three main subsets can be defined to describe the system behavior. This behavior can be divided into 3 main cases.

1) Crossing from System I to System II

2) Crossing from System II to System I

3) The grazing case at which trajectories do not cross but just graze the switch line and stay in their initial system.

Figure 71 shows an illustration for the above mentioned 3 cases.

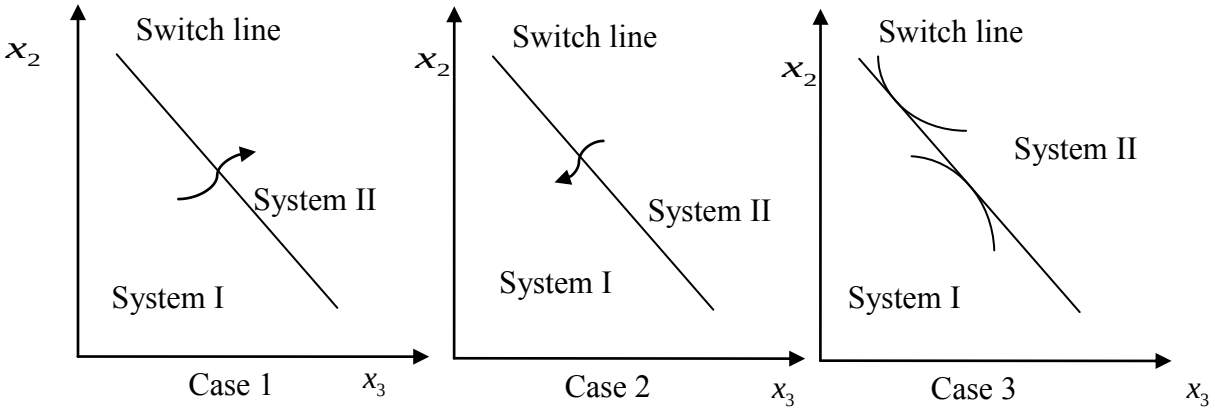

Figure 71: Cases of trajectories behavior at the switch line

The following analysis uses directional derivatives to formally define those subsets that represent the above mentioned cases.

From the equation of the switch line we can define

$$w(x_3, x_2) = x_2 - f(x_3)$$
where,
$$f(x_3) = \mu(\alpha_{stall} - x_3) \qquad (3.39)$$

The switch line can be defined by the unit vector

$$\hat{\mathbf{v}} = (v_1, v_2) = \left(\frac{1}{\sqrt{1+\mu^2}}, \frac{-\mu}{\sqrt{1+\mu^2}}\right) \qquad (3.40)$$

Taking the directional derivative of $w(x_3, x_2)$ along $\hat{\mathbf{v}}$

$$\begin{aligned}\nabla_{\hat{\mathbf{v}}} w(x_3, x_2) &= \frac{\partial w}{\partial x_3} v_1 + \frac{\partial w}{\partial x_2} v_2 \\ &= \frac{-df(x_3)}{dx_3} v_1 + v_2\end{aligned} \tag{3.41}$$

Equating (3.41) to zero will give the following relationship

$$\frac{dx_2}{dx_3} = -\mu \tag{3.42}$$

Applying the chain rule to (3.42)

$$\begin{aligned}&\frac{dx_2/dt}{dx_3/dt} = -\mu \\ &\frac{\dot{x}_2}{\dot{x}_3} = -\mu\end{aligned} \tag{3.43}$$

Substituting the dynamics of the system in (3.3) into (3.43)

$$\begin{aligned}&-x_1 - (p_1 + p_2 \mu c_o) x_{2L} - p_2 \mu^2 c_o x_3 = -\mu x_4 \\ &-x_1 - (p_1 + p_2 \mu c_o)(\mu(\alpha_{stall} - x_3)) - p_2 \mu^2 c_o x_3 = -\mu x_4 \\ &x_1 - \mu x_4 = -p_1 \mu \alpha_{stall} + p_1 \mu x_3 - p_2 \mu^2 c_o \alpha_{stall} + p_2 \mu^2 c_o x_3 - p_2 \mu^2 c_o x_3\end{aligned} \tag{3.44}$$

After simplification and collection of terms (3.44) becomes

$$x_1 - \mu x_4 = -p_1 x_2 - p_2 \mu^2 c_o \alpha_{stall} \tag{3.45}$$

Combining the information in (3.37) and (3.45) the three subsets of L describing the three cases shown in Figure 71 can be defined as follows.

Set of initial conditions for case 1, crossing from System I to System II

$$S_{I-II} = \{\mathbf{x} \mid \mathbf{x} \in L, |x_1 - \mu x_4| < -p_1 x_2 - p_2 \mu^2 c_o \alpha_{stall}\} \tag{3.46}$$

Set of initial conditions for Case 2, crossing from System II to System I

$$S_{II-I} = \{\mathbf{x} \mid \mathbf{x} \in L, |x_1 - \mu x_4| > -p_1 x_2 - p_2 \mu^2 c_o \alpha_{stall}\} \tag{3.47}$$

Set of initial conditions for case 3, Grazing and staying on the same side of the line

$$S_G = \left\{ \mathbf{x} \,|\, \mathbf{x} \in L, \left| x_1 - \mu x_4 \right| = -p_1 x_2 - p_2 \mu^2 c_o \alpha_{stall} \right\} \tag{3.48}$$

By selecting initial conditions according to (3.46), (3.47) and (3.48) and numerically integrating the system forward and backward in time, the results obtained in those equations can be verified as shown in Figure 72 through Figure 75.

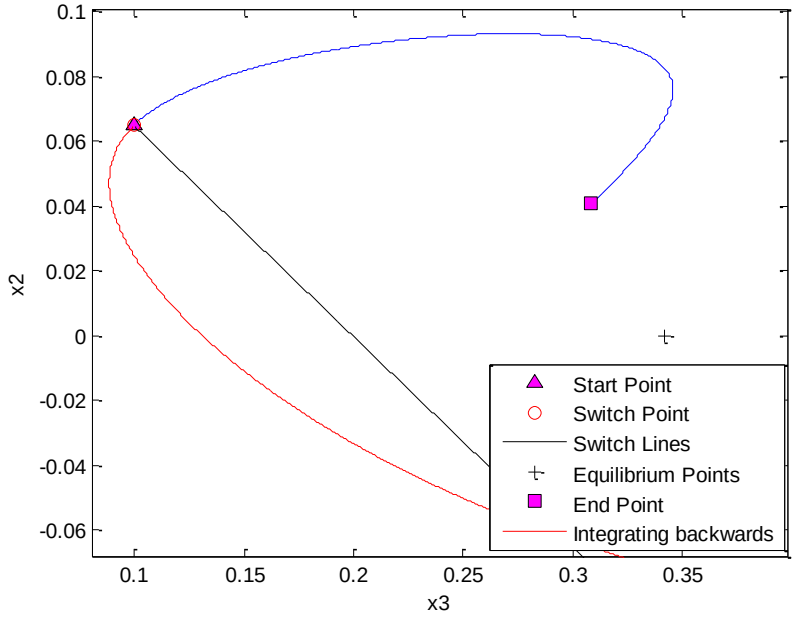

Figure 72: Sets of initial conditions case 1

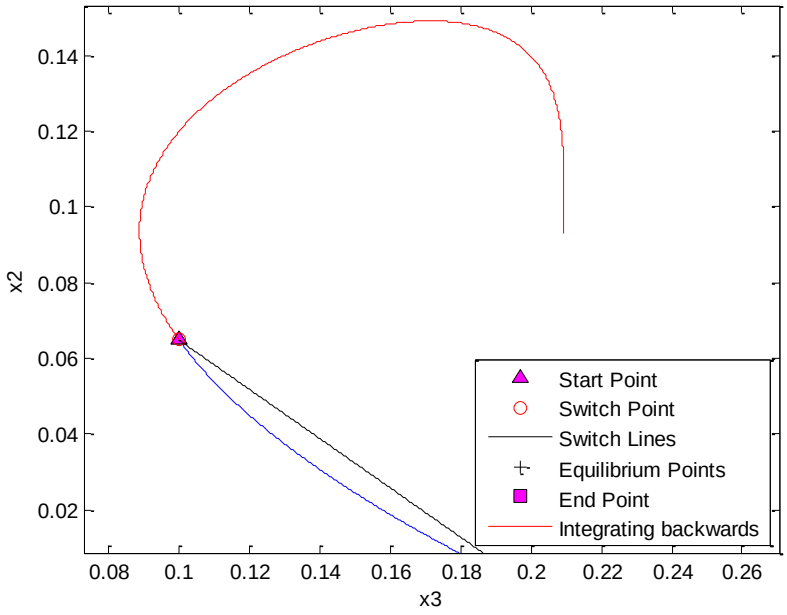

Figure 73: Sets of initial conditions case 2

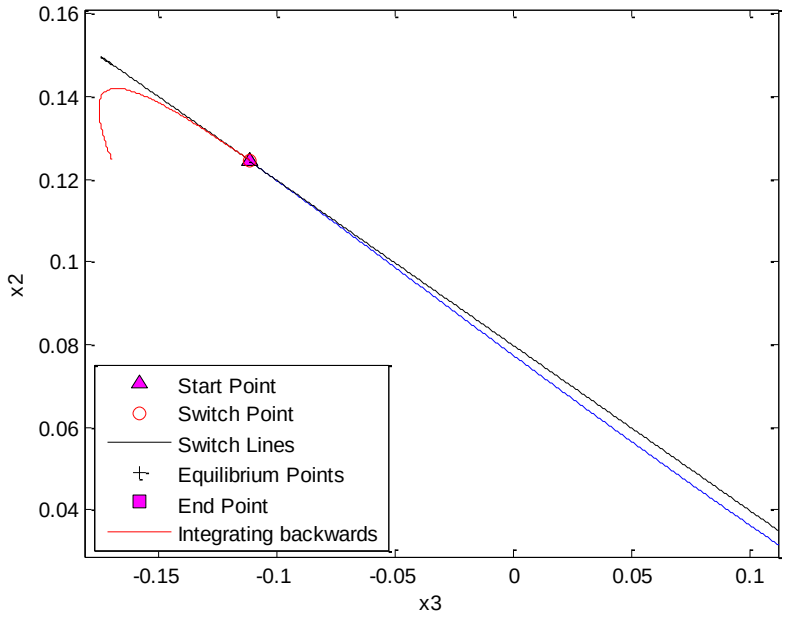

Figure 74: Grazing behavior (System I)

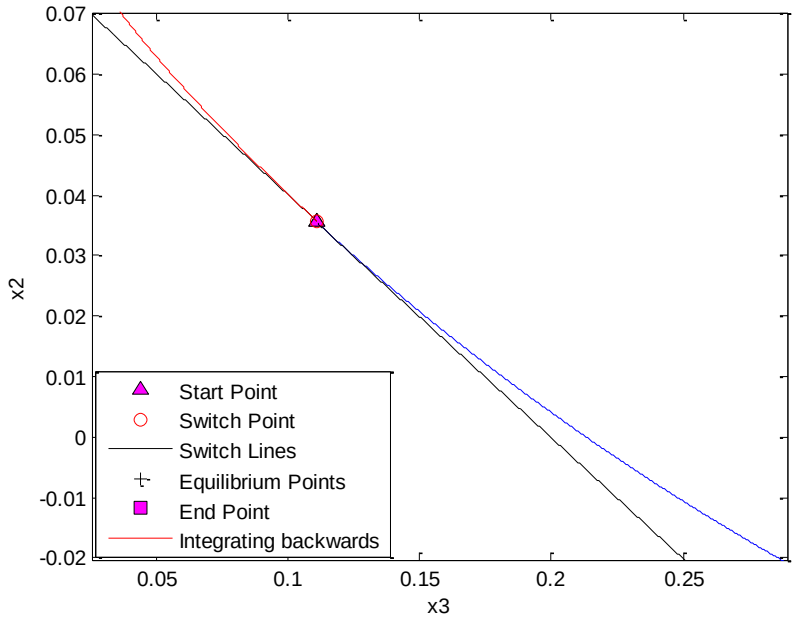

Figure 75: Grazing behavior (System II)

Figure 72 shows the system behavior for initial conditions belonging to S_{I-II}. As shown, trajectory crosses from System I to System II at this point. Figure 72 shows the crossing from System II to I as the initial conditions were selected to be elements of S_{II-I}. Figure 74 and Figure 75 show the third case describing the system behavior. Figure 74 shows the grazing behavior of the system where trajectories stay in System I whereas Figure 75 shows the case of trajectories staying in System II.

This grazing set as defined in (3.48) corresponds to the value of the directional derivative with respect to the switch line exactly equals to $-\mu$. $-\mu$ is the slope of the switch line between System I and System II as presented in (3.37). In other words the trajectory is tangent to the switch line. In the grazing case the trajectory hits the line tangentially but it doesn't cross to the other side.

From their definition in (3.46), (3.47) and (3.48) S_{I-II}, S_{II-I} and S_G are disjoint sets. In other words,

$$\begin{aligned} S_{I-II} \cap S_{II-I} &= 0 \\ S_{I-II} \cap S_G &= 0 \\ S_{II-I} \cap S_G &= 0 \end{aligned} \tag{3.49}$$

Also those three sets are the only components of L. Hence,

$$L = S_{I-II} \cup S_{II-I} \cup S_G \tag{3.50}$$

equations (3.49) and (3.50) can be represented in the following Venn diagram,

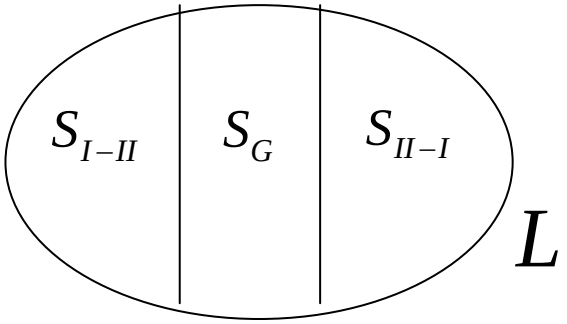

Figure 76: Venn diagram of L

The following set of figures shows numerical results for the subsets of L at different values of μ.

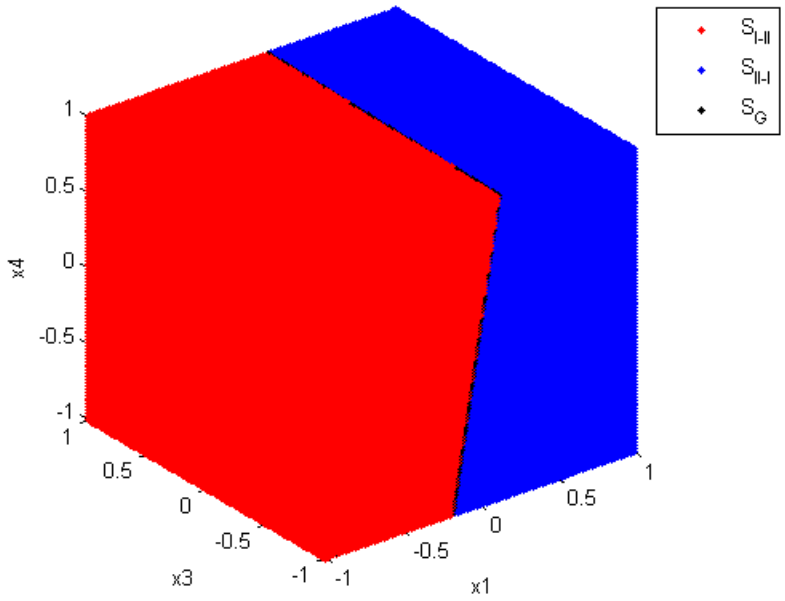

Figure 77: Subsets of L for $0 \le \mu < \mu_{Ieq} (\mu = 0.15)$

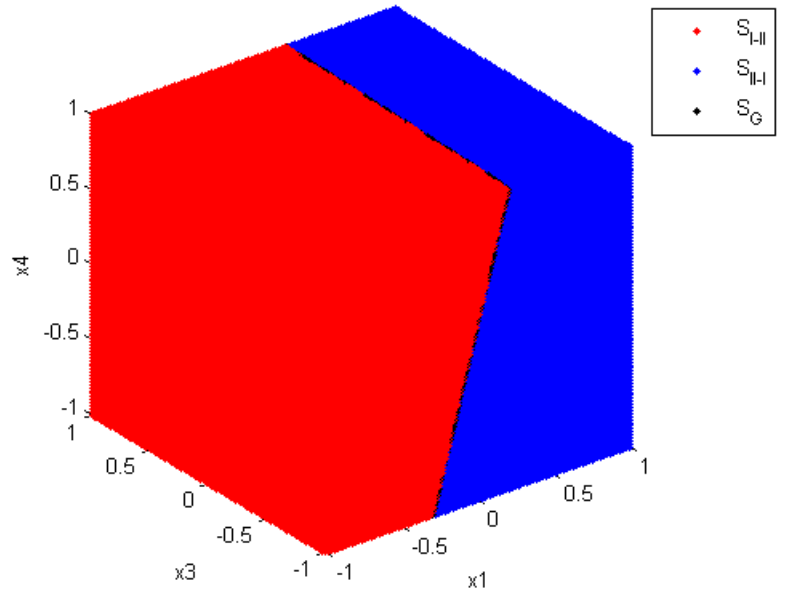

Figure 78: Subsets of L for $\mu_{Ieq} \le \mu \le \mu_{IIeq} (\mu = 0.25)$

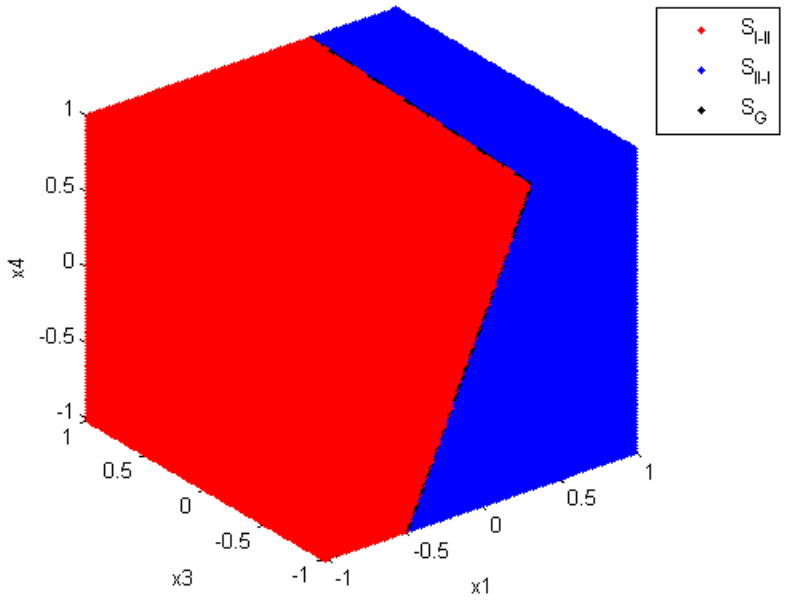

Figure 79: Subsets of L for $\mu_{IIeq} < \mu < \mu_u (\mu = 0.4)$

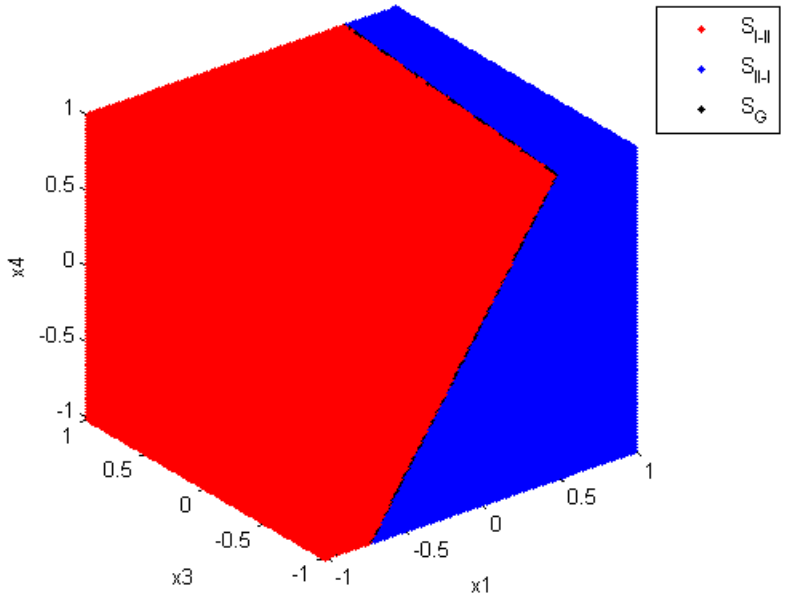

Figure 80: Subsets of L for $\mu_{IIeq} < \mu < \mu_u (\mu = 0.6)$

As shown in Figure 77 through Figure 80 L comprises of the two main sets S_{I-II} and S_{II-I} separated by the grazing set S_G which is acts as a dividing plane in the space of initial conditions belonging to L. As the value of μ changes the slope of this plane changes.

Each of the above represented subsets of L can be further dissected into subsets that describe the evolution of points starting in those sets. Understanding this evolution will lead to drawing relations between each of the above sets and how they will get mapped to one another.

For the evolution of initial conditions belonging to S_{I-II} two main possibilities exist depending on the value of μ with respect to the bilinear system bifurcation diagrams. The solution will either stay bounded or will go unbounded. For values of μ such that $\mu < \mu_{Ieq}$ or $\mu_{Ieq} < \mu < \mu_{IIeq}$ the bounded evolution can be represented in the convergence to the stable equilibrium of System II in case of $\mu_{Ieq} < \mu < \mu_{IIeq}$ or in coming back to the switch line which can take place for either $\mu < \mu_{Ieq}$ or $\mu_{Ieq} < \mu < \mu_{IIeq}$ in which case the condition for either crossing back to System I or grazing and staying in System II cane be checked from S_{II-I} and S_G respectively. For values of μ where $\mu_{IIeq} < \mu < \mu_u$ the bounded behavior can also be checked against S_{II-I} or S_G. In the case of S_{II-I} the behavior can either belong to the stable limit cycle or to the intermittent chaotic behavior.

Similarly the evolution of S_{II-I} can either be bounded or unbounded depending on the value of μ. The bounded behavior can either be converging to System I equilibrium, x_{Ieq}, or going back to the switch line where it will either cross to System II or graze. The only case for which the evolution of points in S_{II-I} will be unbounded is when the eigenvector corresponding to the positive real eigenvalue of System I is exactly parallel to the switch lines between System I and II. Other than that all points in S_{II-I} will hit the switch line as this line is imposing a boundary on System I. This means that there might exist a combination of the value of μ and the initial conditions in S_{II-I} that will lead to trajectories going to infinity parallel to the switch lines. This case will not be considered in this analysis.

The grazing set S_G can also be dissected in similar subsets. In fact the grazing set evolution will have combinations of S_{I-II} and S_{II-I} evolutions. For the purpose of this study only S_{I-II} and S_{II-I} subsets will be formally defined and analyzed since the grazing set is an extension or a combination of those sets evolutions.

The bifurcation diagrams of the system depend on the evolution of points belonging to each set. In the following analysis for each range of values of μ according to the bifurcation diagrams of the system the subsets of S_{I-II} and S_{II-I} will be shown and defined. Figure 81 through Figure 83 show Venn diagrams for L with the subsets of S_{I-II} and S_{II-I} for different values of μ.

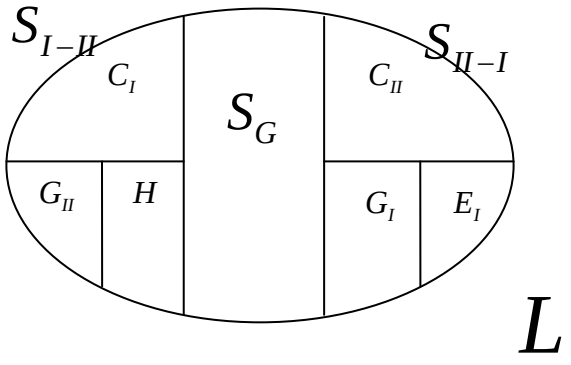

Figure 81: S_{I-II} **and** S_{II-I} **subsets for** $0 \le \mu < \mu_{Ieq}$

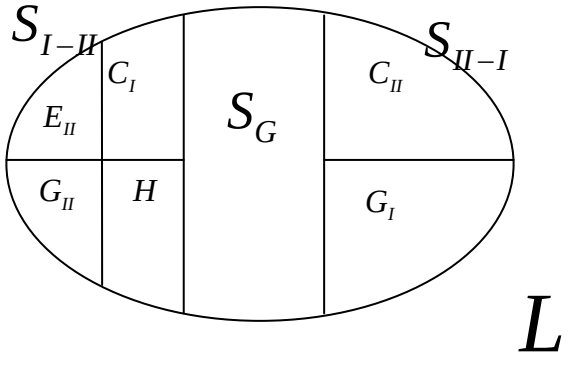

Figure 82: S_{I-II} **and** S_{II-I} **subsets for** $\mu_{Ieq} \le \mu < \mu_{IIeq}$

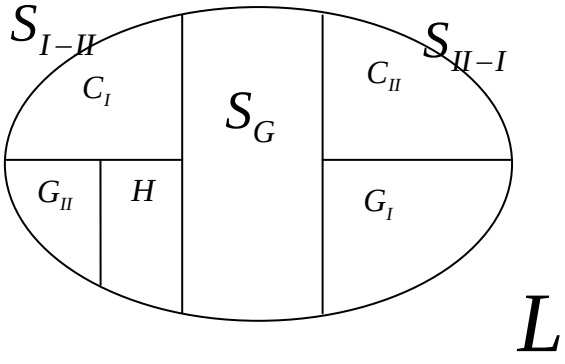

Figure 83: S_{I-II} **and** S_{II-I} **subsets for** $\mu_{IIeq} < \mu < \mu_u$

The following table shows the definitions of the subsets shown in the previous Venn diagrams. The quantity T will be defined as the first instant, if it exists, for which $\mathbf{x}(T) \in L$.

Table 1: Definitions of subsets of S_{I-II} and S_{II-I}

Name	Definition
C_I	$C_I = \{\mathbf{y} \mid \mathbf{y} \in S_{I-II}, \mathbf{x}(T) \in S_{II-I}, \mathbf{x}(0) = \mathbf{y}\}$
E_{II}	$E_{II} = \{\mathbf{y} \mid \mathbf{y} \in S_{I-II}, \lim_{t\to\infty} \mathbf{x}(t) = \mathbf{x}_{IIeq}, \mathbf{x}(0) = \mathbf{y}, \mathbf{x}(t > 0) \notin L\}$
G_{II}	$G_{II} = \{\mathbf{y} \mid \mathbf{y} \in S_{I-II}, \mathbf{x}(T) \in S_G, \mathbf{x}(0) = \mathbf{y}\}$
H	$H = \{\mathbf{y} \mid \mathbf{y} \in S_{I-II}, \lim_{t\to\infty} \lVert\mathbf{x}(t)\rVert = \infty, \mathbf{x}(0) = \mathbf{y}, \mathbf{x}(t > 0) \notin L\}$
C_{II}	$C_{II} = \{\mathbf{y} \mid \mathbf{y} \in S_{II-I}, \mathbf{x}(T) \in S_{I-II}, \mathbf{x}(0) = \mathbf{y}\}$
E_I	$E_I = \{\mathbf{y} \mid \mathbf{y} \in S_{II-I}, \lim_{t\to\infty} \mathbf{x}(t) = \mathbf{x}_{Ieq}, \mathbf{x}(0) = \mathbf{y}\}$
G_I	$G_I = \{\mathbf{y} \mid \mathbf{y} \in S_{II-I}, \mathbf{x}(T) \in S_G, \mathbf{x}(0) = \mathbf{y}\}$

As shown in the table C_I describes the subset of S_{I-II} for which after a finite time T, defined previously, the trajectory will come back to the switch line and cross it to System I. E_{II} describes the subset of S_{I-II} for which the trajectory will converge to System II equilibrium and will not come back to the switch line. G_{II} is a subset of S_{I-II} for which the trajectory will come back to the switch line and graze to come back to System II. H is the subset that trajectories will go unbounded. Similarly, C_{II} is a subset of S_{II-I} for which the trajectory will come back to the switch line and cross to System II.

E_I is the subset for which the trajectories will converge to System I equilibrium and never cross the line again and finally G_I is the subset for which trajectories will come back to the switch line and graze to come back to System I.

The following set of figures shows numerical simulation results that show the distribution of some of the above mentioned subsets in the initial conditions space.

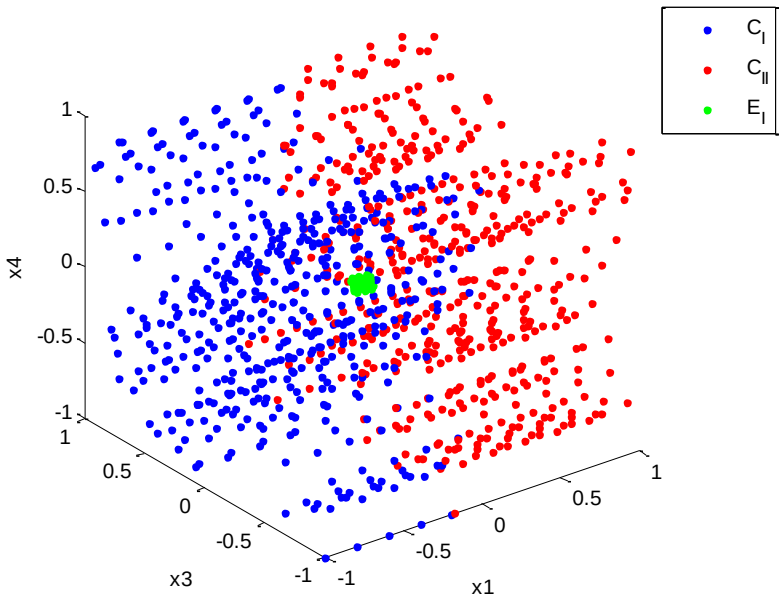

Figure 84: Initial conditions subsets for $0 \le \mu < \mu_{Ieq} (\mu = 0.15)$

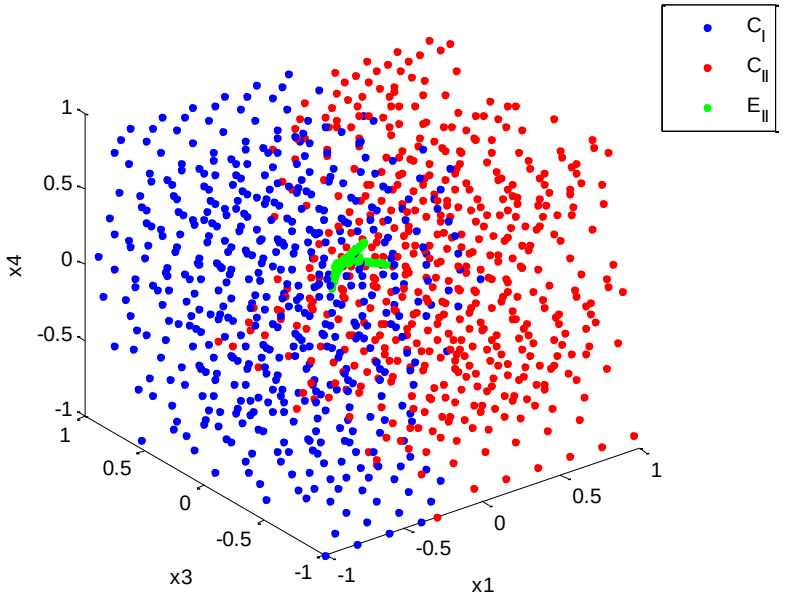

Figure 85: Initial conditions subsets for $\mu_{Ieq} < \mu < \mu_{IIeq} (\mu = 0.25)$

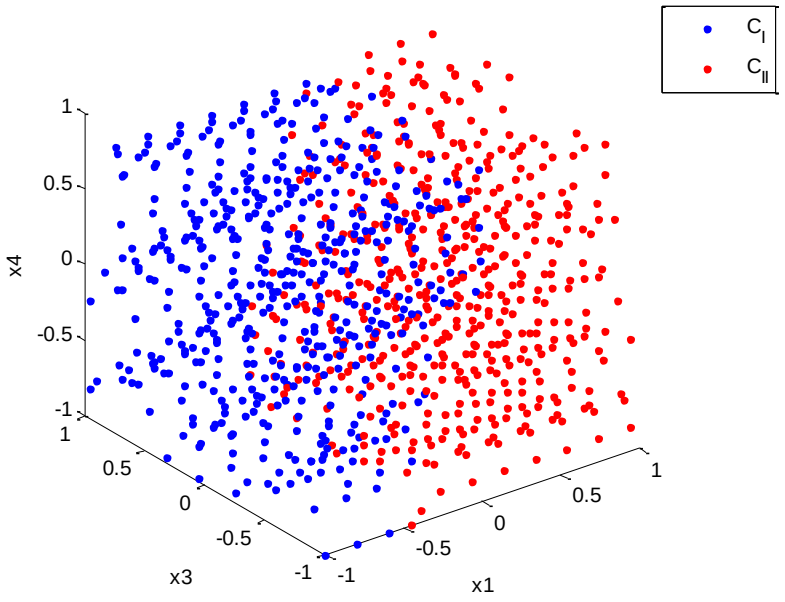

Figure 86: Initial Conditions subsets for $\mu_{IIeq} < \mu < \mu_u (\mu = 0.4)$

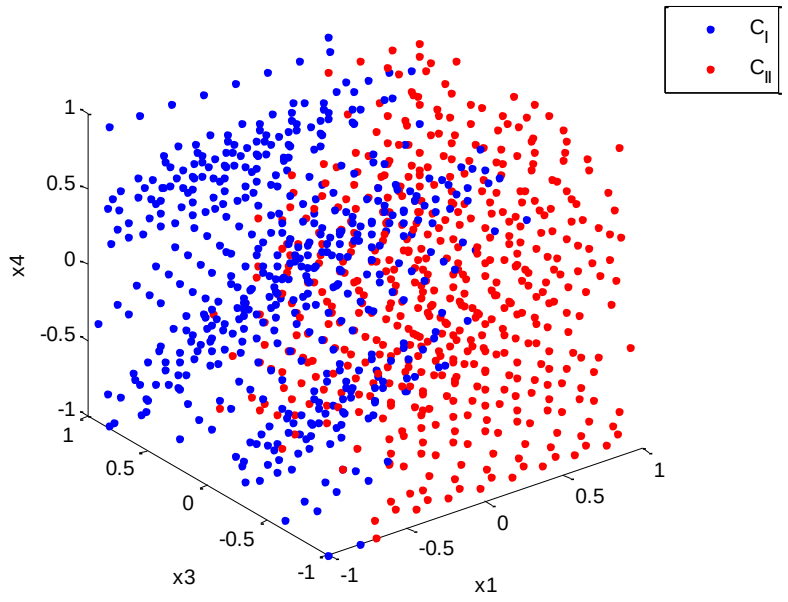

Figure 87: Initial conditions subsets for $\mu_{IIeq} < \mu < \mu_u (\mu = 0.6)$

In Figure 84 through Figure 87 most of the sets presented in Table 1 are shown except for H, G_I and G_{II}. In case of the subset H, the values of initial conditions in L that goes to infinity will exceed the bounds of the numerical simulations and hence it was not shown in the above presented figures. In case of G_I and G_{II} this required implementing a much finer grid of points that to capture points returning back to L on exactly the separating plane presented in Figure 77 through Figure 80.

Based on the above subsets and their associated behavior we can define maps that take from one subset to the other. Two of those maps are,

$$M_1 : C_I \rightarrow C_{II} \tag{3.51}$$

$$M_2 : C_{II} \to C_I \tag{3.52}$$

equations (3.51) and (3.52) define two maps M_1 and M_2. M_1 takes from the subset C_I where trajectories cross from System I to II to the subset C_{II} where trajectories cross from System II to I whereas M_{II} that takes from C_{II} to C_I. The system dynamics can be examined by the interaction of those two maps as shown in the following set of figures.

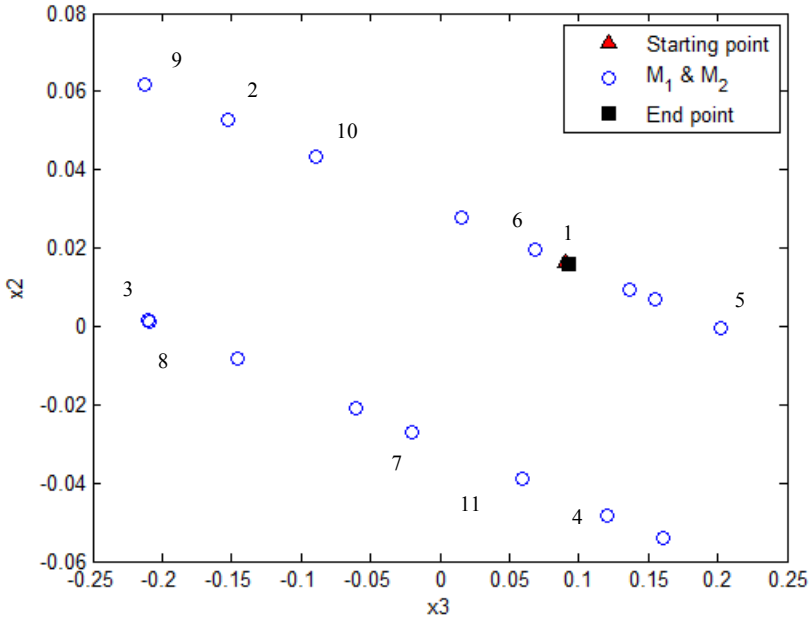

Figure 88: Mapping of a point in C_I for $\mu = 0.15$

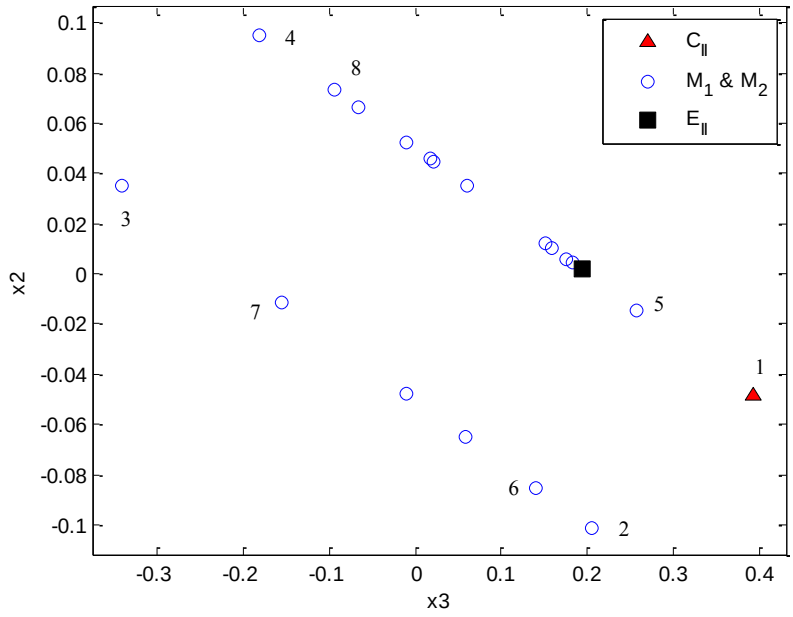

Figure 89: Mapping of a point in C_{II} for $\mu = 0.25$

The numbers shown in each figure indicates the number of iterations for example the starting point is 1 then it get mapped to 2 and then 2 gets mapped to 3 and so on. In Figure 88 the final point, black square, indicate that the trajectory will not come back to the switch line and will converge to the local equilibrium point of System I. In case of Figure 89 the trajectory will converge to the equilibrium of System II.

The maps defined in (3.51) and (3.52) are a very useful tool in understanding the global system behavior. Those maps combined with the various sets defined in Table 1 can be used to verify the system behavior generated from the continuation tools and numerical simulations of the system. In this research project this analysis will not be conducted, instead a general idea will be presented on how to use the work presented here to further analyze the system. By using the sets defined previously for initial

conditions starting in L, those points can be checked for the various subsets of L presented in Table 1. An algorithm can be developed to use those points and by applying an optimization tool those points can be checked against the various sets in Table 1 and against each other. Meaning that if the mapping leads to the same point after a number of iterations the simulation should jump to the next point until all the points are covered. After the simulation is over the array of points in L can be checked to see if all the points belong to a predefined set. This can be used as verification to the bifurcation diagrams and it also can lead to discovering some global behavior that the tools used in this research did not unravel.

Combining the information obtained from defining the sets of initial conditions and the bifurcation diagrams shown in the previous section Poincaré sections can be shown to show the system periodic behavior. Selecting the same value of μ for which a limit cycle exists the Poincaré section is shown for the point of intersection of the trajectory with the switching line. As shown the point gets projected into itself indicating a limit cycle oscillation. Figure 90 shows this for a point on the switch that lies on the limit cycle.

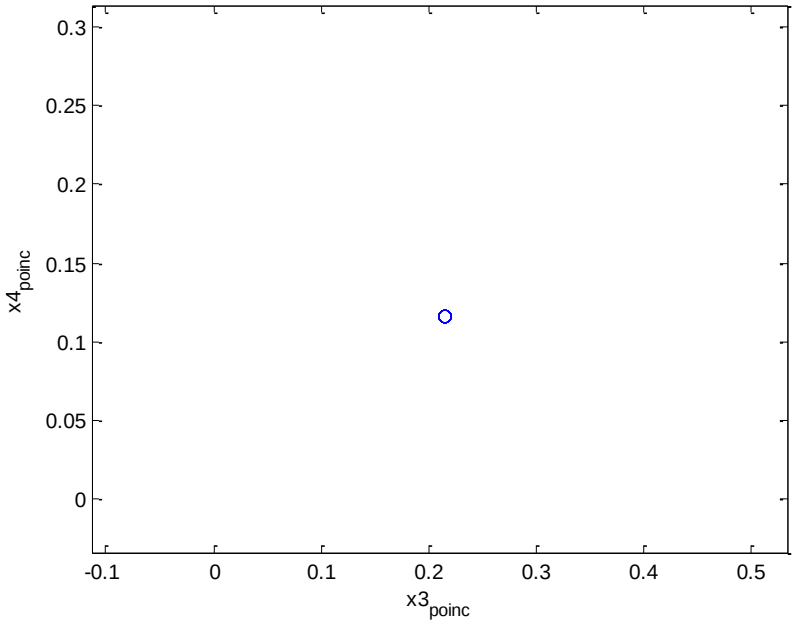

Figure 90: Poincaré section at $\mu = 0.4$

For the chaotic solution presented earlier the following Poincaré section is shown Figure 91.

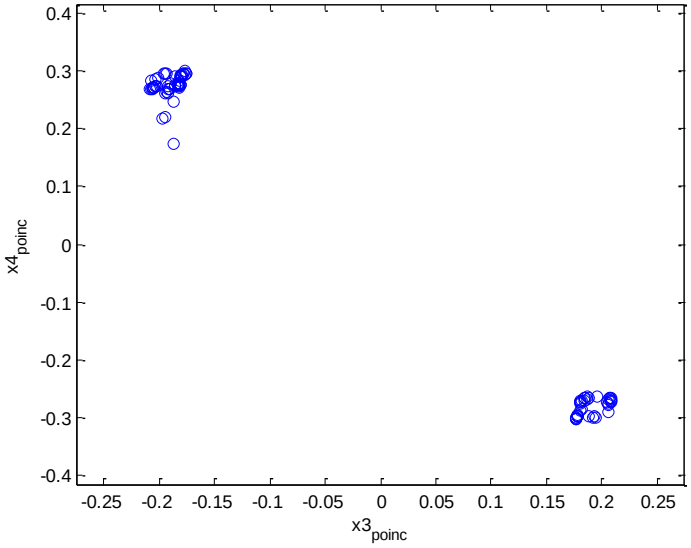

Figure 91: Poincaré section at $\mu = 0.65$

As shown in Figure 91 the intermittent behavior of the system can be understood from the existence of points in both corners of the above plots indicating the jump that takes place from one boundary to the other also the existence of a cluster of points in each corner indicates that trajectories oscillates periodically for a period of time till they jump. It should be noted that none of the points coincide which indicates the absence of pure periodic behavior. Figure 92 shows this behavior in the x3-x2 plane.

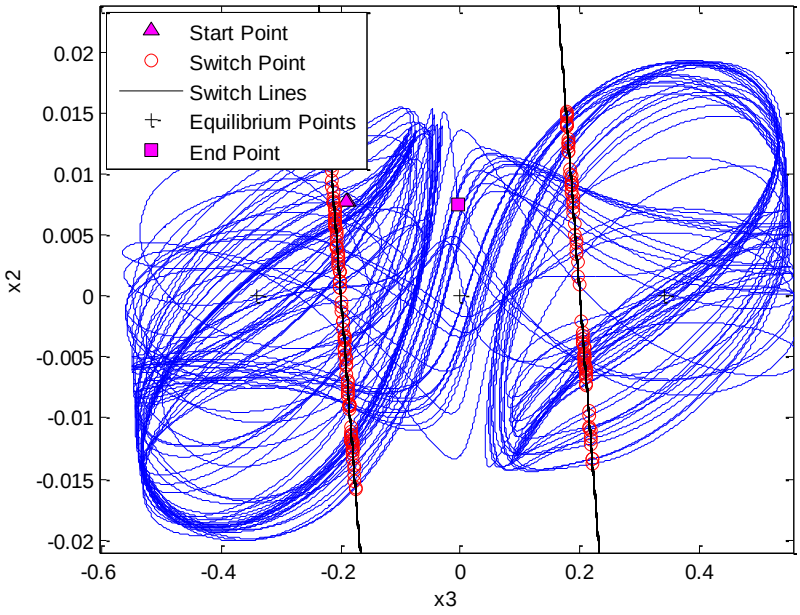

Figure 92: Chaotic behavior x3-x2 plane at $\mu = 0.65$

This concludes the analysis of the bilinear model. In this analysis the equilibrium points of the system were computed and their stability analyzed. The system bifurcation diagrams were introduced and several phase portraits and time evolutions plots were presented as examples for the system behavior at different values of the bifurcation parameter. The chaotic behavior of the system was also observed and presented in the intermittent route to chaos. The results from the bilinear system are compared with numerical simulations using the continuous aerodynamic model and the both generate the same system response. This is a good indication that the piecewise linear approximation can be utilized to explore and analyze such systems. This has the advantage of applying the linear systems analysis techniques to analyze complicate nonlinear systems which can provide more understanding of dynamical systems

behavior. Sets of initial conditions are defined and their behavior analyzed. Numerical simulations were presented to show some of those sets and the mapping between them. Finally Poincaré sections describing both the periodic and the chaotic solutions of the systems are shown.

4. CONCLUSION, DISCUSSION AND FUTURE WORK

4.1 Conclusion and Discussion of Results

Nonlinear analysis of aeroelastic systems is a topic that has been widely covered in the literature. The nonlinearities introduced to aeroelastic systems can be either aerodynamic nonlinearities, structural nonlinearities or a mixture of both. Many models were introduced to address these nonlinearities and study their effects on aeroelastic systems. In this research project aerodynamic nonlinearities arising from the stall behavior of an aeroelastic system were studied. A piecewise linear model utilizing experimental data for the lift coefficient versus the angle of attack for a NACA 0012 airfoil was proposed and analyzed.

The piecewise linear model was proposed to describe the lift coefficient as a function of the effective angle of attack. A model consisting of 4 linear portions covering angles from 0 to 45˚ was first used as a general model. The equations of motion for the system were introduced and nondimensionalized. The nondimensionalizing of the equations introduced both time and length scales. Those scales were used to nondimensionalize and scale the 2 DOF of the system, pitch and plunge, along with the freestream velocity which defines the bifurcation parameter of the system.

A simplified bilinear model was then extracted from the full piecewise linear model and analyzed. Equilibrium points of the bilinear model were found analytically and represented as a function of the bifurcation parameter. The stability of those equilibrium points was then checked using the Routh-Hurwtiz stability criteria and the

Liénard-Chipart theorem. From the stability checks the values of the non dimensional freestream velocity at which equilibrium points loses stability are calculated.

Bifurcation diagrams of the system are then shown utilizing MATCONT, Dhooge et al. (2003). Two types of bifurcations are analyzed; the border collision bifurcation which described the existence of System II equilibrium and the loss of stability of System I equilibrium at the boundary between System I and System II and the rapid bifurcation which is similar to a degenerate Hopf bifurcation in continuous systems but has some differences in the amplitude behavior of the limit cycle. Chaotic behavior was also observed in the intermittent route to chaos. The system exhibited jumps from periodic to chaotic behavior and as the bifurcation parameter increases the chaotic behavior becomes more dominant and the periodic behavior vanished.

Finally sets of initial conditions of the system are introduced to describe the various system behavior examined in the bifurcation diagrams and numerical simulation. Those sets describe initial conditions starting on the boundary between System I and II and how they get mapped with respect to each other. Numerical results were also presented to show those sets and the mapping between them. By defining and understanding the behavior of those sets the system local and global behavior is examined and analyzed.

The above described the nonlinear analysis that was conducted to understand the bilinear system behavior. As a result the local and global system behavior was analyzed and understood. Interesting phenomena was observed in this analysis such as the intermittent chaotic behavior and the jumps between the system boundaries associated

with it. Also the analysis introduced new type of bifurcations that are properties to piecewise systems such as the border collision and the rapid bifurcations.

It is important to highlight that some of the results presented in this research exceed the boundaries of the physical validity of the model for an airfoil. For the model to accurately go in line with the physics of the problem the bilinear model should be bounded till a value of $\alpha_{eff} \approx 0.3 rad$. Nevertheless the analysis was conducted on the bilinear model assuming no restrictions on the range of the angle of attack. This enabled us to understand the full behavior of such models. Also it has to be noted that some of the system interesting behavior, e.g. rapid bifurcation and existence of limit cycles, takes place in the physically valid region of the model.

Hence the bilinear model can be considered as a first step to understand how piecewise linear systems can be applied to physical problems and how those systems can be analyzed. In case of the aeroelastic problem presented in this research and to cover the physics of the whole model more linear portions can be added to cover a larger span of the angles of attack. The same analysis done for the bilinear model can be reapplied to a model with three or four linear pieces. There also exist systems that can utilize this bilinear analysis as it covers the whole physics of those problems. In the literature one of the systems that can get a full advantage of such bilinear analysis is the Wien bridge oscillator presented in Kriegsmann (1987) and Freire et al. (1999).

4.2 Future Work

As previously mentioned this dynamical analysis can be considered a first step in providing a complete dynamical analysis for piecewise linear systems. The scope of the analysis presented was limited to a bilinear model. This can be extended to more complicated model with more linear portions such as the full piecewise linear model presented for the 2 DOF aeroelastic system analyzed in this research.

More refinements can be added to the piecewise linear model by introducing a model that has finite radii of curvature in the transitional regions at the boundaries of each linear portion of the model. The introduction of a smoother function at these transitions has the advantage of emulating the actual physics of the problem as the transitions wouldn't happen abruptly but would take some time to jump from one region to the other.

The chaotic behavior of the system was presented here as the intermittent route to chaos but this can be further analyzed to show the full chaotic behavior of the system and also to show the transition between periodic and chaotic solution as the bifurcation parameter is varied. Also the coexistence of period and chaotic solutions can be further analyzed and examined for the sensitivity of initial conditions to either solution.

Further analysis can be done on the sets of initial conditions defined in Table 1. Analyzing the dimensions of those sets is a topic that was not covered in the analysis. Also how those sets dimensions would be of any impact on the system dynamics or the mapping between one set and the other. Another point is the assumption of the bounded behavior of System I and that trajectories wouldn't go unbounded instead they will

always come back to the switch line between System I and II. A set can be defined to include the unbounded behavior of System I and although this set can be very small or even nonexistent it can have a great impact on the system dynamics. Finally more investigation of those sets and the mapping between them can be implemented to verify the bifurcation diagrams and to show any global behavior of the system that was not captured by the tools at hand.

Finally, the proposed aeroelastic system was assumed to have the center of mass collocated with the elastic axis. This assumption enabled us to have one bifurcation parameter which was the freestream velocity. A more general system can be analyzed by introducing a distance between the elastic axis and the center of mass of the airfoil. This distance will be a second bifurcation parameter and will produce more general results that can be applied to more general aeroelastic systems.

REFERENCES

Andronov, A. A., Vitt, A. A., Khaikin, S. E., 1966. *Theory of Oscillators*. Pergamon Press LTD, New York.

Dhooge, A., Govaerts, W., Kuznetsov, Y. A., 2003, "MATCONT: A MATLAB package for numerical bifurcation analysis of ODEs." *ACM Trans. Math. Softw.* **29(2),** 141-164.

Di Bernardo, M., Budd, C. J., Champneys, A. R., Kowalczyk, P., 2008, "Piecewise-smooth dynamical systems: theory and applications." *Springer Verlag*, London.

Dowell, E. H., Edwards, J., Strganac,T. W., 2003, "Nonlinear aeroelasticity." *Journal of Aircraft* **40(5),** 857-874.

Dubois, M., Rubio, M. A., Berge, P., 1983, "Experimental evidence of intermittencies associated with a subharmonic bifurcation." *Physical Review Letters* **51(16),** 1446-1449.

Freire, E., Ponce, E., Ros, J., 1999, "Limit cycle bifurcation from center in symmetric piecewise-linear systems." *International Journal of Bifurcation and Chaos* **9(5),** 895-907.

Gantmacher, F. R., 1959, *The Theory of Matrices Vol. 2*, Chelsea Publishing Company, New York.

Gilliatt, H. C., 1997, *Investigations of Internal Resonance Phenomena and Related Nonlinear Pathologies in Aeroelastic Systems*. Master thesis, Texas A&M University, College Station.

Gilliatt, H. C., Strganac, T. W., Kurdila, A. J., 1997, "Nonlinear aeroelastic response of an airfoil." *AIAA Paper* 97-0459.

Gilliatt, H. C., Strganac, T. W., Kurdila, A. J., 2003, "An investigation of internal resonance in aeroelastic systems." *Nonlinear Dynamics* **31(1),** 1-22.

Goncalves, J. M., Megretski, A., Dahleh, M. A., 2003, "Global analysis of piecewise linear systems using impact maps and surface Lyapunov functions." *IEEE Transactions on Automatic Control* **48(12),** 2089-2106.

Hammer, P. W., Platt, N., Hammel, S. M., Heagy, J. F., Lee, B. D, 1994. "Experimental observation of on-off intermittency." *Physical Review Letters* **73(8),** 1095-1098.

Hayashi, H., Ishizuka, S., Hirakawa, K., 1983. "Transition to chaos via intermittency in the Onchidium pacemaker neuron." *Physics Letters A* **98(8-9),** 474-476.

Hilborn, R. C., 2000. *Chaos and Nonlinear Dynamics: An Introduction for Scientists and Engineers.* Oxford University Press, New York.

Huang, J. Y., Kim, J. J., 1987. "Type-II intermittency in a coupled nonlinear oscillator: experimental observation." *Physical Review A* **36(3),** 1495-1497.

Jeffries, C., Perez, J., 1982. "Observation of a Pomeau-Manneville intermittent route to chaos in a non-linear oscillator." *Physical Review A* **26(4),** 2117-2122.

Kalmár-Nagy, T., 2007. "Dynamics of a relay oscillator with hysteresis." *46th IEEE Conference on Decision and Control*, New Orleans, LA, pp. 3245-3251.

Kriegsmann, G. A., 1987. "The rapid bifurcation of the Wien bridge oscillator." *IEEE Transactions on Circuits and Systems* **34(9),** 1093-1096.

Lee, B. H. K., Price, S. J., Wong, Y.S., 1999. "Nonlinear aeroelastic analysis of airfoils: bifurcation and chaos." *Progress in Aerospace Sciences* **35(3),** 205-334.

Leine, R. I., 2006. "Bifurcations of equilibria in non-smooth continuous systems." *Physica D-Nonlinear Phenomena* **223(1),** 121-137.

Mahfouz, I. A., Badrakhan, F., 1990a. "Chaotic behavior of some piecewise-linear systems .1. Systems with set-up spring or with unsymmetric elasticity." *Journal of Sound and Vibration* **143(2),** 255-288.

Mahfouz, I. A., Badrakhan, F., 1990b. "Chaotic behavior of some piecewise-linear systems, .2. Systems with clearance." *Journal of Sound and Vibration* **143(2),** 289-328.

McAlister, K. W., Lambert, O., Petot, D., 1984. "Application of the ONERA model of dynamic stall." NASA Technical Paper 2399.

O'Neil, T. G., Gilliatt, H. C., Strganac, T. W., 1996. "Investigations of aeroelastic response for a system with continuous structural nonlinearities." *AIAA Paper* 96-1390

O'Neil, T. G., Strganac, T. W., 1998a. "Aeroelastic response of a rigid wing supported by nonlinear springs." *Journal of Aircraft* **35(4),** 616-622.

O'Neil, T.G., Strganac, T.W., 1998b. "An experimental investigation of nonlinear aeroelastic response." *AIAA Journal of Aircraft*, **35(4),** 616-622.

Platt, N., Spiegel, E. A., Tresser, C., 1993. "On-Off intermittency: a mechanism for bursting." *Physical Review Letters* **70(3),** 279-282.

Pratap, R., Mukherjee, S., Moon, F. C., 1994a. "Dynamic behavior of a bilinear hysteretic elastoplastic oscillator, .1. Free oscillations." *Journal of Sound and Vibration* **172(3),** 321-337.

Pratap, R., Mukherjee, S., Moon, F. C., 1994b. "Dynamic behavior of a bilinear hysteretic elastoplastic oscillator .2. Oscillations under periodic impulse forcing." *Journal of Sound and Vibration* **172(3),** 339-358.

Price, S. J., Alighanbari, H., Lee, B. H. K., 1995. "The aeroelastic response of a 2-dimensional airfoil with bilinear and cubic structural nonlinearities." *Journal of Fluids and Structures* **9(2),** 175-193.

Reddy, T. S. R., Kaza, K. R.V., 1987. "A comparative study of some dynamic stall models." NASA TM-88917.

Seiranyan, A. P., 1994. "Collision of eigenvalues in linear oscillatory systems." *Journal of Applied Mathematics and Mechanics* **58(5),** 805-813.

Shaw, S. W., Holmes, P. J., 1983. "A periodically forced piecewise linear-oscillator." *Journal of Sound and Vibration* **90(1),** 129-155.

Sheldahl, R. E., Klimas, P. C., 1981. "Aerodynamic characteristics of seven symmetrical airfoil sections through 180-degree angle of attack for use in aerodynamic analysis of vertical axis wind turbines," SANDIA Report, SAND80-2114.

Strogatz, S. H., 2000. *Nonlinear Dynamics and Chaos: with Applications to Physics, Biology, Chemistry and Engineering*. Westview Press, Cambridge, MA.

Tang, D. M., Dowell, E. H., 1992. "Flutter and stall response of a helicopter blade with structural nonlinearity." *Journal of Aircraft* **29(5),** 953-960.

Tang, D. M., Dowell, E. H., 1993. "Comparison of theory and experiment for nonlinear flutter and stall response of a helicopter blade." *Journal of Sound and Vibration* **165(2),** 251-276.

Ueda, T., Dowell, E. H., 1984. "Flutter analysis using nonlinear aerodynamic forces." *Journal of Aircraft* **21(2),** 101-109.

Weaver, JR., W., Timoshenko, S. P., Young, D.H., 1990. *Vibration Problems in Engineering*. Wiley, New York, NY.

Woolston, D. S., Runyan, H. L., Andrews, R. E., 1957. "An investigation of effects of certain types of structural nonlinearities on wing and control surface flutter." *Journal of the Aeronautical Sciences* **24(1),** 57-63.

Yeh, W. J., Kao, Y. H., 1982. "Universal scaling and chaotic behavior of a Josephson-Junction analog." *Physical Review Letters* **49(26),** 1888-1891.

Zhusubaliyev, Z. T., Mosekilde, E., 2003. *Bifurcations and Chaos in Piecewise-Smooth Dynamical Systems*. World Scientific, River Edge, NJ.

APPENDIX A

Table 2: System parameters values and dimensions, Gilliatt et al. (1997)

Parameter	Description	Value	Units
b	Semichord of the wing	0.1064	m
s	Span	0.6	m
m	mass of the system	12	Kg
k_y	Structural spring constant for vertical motion	2844.4	N/m
k_α	Structural spring constant for rotational motion	2.82	N.m/rad
c_y	Viscous damping coefficient of plunge DOF	27.43	Kg/s
c_α	Viscous damping coefficient for pitch DOF	0.036	$Kg.m^2 / s$
I_{cg}	Mass moment of inertia about center of mass	0.0433	$Kg.m^2$
ρ	Air density	1.2	Kg / m^3
M	Moment		N.m
L	Lift		N
α	Displacement coordinate for pitch		rad
y	Displacement coordinate for plunge		m
U	Freestream velocity		m/s

Table 3: Data points, Sheldahl and Klimas (1981)

α_{eff}		C_l **(Lift Coefficient)**
Degrees	**Radians**	
0	0	0
1	0.017	0.1
2	0.035	0.22
3	0.052	0.33
4	0.069	0.44
5	0.087	0.55
6	0.104	0.66
7	0.122	0.77
8	0.139	0.88
9	0.157	0.9661
10	0.175	1.0512
11	0.192	1.1097
12	0.209	1.1212
13	0.227	1.0487
14	0.244	0.8846
15	0.262	0.7108
16	0.279	0.606

Table 3: Continued

α_{eff}		C_l **(Lift Coefficient)**
Degrees	**Radians**	
17	0.297	0.5906
18	0.314	0.603
19	0.332	0.6334
20	0.349	0.6716
21	0.367	0.7162
22	0.384	0.7613
23	0.401	0.8097
24	0.419	0.8589
25	0.436	0.9093
26	0.454	0.9618
27	0.471	1.0144
30	0.524	0.915
35	0.611	1.02
40	0.698	1.075
45	0.785	1.085

Table 4: Continuous aerodynamic model parameters

Parameter	Description	Value
a_1	Coefficient of the first sin term	0.8799
b_1	Coefficient of α_{eff} in the first sin term	3.788
c_1	Constant in the first sin term	0.403
a_2	Coefficient of the second sin term	0.2939
b_2	Coefficient of α_{eff} in the second sin term	20.68
c_2	Coefficient of α_{eff} in the second sin term	-2.004
a_3	Coefficient of the third sin term	0.07447
b_3	Coefficient of α_{eff} in the third sin term	42.96
c_3	Coefficient of α_{eff} in the third sin term	-1.08
a_4	Coefficient of the fourth sin term	0.02258
b_4	Coefficient of α_{eff} in the fourth sin term	65.88
c_4	Coefficient of α_{eff} in the fourth sin term	-0.4469
C	Constant to adjust curve to go through origin	$C = -\sum_{i=1}^{4} a_i \sin(c_i) = -0.0029$

Table 5: Piecewise linear aerodynamic model parameters

Parameter	Description	Value
c_o	Slope of the first linear piece of the lift model C_{lI}	5.932
c_1	Slope of the second linear piece of the lift model C_{lII}	-6.846
c_2	Constant of the second linear piece of the lift model C_{lII}	2.56
c_3	Slope of the third linear piece of the lift model C_{lIII}	2.662
c_4	Constant of the third linear piece of the lift model C_{lIII}	-0.2515
c_5	Constant of the final piece of the lift coefficient C_{lIV}	1.0029
α_{stall}	Stall angle of attack (switching angle between C_{lI} and C_{lII})	0.2 radians
α_{sw}	Switching angle between C_{lII} and C_{lIII}	0.2957 radians
α_{sat}	Saturation angle of attack (between C_{lIII} and C_{lIV})	0.4712 radians

Table 6: Non dimensional quantities values

Non dimensional quantity	Expression	Dimensional check	Value
γ_1	$T\frac{c_y}{m_T}$	$s\frac{kg/s}{kg}=1$	$(2.286(\frac{1}{s}))$T
γ_2	$L\frac{\rho bs}{m}$	$m\frac{kg.m.m}{m^3.kg}=1$	$(0.00638(\frac{1}{m}))$L
γ_3	$T^2\frac{k_y}{m_T}$	$s^2\frac{kg.m}{s^2.m.kg}=1$	$(237.03(\frac{1}{s^2}))T^2$
γ_4	$T\frac{c_\alpha}{I_{cg}}$	$s\frac{kg.m^2}{s.kg.m^2}=1$	$(0.8314(\frac{1}{s}))$T
γ_5	$T^2\frac{k_\alpha}{I_{cg}}$	$s^2\frac{kg.m^2}{s^2.kg.m^2}=1$	$65.13(\frac{1}{s^2})\,T^2$
γ_6	$L^2\frac{\rho b^2 s}{I_{cg}}$	$m^2\frac{kg.m^2.m}{m^3.kg.m^2}=1$	$(0.1882(\frac{1}{m^2}))L^2$

Table 7: Non dimensional parameters

Non dimensional parameter	Expression	Dimensional check	Value
p_1	$\frac{c_y}{\sqrt{m_T k_y}}$	$\frac{kg}{s}.\frac{1}{\sqrt{\frac{kg}{s^2}.kg}}=1$	0.15
p_2	$\frac{\sqrt{\rho I_{cg} s}}{m}$	$\frac{\sqrt{\frac{kg}{m^3}.kg.m^2.m}}{kg}=1$	0.015
p_3	$\frac{c_\alpha}{I_{cg}}\sqrt{\frac{m}{k_y}}$	$\frac{kg.m^2}{s.kg.m^2}\sqrt{\frac{kg.s^2}{kg}}=1$	0.054
p_4	$\frac{k_\alpha m}{I_{cg} k_y}$	$\frac{kg.\frac{m^2}{s^2}.kg}{\frac{kg}{s^2}.kg.m^2}=1$	0.275

APPENDIX B

Numerical Routh – Hurwitz Stability Analysis

The Hurwitz determinants in (3.20) are computed as shown.

For System I

$$\Delta_1 = p_2 c_o \mu + p_1 + p_3 \tag{B.1}$$

$$\Delta_2 = -p_2 c_o^2 \mu^3 + \left(p_2^2 p_3 c_o^2 - p_3 c_o \right) \mu^2 + \left(p_2 p_3^2 c_o + 2 p_1 p_2 p_3 c_o + p_2 c_o \right) \mu + p_3 p_4 + p_3^2 p_3 + p_1 \tag{B.2}$$

$$\begin{aligned} \Delta_3 = {} & p_1 p_2 c_o^3 \mu^5 + \left(-p_2^2 p_4 c_o^3 + p_1 p_3 c_o^2 - p_1 p_2^2 p_3 c_o^3 + p_2^2 c_o^3 \right) \mu^4 \\ & + \begin{pmatrix} -p_1 c_o^2 p_4 p_2 - p_3^2 p_2 c_o^2 p_1 - 2 p_3 p_2 c_o^2 p_1^2 + p_2^3 c_o^3 p_3 p_4 - p_3 c_o^2 p_4 p_2 \\ + p_3 c_o^2 p_2 + c_o^2 p_2 p_2 \end{pmatrix} \mu^3 \\ & + \begin{pmatrix} -p_3^2 p_1^2 c_o + 3 p_1 p_3 p_2^2 c_o^2 p_4 - p_3 p_1^3 c_o - 2 p_3 p_4 c_o p_1 + 2 c_o p_1 p_3 \\ + p_3^2 p_2^2 c_o^2 p_4 + p_2^2 c_o^2 p_3^2 \end{pmatrix} \mu^2 \\ & + \begin{pmatrix} p_3 p_2 c_o + 2 p_3^2 p_1 p_4 p_2 c_o + p_3 p_1^2 p_4 p_2 c_o + p_3 p_4^2 p_2 c_o + p_3^3 p_2 c_o \\ + 2 p_1 p_3^2 p_2 c_o - 2 p_4 p_2 c_o p_3 \end{pmatrix} \mu \\ & + p_3 p_1 + p_3 p_1^3 p_4 + p_3^2 p_1^2 p_4 - 2 p_4 p_1 p_3 + p_3 p_4^2 p_1 + p_3^3 p_1 + p_3^2 p_1^2 \end{aligned} \tag{B.3}$$

$$
\begin{aligned}
\Delta_4 = & -p_2 c_o^4 p_1 \mu^7 + \left(p_2^2 c_o^4 p_3 p_1 - p_3 c_o^3 p_1 - p_2^2 c_o^4 + p_2^2 c_o^4 p_4 \right) \mu^6 \\
& + \begin{pmatrix} -p_2 c_o^3 p_1 + p_3^2 p_2 c_o^3 p_1 + 2 p_1 c_o^3 p_4 p_2 + 2 p_3 p_2 c_o^3 p_1^2 \\ -p_2^3 c_o^4 p_3 p_4 + p_3 c_o^3 p_4 p_2 - p_3 p_2 c_o^3 \end{pmatrix} \mu^5 \\
& + \begin{pmatrix} p_3 p_1^3 c_o^2 + 3 p_3 p_4 c_o^2 p_1 + p_2^2 c_o^2 p_4 - p_3^2 p_2^2 c_o^3 p_4 + p_3^2 p_1^2 c_o^2 \\ -p_2^2 c_o^3 p_4^2 - p_2^2 c_o^3 p_3^2 - 4 p_1 p_3 p_2^2 c_o^3 p_4 - 2 p_3 c_o^2 p_1 \end{pmatrix} \mu^4 \\
& + \begin{pmatrix} 3 p_3 c_o^2 p_4 p_2 + p_1 c_o^2 p_4 p_2 + p_2^3 c_o^3 p_3 p_4^2 - p_3 c_o^2 p_2 - 3 p_3^2 p_1 p_4 p_2 c_o^2 \\ -p_3^3 p_2 c_o^2 - 2 p_3^2 p_2 c_o^2 p_1 - 2 p_3 p_4^2 p_2 c_o^2 - 5 p_3 p_1^2 p_4 p_2 c_o^2 - p_1 p_4^2 p_2 c_o^2 \end{pmatrix} \mu^3 \\
& + \begin{pmatrix} -p_3^2 p_1^2 c_o + p_3^2 p_2^2 c_o^2 p_4 - c_o p_1 p_3 + p_3^2 p_2^2 c_o^2 p_4^2 + 4 p_3 p_4 c_o p_1 \\ -3 p_3 p_4^2 p_1 c_o - 2 p_3 p_1^3 p_4 c_o + 3 p_1 p_3 p_2^2 c_o^2 p_4^2 - p_3^3 p_1 c_o - 2 p_3^2 p_1^2 p_4 c_o \end{pmatrix} \mu^2 \\
& + \begin{pmatrix} p_3^3 p_2 c_o p_4 + 2 p_3^2 p_1 p_4^2 p_2 c_o + 2 p_3^2 p_1 p_4 p_2 c_o \\ +3 p_3 p_1^2 p_4^2 p_2 c_o + p_3 p_4^3 p_2 c_o + p_4 p_2 c_o p_3 - 2 p_3 p_4^2 p_2 c_o \end{pmatrix} \mu \\
& - 2 p_3 p_4^2 p_1 + p_3^2 p_1^2 p_4 + p_3 p_1^3 p_4^2 + p_4 p_1 p_3 + p_3^3 p_1 p_4 + p_3^2 p_1^2 p_4^2 + p_3 p_4^3 p_1
\end{aligned}
\tag{B.4}
$$

For System II

$$
\Delta_1 = p_2 c_1 \mu + p_1 + p_3 \tag{B.5}
$$

$$
\begin{aligned}
\Delta_2 = & -p_2 c_1^2 \mu^3 + \left(p_2^2 p_3 c_1^2 - p_3 c_1 \right) \mu^2 + \left(p_2 p_3^2 c_1 + 2 p_1 p_2 p_3 c_1 + p_2 c_1 \right) \mu \\
& + p_3 p_4 + p_3^2 p_3 + p_1
\end{aligned}
\tag{B.6}
$$

$$
\begin{aligned}
\Delta_3 = & \, p_1 p_2 c_1^3 \mu^5 + \left(-p_2^2 p_4 c_1^3 + p_1 p_3 c_1^2 - p_1 p_2^2 p_3 c_1^3 + p_2^2 c_1^3 \right) \mu^4 \\
& + \begin{pmatrix} -p_1 c_1^2 p_4 p_2 - p_3^2 p_2 c_1^2 p_1 - 2 p_3 p_2 c_1^2 p_1^2 + p_2^3 c_1^3 p_3 p_4 - p_3 c_1^2 p_4 p_2 \\ + p_3 c_1^2 p_2 + c_1^2 p_2 p_2 \end{pmatrix} \mu^3 \\
& + \begin{pmatrix} -p_3^2 p_1^2 c_1 + 3 p_1 p_3 p_2^2 c_1^2 p_4 - p_3 p_1^3 c_1 - 2 p_3 p_4 c_1 p_1 + 2 c_1 p_1 p_3 \\ + p_3^2 p_2^2 c_1^2 p_4 + p_2^2 c_1^2 p_3^2 \end{pmatrix} \mu^2 \\
& + \begin{pmatrix} p_3 p_2 c_1 + 2 p_3^2 p_1 p_4 p_2 c_1 + p_3 p_1^2 p_4 p_2 c_1 + p_3 p_4^2 p_2 c_1 + p_3^3 p_2 c_1 \\ + 2 p_1 p_3^2 p_2 c_1 - 2 p_4 p_2 c_1 p_3 \end{pmatrix} \mu \\
& + p_3 p_1 + p_3 p_1^3 p_4 + p_3^2 p_1^2 p_4 - 2 p_4 p_1 p_3 + p_3 p_4^2 p_1 + p_3^3 p_1 + p_3^2 p_1^2
\end{aligned}
\tag{B.7}
$$

$$
\begin{aligned}
\Delta_4 = & -p_2 c_1^4 p_1 \mu^7 + \left(p_2^2 c_1^4 p_3 p_1 - p_3 c_1^3 p_1 - p_2^2 c_1^4 + p_2^2 c_1^4 p_4 \right) \mu^6 \\
& + \begin{pmatrix} -p_2 c_1^3 p_1 + p_3^2 p_2 c_1^3 p_1 + 2 p_1 c_1^3 p_4 p_2 + 2 p_3 p_2 c_1^3 p_1^2 \\ -p_2^3 c_1^4 p_3 p_4 + p_3 c_1^3 p_4 p_2 - p_3 p_2 c_1^3 \end{pmatrix} \mu^5 \\
& + \begin{pmatrix} p_3 p_1^3 c_1^2 + 3 p_3 p_4 c_1^2 p_1 + p_2^2 c_1^2 p_4 - p_3^2 p_2^2 c_1^3 p_4 + p_3^2 p_1^2 c_1^2 \\ -p_2^2 c_1^3 p_4^2 - p_2^2 c_1^3 p_3^2 - 4 p_1 p_3 p_2^2 c_1^3 p_4 - 2 p_3 c_1^2 p_1 \end{pmatrix} \mu^4 \\
& + \begin{pmatrix} 3 p_3 c_1^2 p_4 p_2 + p_1 c_1^2 p_4 p_2 + p_2^3 c_1^3 p_3 p_4^2 - p_3 c_1^2 p_2 - 3 p_3^2 p_1 p_4 p_2 c_1^2 \\ -p_3^3 p_2 c_1^2 - 2 p_3^2 p_2 c_1^2 p_1 - 2 p_3 p_4^2 p_2 c_1^2 - 5 p_3 p_1^2 p_4 p_2 c_1^2 - p_1 p_4^2 p_2 c_1^2 \end{pmatrix} \mu^3 \\
& + \begin{pmatrix} -p_3^2 p_1^2 c_1 + p_3^2 p_2^2 c_1^2 p_4 - c_1 p_1 p_3 + p_3^2 p_2^2 c_1^2 p_4^2 + 4 p_3 p_4 c_1 p_1 \\ -3 p_3 p_4^2 p_1 c_1 - 2 p_3 p_1^3 p_4 c_1 + 3 p_1 p_3 p_2^2 c_1^2 p_4^2 - p_3^3 p_1 c_1 - 2 p_3^2 p_1^2 p_4 c_1 \end{pmatrix} \mu^2 \\
& + \begin{pmatrix} p_3^3 p_2 c_1 p_4 + 2 p_3^2 p_1 p_4^2 p_2 c_1 + 2 p_3^2 p_1 p_4 p_2 c_1 \\ +3 p_3 p_1^2 p_4^2 p_2 c_1 + p_3 p_4^3 p_2 c_1 + p_4 p_2 c_1 p_3 - 2 p_3 p_4^2 p_2 c_1 \end{pmatrix} \mu \\
& -2 p_3 p_4^2 p_1 + p_3^2 p_1^2 p_4 + p_3 p_1^3 p_4^2 + p_4 p_1 p_3 + p_3^3 p_1 p_4 + p_3^2 p_1^2 p_4^2 + p_3 p_4^3 p_1
\end{aligned}
\tag{B.8}
$$

Using the system parameters values presented in Table 5 and Table 7 and solving (B.1) through (B.8) for μ the following values for the nondimensional freestream velocity are obtained.

For System I

$$
\begin{aligned}
&\Delta_1 = 0, \mu = -2.32 \\
&\Delta_2 = 0, \mu = 0.59, -0.6 \pm 0.42i \\
&\Delta_3 = 0, \mu = -0.75, 0.082 \pm 0.31i, -0.051 \pm 0.34i \\
&\Delta_4 = 0, \mu = \pm 0.2152, 0.082 \pm 0.31i, -0.051 \pm 0.34i, -0.75
\end{aligned}
\tag{B.9}
$$

For System II

$$\begin{aligned}
&\Delta_1 = 0, \mu = 2.01 \\
&\Delta_2 = 0, \mu = 0.75, -0.11 \pm 0.55i \\
&\Delta_3 = 0, \mu = 0.303, 0.39 \pm 0.23i, -0.29, -0.33 \\
&\Delta_4 = 0, \mu = \pm 0.2i, 0.303, 0.39 \pm 0.23i, -0.294, -0.335
\end{aligned} \tag{B.10}$$

Hence the minimum real positive value of μ at which System I hits the imaginary axis is $\mu_I = 0.2152$, and for System II $\mu_{II} = 0.3034$.

VITA

Name:	Tarek Adel Abdelsalam Elgohary
Address:	Texas A&M University Department of Aerospace Engineering H.R. Bright Building, Rm. 620D, Ross Street - TAMU 3141 College Station TX 77843-3141
Email Address:	tag2892@aeromail.tamu.edu
Education:	B.S., Mechanical Engineering, The American University in Cairo, 2006 M.S., Aerospace Engineering, Texas A&M University, 2010